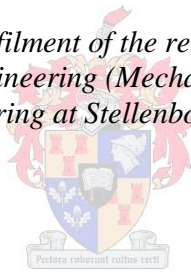# Investigation of the effect of a new splash grid on natural draught wet cooling tower (NDWCT) performance

by

Alain Juan-Pierre Michaels

Thesis presented in partial fulfilment of the requirements for the degree of Master of Engineering (Mechanical) in the Faculty of Engineering at Stellenbosch University

Supervisor: Prof Hanno Carl Rudolph Reuter

March 2015

DECLARATION

By submitting this thesis electronically, I declare that the entirety of the work contained therein is my own, original work, that I am the sole author thereof (save to the extent explicitly otherwise stated), that reproduction and publication thereof by Stellenbosch University will not infringe any third party rights and that I have not previously in its entirety or in part submitted it for obtaining any qualification.

Signature:………………………

Date: 02 December 2014

SUMMARY

A thermal power plant's efficiency is greatly dependent on the temperature of the saturated steam in the condenser. Wet-cooling provides low temperatures economically where water is readily available. Increasing the effectiveness of these wet-cooling towers through performance enhancement could result in a decrease in life cycle cost. Reuter has found that the rain zone, often overlooked as a region for performance enhancement, can have a considerable effect on the performance characteristics of a cooling tower.

In this thesis, the effect of installing a newly developed splash type grid below a conventional film type fill on the performance characteristics of the rain zone is investigated experimentally. The proposed grid reduces the mean drop size in the rain zone to enhance the performance characteristics. The following experimental performance tests are conducted in a fill test facility: film fill only, fill with rain zone, fill with rain zone and one layer of splash grids for different placements and inclination angles below the fill, fill with rain zone and two layers of splash grids for different placements below the fill. From the experimental performance characteristics, a Sauter mean drop diameter is calculated, which shows that a significant reduction in drop size is achieved by means of the grid.

The experimental results are ultimately used in a natural draught wet cooling tower one dimensional performance model to determine the effect of different fills and the grid below the fill on the cooling tower re-cooled water temperature and range.

OPSOMMING

'n Termiese kragtasie se doeltreffenheid is hoogs afhanklik van die temperatuur van die versadigde stoom in die kondensators. Nat verkoeling bied tans die laagste temperatuur wat ekonomies lewensvatbaar is waar water redelik beskikbaar is. Die verhoging in nat verkoeling torings se effektiwiteit deur die verbetering in werksverrigting kan 'n daling in lewensiklus koste tot gevolg bring. Reuter het gevind dat die reënsone, 'n aansienlike effek kan hê op die werksverrigting karakteristieke van 'n koeltoring.

In hierdie tesis, word die effek van 'n nuutontwikkelde spatpakrooster onder 'n konvensionele film tipe pakking op die werkverrigtingskarakteristieke van die reënsone eksperimenteel ondersoek. Die voorgestelde rooster verklein die gemiddelde druppelgrootte in die reënsone om sodoende die werkverrigtingskarakteristieke te verbeter. Die volgende eksperimentele werkverrigtingstoetse is gedoen in 'n koeltoringpakking toetsfasiliteit.: filmpakking alleen, filmpakking met reënsone, filmpakking met reënsone en een laag van spatpakroosters vir verskillende plasings en hoeke onder die pakking, filmpakking met reënsone en twee lae van spatpakroosters vir verskillende plasings onder die pakking. Vanaf die eksperimentele werkverrigtingskarakteristieke, word daar 'n Sauter gemiddelde druppeldeursnee bereken, wat toon dat 'n noemenswaardige verlaging in druppelgrootte met behulp van die spatpakrooster verkry kan word.

Die eksperimentele resultate word uiteindelik gebruik in 'n een dimensionele natuurlik trek natkoeltoring werkverrigtingsmodel om die effek van die spatpakrooster onder die pakking in 'n natuurlike trek nat koeltoering se herverkoelde water temperatuur en temperatuurverskil te bepaal.

ACKNOWLEDGEMENTS

TABLE OF CONTENTS

LIST OF FIGURES

LIST OF TABLES

NOMENCLATURE

Symbols

a	wetted surface area or "a" coefficient
Cu	Christiansen coefficient
d	diameter
D	diameter
i	enthalpy
h	mass or heat transfer coefficient
H	height
g	gravitational acceleration
G	mass velocity
K	loss coefficient
L	fill height
m	mass or mass flow rate
Me	transfer coefficient or Merkel number
n	number
Q	heat transfer
p	pressure
R	gas constant
T	temperature
v	velocity
w	humidity ratio
z	depth

Greek symbols

δ	differential
Δ	differential
ρ	density
μ	viscosity
σ	surface tension

Subscripts

a	air, or based on air side area

air	air
app	approach
ave	average
c	convection
condenser	condenser
cw	circulating water
d	drop, or dynamic
f	friction
fg	fill and first grid
fi	fill
fr	frontal
gg	first grid and second grid
gr	grid
i	inlet
ITD	initial temperature difference
L	length
m	mean or mass transfer
o	outlet
out	outlet
rz	rain zone
s	saturated
sp	spray zone
TTD	terminal temperature difference
v	vapour
w	water
wb	wetbulb

Abbreviations

NDWCT	natural draught wet cooling tower
T/C	thermocouple

CHAPTER 1 INTRODUCTION

1.1   Wet cooling towers

A natural draught wet cooling tower (NDWCT) as shown in Figure 1-1, rejects waste heat from re-circulating cooling water to the atmosphere and provides the lowest possible temperatures when using the atmosphere as a low temperature reservoir. It is a preferred option where water is readily available at low cost. Heated re-circulating cooling water, which is typically from a surface condenser- or process type heat exchanger, enters a wet cooling tower from the bottom and flows upwards in a riser before it is distributed to a grid of sprayers (Figure 1-2a). The sprayers spray the water as small drops onto the fill. The fill zone, which can either contain splash- (Figure 1-2b), trickle-(Figure 1-2c) or film fill (Figure 1-2d), increases the water-air interfacial area, which is achieved by the water splashing, trickling or running down the fill as a thin film, depending on the type of fill. The type of fill used in cooling towers depends on several factors including the size of the cooling tower (existing towers), the hydraulic head available (existing towers), water quality, water temperature and cost. After the water passes through the fill zone it falls, under the force of gravity, through the so called rain zone as water drops with a polydisperse size distribution and falls into a water collecting pond from where it is pumped back to the surface condenser or process heat exchanger.
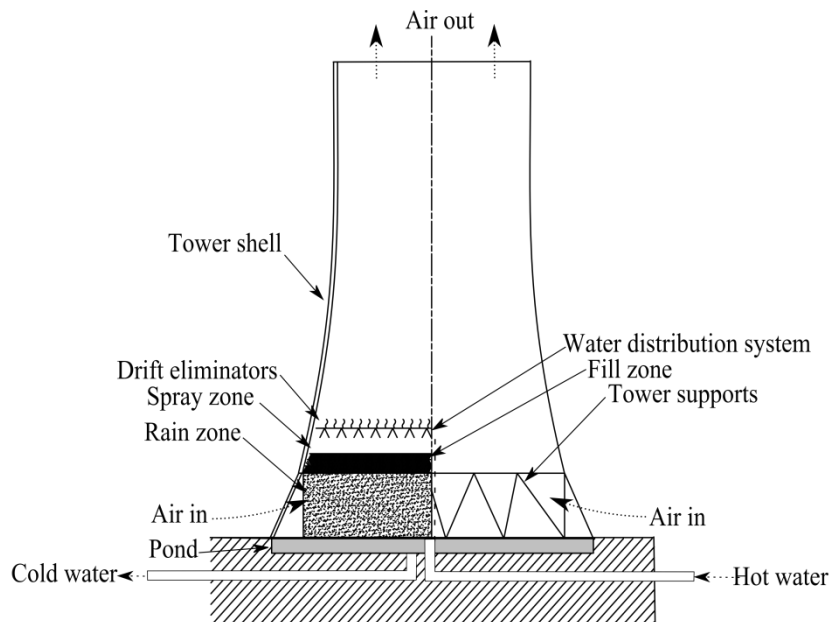
Figure 1-1: Schematic of natural draught wet cooling

The re-circulating water is cooled by ambient air which is drawn in at the bottom of the cooling tower due to a low pressure induced by buoyancy effects as a result of density difference between the air inside the cooling and the air outside the

cooling tower. This is known as natural draught. The low pressure can also be induced by fans (mechanical draught). The air enters the cooling tower, passing through the rain zone where between 10-20% of the heat and mass transfer occurs (Kröger, 2004). It then enters the fill zone, which can either contain splash-, trickle-or film fill, where most of the heat and mass transfer occurs. The now saturated to super saturated air leaves the fill zone, passing through the spray zone, water distribution system and drift eliminators. The drift eliminators remove any water drops that might have become entrained in the upward flowing air. After the air passes through the drift eliminators it flows through the remainder of the tower and exits to the atmosphere.

a). Sprayer   b). Splash fill   c). Trickle fill

d). Film fill   e). Drift eliminators
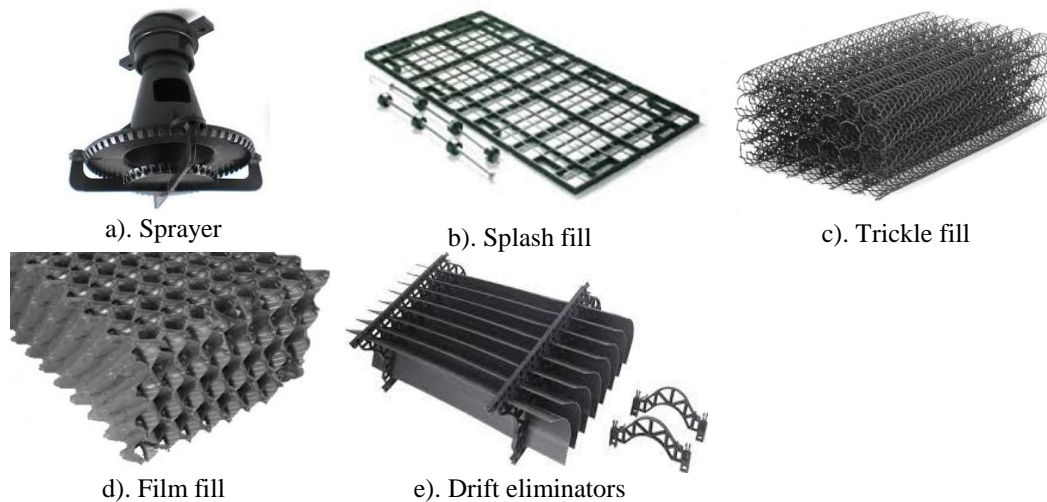
Figure 1-2: Wet cooling tower internals

A NDWCT performance affects a power plant performance since it affects the turbine exhaust temperature i.e. condenser steam temperature. In a typical power plant water/steam cycle with a NDWCT re-circulating cooling water circuit, as shown in figure 1-3, a steam turbine exhausts wet steam to a surface condenser where the steam is condensed so that it can be pumped back to a boiler via feedwater heaters. This condensate is heated and turned back into superheated steam which is fed to a turbine to complete the power generation cycle.

Reuter (2010) found that the gross efficiency of a typical modern coal fired-power plant increases between 0.3 to 0.5 % per 1 K decrease in turbine exhaust steam temperature i.e. condenser steam temperature.

A temperature versus condenser heat load diagram for a typical wet cooled power plant system is shown in figure 1-4. It can be seen from figure 1.4 that the condenser steam temperature can be decreased by either decreasing the initial temperature difference (ΔT_{ITD}) and/or the tower's approach (ΔT_{App}). The initial temperature difference can typically be decreased by increasing the condenser heat transfer surface area and the cooling water mass flow rate to reduce the cooling water temperature rise. The approach can be decreased by either installing fill with better performance characteristics than the current installed fill,

2

decreasing the flow losses, increasing the size of the tower or increasing the performance of the rain zone.
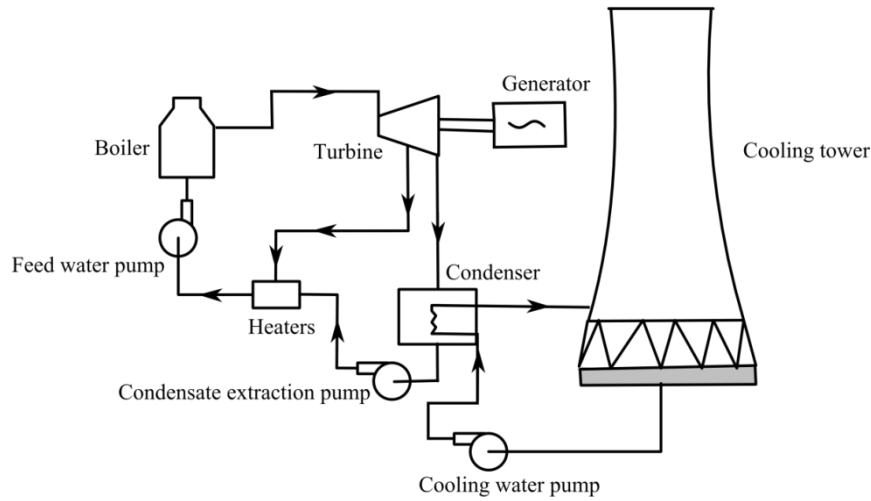
Figure 1-3: Schematic drawing of a typical power plant water/steam cycle and natural draught wet cooling tower re-circulating water circuit
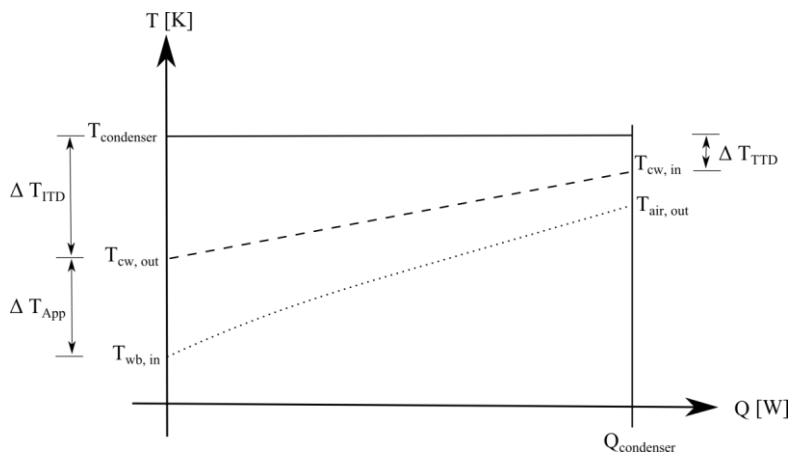
Figure 1-4: T vs Q diagram for a typical wet cooling system diagram

Eskom (South Africa's parastatal power utility) NDWCT's of Eskom (which comprise approximately 75 % of its heat ejection systems) are currently under-performing. The under-performance can be ascribed to various factors which include degradation of cooling tower internals as a result of lack of maintenance, ineffective water treatment and deteriorating water quality.

The performance of the Eskom cooling towers can be improved by introducing a splash type grid beneath the currently installed fills to reduce the average rain zone drop size thereby increasing the air-water interface and thus the heat and mass transfer of this zone.

This thesis presents the effect of reducing the rain zone drop size by introducing a specially designed splash type grid below a conventional cross fluted film fill on the overall performance characteristics of a natural draught wet cooling tower.

1.2 Literature review

This literature review presents the theory and literature concerning NDWCT's, drop size reduction, splash grid design, rain zone performance modelling, fill performance testing and cooling tower modelling.

1.2.1 NDWCT theory

A NDWCT uses two mechanisms to transfer heat from the heated circulating cooling water to the atmosphere, namely sensible (convection heat transfer) and latent heat transfer (diffusion mass transfer). The sensible heat transfer is as a result of the temperature difference that exists between the water and the air and the latent heat transfer is as a result of a concentration difference between the air at the surface of the water and the free stream air. This is illustrated in figure 1-3 and mathematically in equation 1-1, where the subscripts m and c is the heat transfer due to mass and convection respectively.

$$dQ = dQ_m + dQ_c \qquad \text{1-1}$$

According to Fick's law the mass transfer from a differential control volume is given by equation 1-2.

$$\frac{dm_w}{dz} = h_d(w_{sw} - w)dA \qquad \text{1-2}$$

Where h_d is known as the mass transfer coefficient.

The energy thus required to evaporate this mass from the water surface to the adjacent air is given by equation 1-3.

$$dQ_m = i_v \frac{dm_w}{dz} dz = i_v h_d(w_{sw} - w)dA \qquad \text{1-3}$$

The enthalpy of the water vapour is given by the expression shown in equation 1-4.

$$i_v = i_{fgwo} + c_{pv}T_w \qquad \text{1-4}$$

The sensible heat transfer is given by equation 1-5

$$dQ_c = h(T_w - T_a)dA \qquad \text{1-5}$$

The enthalpy of the saturated air at the water's surface is given by equation 1-6

$$i_{masw} = c_{pa}T_w + w_{sw}(i_{fgwo} + c_{pv}T_w) = c_{pa}T_w + w_{sw}i_v \qquad \text{1-6}$$

Where the term $c_{pa}T_w$ is the enthalpy associated with the dry air and $w_{sw}(i_{fgwo}+c_{pv}T_w)$ the enthalpy associated with the water vapour in the air.

Rewriting equation 1-6 to the expression shown below.

$$i_{masw} = c_{pa}T_w + wi_v + (w_{sw} - w)i_v \qquad \text{1-7}$$

The enthalpy associated with the free stream air away from the surface of the water is given by equation

$$i_{ma} = c_{pa}T_a + w(i_{fgwo} + c_{pv}T_a) \qquad \text{1-8}$$

Where the term $c_{pa}T_w$ is the enthalpy associated with the dry air and $w(i_{fgwo}+c_{pv}T_a)$ the enthalpy associated with the water vapour in the air.

By subtracting equation 1-7 from 1-8 and assuming the difference between the specific heats are negligible at the different temperatures they are evaluated at equation 1-9 is obtained.

$$i_{masw} - i_{ma} \approx (c_{pa} + wc_{pv})(T_w - T_a) + (w_{sw} - w)i_v \qquad \text{1-9}$$

Rearranging equation 1-9 to make (T_w-T_a) the subject equation 1-10 is obtained.

$$T_w - T_a = [(i_{masw} - i_{ma}) - (w_{sw} - w)]/c_{pma} \qquad \text{1-10}$$

Where $c_{pma} = c_{pa} + wc_{pv}$

Equation 1-1 can now be written as equation 1-11 after substituting equation 1-3, 1-5 and 1-10.

$$dQ = h_d \left[\frac{h}{c_{pma}h_d}(i_{masw} - i_{ma}) + \left(1 - \frac{h}{c_{pma}h_d}\right)i_v(w_{sw} - w)\right] dA \qquad \text{1-11}$$

The term $\frac{h}{c_{pma}h_d}$ is known as the Lewis factor (Le_f) and shows the relative rate of heat and mass transfer.

It can be said that the enthalpy transfer from the water to the air is also the change in the enthalpy of the air from equation 1-10 we have equation 1-12

$$\frac{di_{ma}}{dz} = \frac{1}{m_a}\frac{dQ}{dz} = \frac{h_d}{m_a}\frac{dA}{dz}\left[Le_f(i_{masw} - i_{ma}) + (1 - Le_f)i_v(w_{sw} - w)\right] \qquad \text{1-12}$$

The area for a one dimensional model of a cooling tower can be written as

$$dA = a_{fi}A_{fr}dz \qquad \text{1-13}$$

Substituting equation 1-13 into 1-12 and assuming the Lewis factor is unity equation 1-12 reduces to equation 1-14.

$$\frac{di_{ma}}{dz} = \frac{h_d a_{fi} A_{fr}}{m_a}(i_{masw} - i_{ma}) \qquad \text{1-14}$$

The change in water temperature across a control volume over distance dz can be obtained by performing a mass and energy balance across a control volume, which is shown in figure 1-3. By combining the mass and energy balance and neglecting second order terms the expression below for the change in water temperature across a control volume of distance dz is obtained.

$$\frac{dT_w}{dz} = \frac{m_a}{m_w}\left(\frac{1}{c_{pw}}\frac{di_{ma}}{dz} - T_w\frac{dw}{dz}\right) \qquad \text{1-15}$$
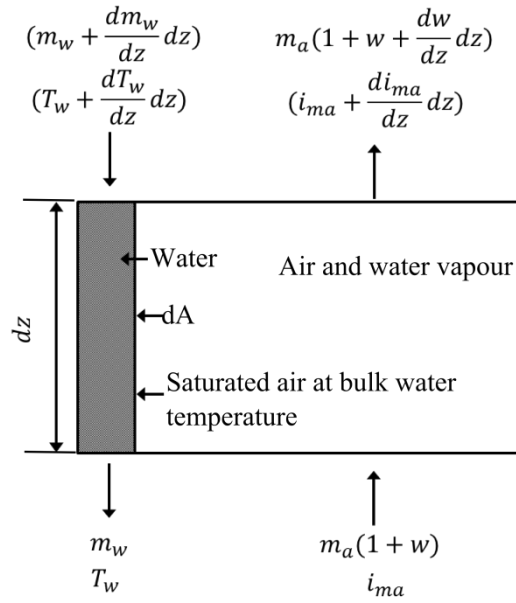
Figure 1-5: Counter flow fill control volume (adapted from Kröger, 2004)

Substituting equation 1-14 into 1-15 and assuming the evaporation rate is negligible equation 1-16 is obtained.

$$\frac{dT_w}{dz} = \frac{m_a}{m_w}\frac{1}{c_{pw}}\frac{h_d a_{fi} A_{fr}}{m_a}(i_{masw} - i_{ma})$$

1-16

By rearranging equation 1-16 the expression shown in equation 1-17 is obtained. The term on the left is known as the transfer coefficient or Merkel number.

$$Me = \frac{h_d a_{fi} L_{fi}}{G_w} = \int_{T_{wo}}^{T_{wi}} \frac{c_{pw} dT_w}{i_{masw} - i_{ma}}$$

1-17

The process of enthalpy transfer from the water to the air heats and saturates the air along the height of the tower resulting in a density difference between the air inside the tower and the air outside the tower. The buoyancy effect causes the air to flow through the tower.
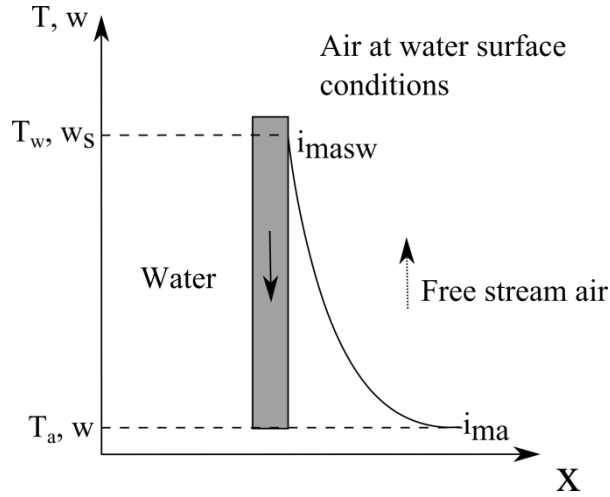
Figure 1-6: Illustration of Merkel theory

The air flow rate in a NDWCT is determined by the density difference between the air inside the tower and the air outside the tower. This buoyancy effect causes the draught through the tower. The draught through the tower can however be decreased as a result of flow losses in the cooling tower. The overall loss coefficient, which is defined as Total loss coefficient = Frictional losses + momentum losses + static losses and given in equation 1-18.

$$K_{fdm} = \frac{2\left[\Delta p_{fi} - (\rho_{avo}v_{avo}^2 - \rho_{avi}v_{avi}^2) + (\rho_{avi} - \rho_{avm})gL_{fi}\right]\rho_{avm}A_{fr}^2}{m_{avm}^2} \quad \textbf{1-18}$$

1.2.2   *Drop size reduction*

The purpose of drop size reduction is to increase the air-water interface, which increases the rain zone's heat and mass transfer.

Holland (1974) conducted tests on a tower devoid of fill with a water distribution system distributing the water drops evenly across the tower at a known drop size distribution. He found that a uniform drop distribution and a drop diameter of between 1- and 2 mm provide the highest performance.

There are three modes of drop modification, i.e. splashing, dripping and cutting in a splash pack. Dreyer and Erens (1996) found that the slat width, the drop impact velocity on the grid and the position of the impact on the grid has a significant effect on the mechanism of drop break up when drops hits a slat. Splashing (also known as disintegration) occurs when the impact surface is relatively large compared to the incoming drop size and/or the impact velocity is high. Splashing produces a poly-dispersed drop size distribution and forms a mist which can be carried away by the incoming air. Dripping occurs when the drop size is relatively large compared to the impact surface or the drop velocity low. Dripping produces larger drop sizes compared to the incoming drop size. Cutting occurs when the impact surface is comparable with the drop size. This drop break up mechanism produces a more uninform drop distribution compared to splashing and smaller

7

drops compared to dripping. Hung and Yao (1999) conducted experiments on the impact of mono-dispersed droplets on finite cylindrical surfaces. They varied the droplet impact velocity and the size of the cylindrical surface and determined the effect on the drop break up. Their research was however limited to small droplets, with their reference droplet size at 350 μm and also testing droplet sizes of 110 μm and 680 μm. They used stainless steel wire with a diameter of 113, 254, 381, 508, 813, 1190, 1588 μm. The result was that most of the droplets either disintegrated or dripped.

Steenmans (2010) conducted a study where he investigated the drop break up mechanism for a drop impacting on a single cylindrical surface. He took high speed digital images of drops after impact and determined the drop size distribution and average drop diameter. The drop falling height before impact, wire position, drop size, wire diameter, the drop offset from the wire centre line, wire shape, tension in wire and wire material were varied systematically to determine its effect on drop break up. Studies were aimed at producing the smallest average drop size after impact. The reference conditions for the experiments were a drop diameter before impact of 4 mm, falling height before impact of 500 mm, wire diameter of 2 mm, drop offset from wire centreline of 0 mm, wire material of stainless steel, zero tension in the wire and a round shape. He found that the reference conditions produced a drop size of 1.93 mm after impact.

The drop size before impact was varied between 2.7 mm and 5.5 mm. There was a gradual increase of drop size after impact with increasing drop size before impact. The result was that drop size before impact has an effect on the drop size after impact similar to the findings of Kröger (2004) and Terblanche (2008). Steenmans also found that drops deflect at an angle of 20° after impact.

Drop height before impact was varied between 200 mm to 800 mm in increments of 100 mm. The drop size after impact initially decreased with increasing height, reached an optimum of 400 mm and then increased for the remainder of the tests.

The wire material was changed from stainless steel to nylon. The tension in the wire and the wire diameter were varied and found the 1 mm wire diameter and 0 tension produced the smallest drop size after impact and the type of material had a negligible effect on the drop size after impact.

The investigation was later expanded to multiple wire configurations and its effect on drop break up. A staggered pattern of single filament nylon 1 mm diameter wire and drop size reduction were investigated. The wires were placed at an angle of 15° at a distance of 2.3 mm apart. This configuration produced a drop size after impact of 1.6 mm. Steenmans later used these parameters in designing a splash grid to place below the fill.

1.2.3   Splash grid design

Several studies have been done, which include Terblanche et al. (2009), Oosthuizen (1995) and Steenmans (2010), in designing a splash grid to be placed under a conventional fill for reducing the rain zone drop size. The drop size in the rain zone is largely dependent on the fill above. Three types of fill are most commonly found in wet cooling towers, including splash, trickle and film fill. Terblanche et al. (2009) found the Sauter mean drop diameter, for which the definition is given in equation 1-19, below the fill to range between 5 and 6 mm for trickle- and film fill and 3.5 mm for splash fill. Modern power stations prefer the use of film fills since they achieve the highest performance per meter of fill. The use of film fills is however not conducive to high performance in the rain zone due to the larger drops exiting the fill.

$$Sauter\ mean\ diameter\ (SMD) = d_{32} = \frac{\sum nd^3}{\sum nd^2} \qquad \textbf{1-19}$$

Methods for reducing the drop size and its effect on the performance of the rain zone below the fill region have been done in the past. Oosthuizen (1995) investigated the effect of a splash grid below a trickle fill on the drop size of the rain zone. The splash grid, which was made out of a course expanded metal grid, would reduce the drop size in the rain zone without contributing significantly to the total pressure drop. He did this by placing two layers of splash grid, spaced 0.1 m apart, at various heights below the trickle fill. He investigated the optimum distance i.e. the drop height before impact producing the smallest Sauter mean diameter drop size, of the grid below the fill, drop size distribution as well as the transfer characteristics associated with such a configuration. He found the Sauter mean drop diameter to be 4.05 mm for an optimum fill to grid spacing of 0.67 m.

Terblanche (2008) also investigated methods to reduce the rain zone drop size and its effect on the performance of this zone. He measured the drop size distribution for horizontal grid which comprised of 3 mm wide, 12 mm high PVC slats spaced 10 mm apart as well as expanded metal sheeting placed below trickle fill. He also determined the optimum distance between the fill and grid which was based on the smallest Sauter mean drop diameter obtained. He found the smallest Sauter mean drop diameter of 2.73 mm below a double slat grid configuration placed 0.8 m below the trickle fill.

Steenmans (2010) did several experiments on various parameters concerning single drop impacting on a single wire as discussed earlier. He used the results to design a grid. The grid consisted of a 910 mm x 910 mm steel frame, with metal strips either side of the frame. He used 1 mm Nylon string spanning the cross sectional area of the frame in a staggered pattern placed at an angle of 20° with respect to each other, with fourteen wires per diagonal row, grid height of 73 mm and width between wire centres at 8.8 mm He tested the grid in a cross flow wet cooling tower test facility at various orientations to determine the smallest Sauter

mean drop diameter. The drop size was inferred from the experimental transfer coefficient. The smallest Sauter mean drop diameter was found to be 2.5 mm.

1.2.4   Rain zone performance modelling

The rain zone was previously ignored in the modelling of NDWCT due to its complexity to model. The rain zone contributes considerably to the overall transfer coefficient and can thus not be ignored. Several attempts have been made to include the contribution of the rain- and spray zone by modelling the aforementioned zones (Rish, 1961; Lowe and Christi, 1961; Missimer and Bracket, 1986; Sedina, 1992). Some even approached the modelling of the rain zone numerically (Majumdar and Singhal, 1983, Benocci et al., 1986; Benton and Rehberg, 1986), however these methods either proves to be only applicable for either counter-or cross flow. A rain zone is however combination of counter- and cross flow which is taken into account in the model developed by De Villiers and Kröger (1997). De Villiers and Kröger made the following assumptions in developing the model: no drop agglomeration, uniform water flow rate through the fill, uniform rain zone drop diameter, zero absolute drop velocity for drops entering the rain zone, the air velocity profile is not influenced by the falling drops and constant thermophysical properties throughout the rain zone.

1.2.5   Fill performance testing

Fill performance testing is used for generating correlations to describe the performance characteristics of fill. These correlations can for example later be used for modelling to determine the effect of the fill on the performance of a cooling tower.

Experimentally determined correlations are currently the most accurate way to describe fill performance although attempts have been made to model the performance (Dreyer and Erens, 1995). There are several test facilities for fill testing and researchers who produce fill performance results, however neither the test facility nor the procedure and results are standardised and as a result cannot be compared directly with each other (Bertrand, 2009). The test conditions or data to produce the results are most often also not given to verify the correlations. Bertrand (2009) quantify to what accuracy, reliability and repeatability fill performance results, be produced in a 1.5 m x 1.5 m counterflow test facility at the University of Stellenbosch. He also gives the form of the correlations to use which accurately accounts and describes the transfer- and loss coefficients as found and verified by Kloppers and Kröger (2003) and are given in equation 1-20 and 1-21 respectively.

$$Me_{fi}/L_{fi} = a_1 G_w^{a_2} G_a^{a_3} T_{wi}^{a_4} \qquad\qquad \text{1-20}$$

$$K_{fdm}/L_{fi} = b_1 G_w^{b_2} G_a^{b_3} + c_1 G_w^{c_2} G_a^{c_3} \qquad\qquad \text{1-21}$$

The exponents in equations 1-20 and 1-21 are determent experimentally through multi variable linear regression.

1.2.6   One-, two- and three dimensional NDWCT performance modelling

 One-, two- and three dimensional NDWCT performance modelling depends on the density difference between the air inside the tower and the air outside the tower at the same elevation. The flow rate is dependent on the various flow resistances due to the cooling tower internals, transfer characteristics of the rain, fill and spray zones and the cooling tower dimensions (Kröger, 2004).

The Merkel method is still commonly employed for cooling tower analysis in one, two and three dimensional modelling. The more rigorous Poppe method is employed in situations where the assumptions made by Merkel are not valid especially hybrid systems where the outlet air cannot be assumed to be saturated.

One dimensional modelling is still widely used in industry for the design of NDWCT (Reuter, 2010) due to its relative ease of use, low expense and relatively accurate results. The one dimensional models do not however take variation of radial flow, non-uniformities e.g. variation in packing height, shape of the tower and the effect of cross wind into account. Two and three dimensional model was introduced to account for the non-uniformities (Al-Waked and Behnia, 2005; Williamson et al*.,* 2008; Reuter, 2010; Klimanek, 2013). These two- and three dimensional models however still make use of experimental data to account for fill performance characteristics.

Williamson et al. (2008) conducted a study by comparing the difference in cooling range for a one- and two dimensional cooling tower performance models with different input parameters. They found a difference of 2% between the models.

1.3   Objectives

The main objective of this thesis is:

- To experimentally evaluate the effect of installing a newly designed splash grid below a conventional packing cross fluted film fill on rain zone performance characteristics.
- To investigate the effect of such a splash grid on full scale natural draught wet-cooling tower performance, using a one-dimensional performance model developed by Kröger (2004) and improved by Reuter (2010).

1.4   Motivation

The rain zone can contribute more to the overall heat and mass transfer, also known as the transfer coefficient and Merkel number, than is currently the case. The transfer coefficient of the rain zone can be increased by decreasing the Sauter mean drop diameter of the rain zone.

Reducing the rain zone Sauter mean drop diameter from 6 mm to 2.5 mm increases the rain zone transfer coefficient of a typical NDWCT cross-counterflow

rain zone by a factor of 4.5 and the loss coefficient by a factor of 1.5. Based on the NDWCT performance model example given in Kröger (2010), this can reduce the cooling water outlet temperature by as much as 1.2 $^{\circ}$C.

1.5   Scope of work

In order to meet the objectives of this thesis the methodology listed below is followed:

- A new splash type grid is designed and manufactured for testing.
- A test facility is prepared for testing of the new splash type grid and conventional fill.
- A software interface program is developed in visual basic to log and process data during tests.
- Various tests are conducted to investigate the effect of installing the grid below a conventional film pack on rain zone performance characteristics (Merkel number and loss coefficient) based on the Merkel method of analysis
- Computational models are developed for inferring the rain zone drop size from the experimentally determined transfer coefficients
- A theoretical one-dimensional cooling tower model is programmed for a full size cooling tower to investigate the effect of different drop sizes in the rain zone on cooling tower performance

1.6   Thesis summary

Below is an overview of the chapters in this thesis.

CHAPTER 1 – INTRODUCTION

The introduction section introduces the reader to a NDWCT, how it operates, the affect the performance has on a power plant's performance, NDWCT performance issues, typical problems faced by the Eskom power utility and general solutions to these problems and methods for enhancing the performance of a NDWCT. This section also provides the reader with the objectives, motivation and research methodology to achieve the objectives. Lastly the introduction section provides a thesis summary of all the chapters.

CHAPTER 2– COUNTERFLOW WET COOLING TOWER FILL TEST FACILITY

This chapter provides an overview of the wet cooling tower test facility (both counter-and cross flow) located at the University of Stellenbosch. This chapter also gives the aim of the experimental work, the previous work that was done and published using the test facility, description and operation of the test facility, providing more detail on the counterflow test section, which also includes a description of test grid used as the performance enhancing device during testing. A description of the measurement techniques and instrumentation is also given.

The experimental procedure used, which include heating of process water, test facility preparation, testing and data logging is given in this section as well.

CHAPTER 3– EVALUATION OF THE EFFECT OF A GRID ON THE PERFORMANCE CHARACTERISTICS OF A NDWCT RAIN ZONE

The experimental results for the effect of different fill/grid configurations on the overall transfer- and loss coefficient, more specifically the transfer- and loss coefficient for the rain zone below these configurations are given in this chapter. The performance characteristics of the rain zone below these configurations are compared with a reference case, where the reference case is the performance characteristics of the rain zone below a conventional type film fill. Other content of this chapter also include the procedure used for determining the rain zone performance characteristics below the fill configurations, a description of the specific fill configurations tested, the necessity for the configurations tested and finally the results are presented.

CHAPTER 4 – RAIN ZONE SAUTER MEAN DROP DIAMETER

The effect of the grid on the rain zone drop size is given in this chapter. The method used for determining the drop size based on the experimental transfer coefficient is also given.

CHAPTER 5 – THE EFFECT OF DIFFERENT FILL CONFIGURATIONS ON THE PERFORMANCE OF A NDWCT

This chapter contains the NDWCT model used, the design data of the cooling tower being modelled and the type of fill currently installed in the tower. A comparison of the original design performance and the performance as calculated using the one dimensional model is given. The current performance of the cooling tower is incorporated in the one dimensional model. Lastly different fill and fill/grid configurations are modelled and the best performing configuration recommended.

CHAPTER 6 – CONCLUSION

The conclusion based on the work presented in this thesis is given.

CHAPTER 2 COUNTERFLOW WET COOLING TOWER FILL TEST FACILITY

2.1 Introduction

This section of the thesis provides an overview of the wet cooling tower fill performance test facility, as shown in Figure 2-1, located at the University of Stellenbosch.

The aim of the experimental work is to determine the performance characteristics of a conventional film fill as well as a conventional film fill with a grid placed below it. The results obtained are ultimately used in a one dimensional NDWCT model to model the effect of the conventional film fill and grid configuration on the cooling tower performance.

Several experiments have been done, of which the results were also published (Oosthuizen, 1995; Kloppers and Kröger, 2003; Bertrand, 2011; Grobbelaar, 2012), on the test facility to determine performance characteristics of fill and different fill configurations. Oosthuizen (1995) used the counteflow test facility to measure the performance characteristics and drop size distribution below a trickle fill. He then introduced a splash grid below the trickle fill and determined the effect of this splash grid on the performance characteristics and drop size distribution of the rain zone. Kloppers and Kröger (2003) tested film-, trickle-, and splash fill to generate experimental data which was used for determining the best fit correlation for describing the loss coefficient. Grobbelaar (2012) used the cross flow test section to determine a trickle fill's performance characteristics and compares it with the same trickle fill performance characteristics, however tested in the counterflow test facility. The experimental results were also used for validating a two dimensional model. Bertrand (2011) investigated several non-ideal factors associated with the counterflow test facility. This includes: air flow uniformity, air fill bypass, location of water inlet and outlet temperature measurement points and location of pressure measurement probes. He also quantified the water distribution obtained with a newly designed water distribution system. He then tested a film-, trickle- and splash fill to determine whether these fills can be tested accurately in this test facility. He found that film- and trickle fill can accurately be tested in the counterflow test facility and to a lesser degree of accuracy for splash fills where the wall effect i.e. where the water migrates to the wall of the test facility bypassing the fill, start to dominate.

2.2 Description of test facility

A description of the cooling tower fill test facility measurement, techniques and instrumentation are given in this section. It comprises of the water flow, air flow, process water heating and description of the equipment and instrumentation.

The process water is drawn from the top of a 45 000 litre reservoir to the test facility. The process water is heated by a 150 kW diesel fired boiler. The water is

drawn from the bottom of the reservoir and fed to the boiler where it is heated approximately 1.5 ^{o}C every hour before it returns to the top of the reservoir to avoid warm water to be drawn and fed to the boiler. This cycle continues until the process water is heated to 3 ^{o}C above the desired temperature to negate the effect of heat losses to the environment during start-up of the test facility.

1. Round Inlet
2. Cross flow test section
3. Mixing vanes
4. Settling screens
5. Nozzle dry and wet bulb T/C
6. Differential pressure point across nozzle
7. Air flow nozzles
8. Centrifugal fan
9. Counter flow dry-and wet bulb T/C
10. Water outlet T/C
11. Water catchment system
12. Differential pressure point across fill
13. Counterflow test section
14. Water distribution system
15. Water inlet T/C

Figure 2-1: Schematic drawing of experimental test facility

The process water is pumped from the reservoir to the counter flow test section where it is distributed evenly onto the fill material by means of a water distribution system (14, Fig. 2-1 and Fig. 2-2).

The temperature of the water is measured by T/C's (15, Fig 2-1) upstream of the water distribution system in the common inlet pipe line. The water flows through the packing and exits to the rain zone as drops with a poly-dispersed drop distribution after which it is caught by the water collecting troughs (11, Fig. 2-1). The water drains from the water collecting troughs to the side manifolds and outlet pipes. Three T/C's in each outlet pipe measure the outlet temperature (10, Fig. 2-1). The two outlet pipes join to form a common line which drains to a collecting sump at ground level. From the collecting sump it is pumped back to the bottom of the hot water reservoir thereby ensuring the warmest water remains at the top.

The air used in the test facility is drawn through a rounded inlet (1, Fig. 2-1) into a square duct with a cross-sectional area of 4 m^{2}, as shown in Figure 2-1 where the flow is induced by the centrifugal fan (8, Fig. 2-1). It flows through the cross flow test section (2, Fig. 2-1) which is not in use during counterflow tests. There is a pair of mixers in the test facility with each pair containing a horizontal and vertical mixer. This is to ensure good mixing and uniform temperature distribution during cross flow fill tests. The horizontal and vertical mixing vanes are similar in

design, differing only in orientation, where the horizontal vanes are at a 90° angle to the vertical mixing vanes.

The mixing, however induces large eddies and vortices, which are broken up by the settling screens (4, Fig. 2-1). From the settling screens the air moves through the flow nozzles (7, Fig. 2-1) with the pressure drop measured across them (6, Fig. 2-1) and wet- and dry bulb temperature upstream of them (5, Fig. 2-1) used for the calculation of the air mass flow rate. The air moves via the 50 kW variable speed drive fan through three 90° bends fitted with guiding vanes to minimize losses. Before the air enters the last 90° bend it flows through air resistance packing of varying thickness to create a uniform air flow distribution to the counterflow test section. From there it enters the vertical/counterflow test section as an approximately vertical stream. The dry- and wet bulb temperatures are measured (9, Fig. 2-1) before the air flows through the water collecting troughs (11, Fig. 2-1) fill, spray, water distribution system and drift eliminator zones before exiting to the atmosphere.

2.3   Description of the counterflow test section

The primary outcome of this thesis is to determine performance characteristics of fill grid combinations. The counterflow test section shown in Figure 2-2 is utilized to determine these characteristics. The various sections of the counterflow test facility are discussed below.
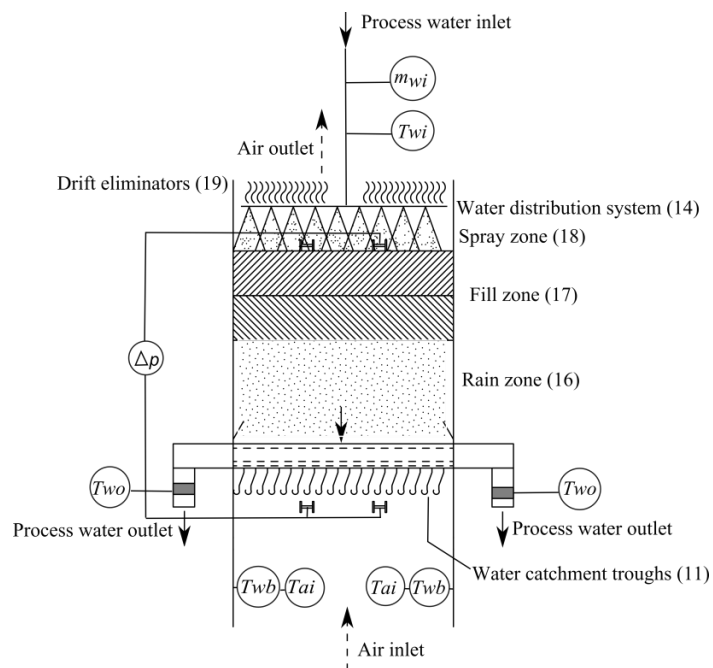
a). Test facility   b). Schematic drawing

Figure 2-2: Counterflow wet cooling fill test section

16

2.3.1   Water distribution system

The water distribution system (marked 14 in Figure 2-2) shown in Figure 2-3, distributes the water approximately uniformly across the fill. It consists of a common inlet pipe, distribution header, down pipes and a double pipe distribution system. Figure 2-3c shows the water flow through one of the inner- and outer pipe configuration that branch off from the common manifold. There are 57 distribution pipes arranged in a staggered pattern and spaced 50 mm apart and 50 mm pitch. The distribution pipes (shown in Fig. 2.3c) consists of an inner pipe with 2 mm holes at the top to prevent air pockets from forming and an outer pipe with 1 mm holes. The 1 mm holes are arranged in a staggered pattern at a pitch of 10 mm. The bottom row (can be seen in Fig. 2.3b) are set at an angle of 30° while the top row at an angle of 20°. The angle allows the drops exiting the water distribution system to have a horizontal component preventing it from falling through the fill. There are several of these pipes and are arranged in a staggered pattern as can be seen in Figure 2-3b.

a). Isometric view

b). Front view

c). Water flow

d). Water distribution system
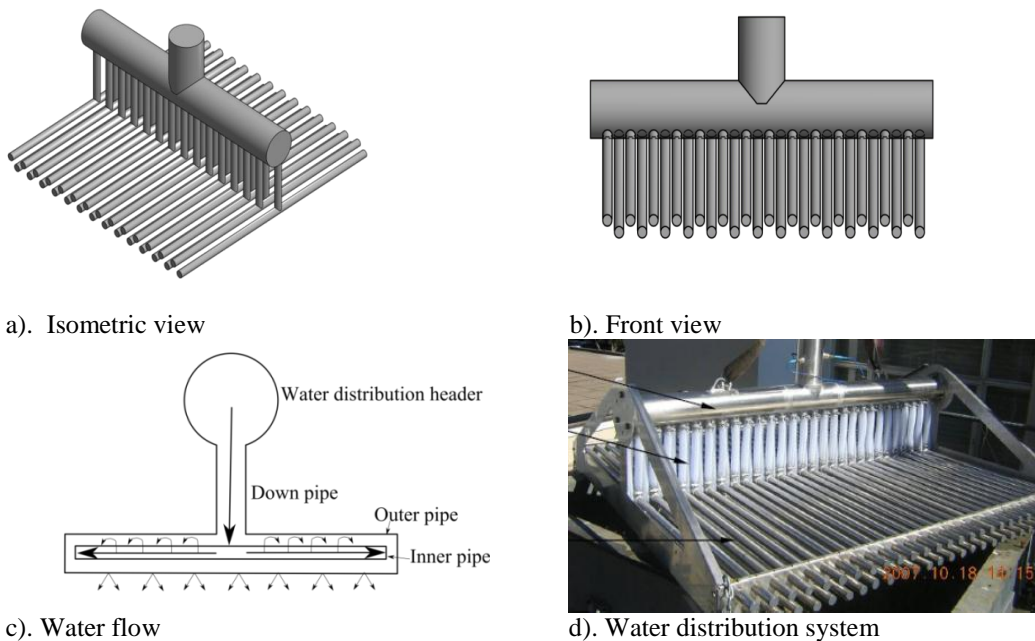
Figure 2-3: Water distribution system

One of the Merkel theory assumptions is a uniform water distribution across the fill. A non-uniform water distribution across the fill will lead to the under-prediction of the transfer coefficient. Bertrand (2009) measured the water distribution below the spray frame at water mass velocities of 1.496, 2.997 and 4.485 kg/s m^2. He quantified the water distribution achieved by the spray frame using the Christiansen coefficient which is defined as:

$$Cu = 1 - \frac{1}{n^2 m_{ave}} \sum |m_{ave} - m_i| \qquad\qquad 2\text{-}1$$

A Christiansen coefficient of 1 corresponds to a uniform distribution i.e. highest transfer coefficient achievable for the given conditions. Bertrand found a Christiansen coefficient of 0.95, 0.96 and 0.94 for 1.49-, 2.99- and 4.49 kg/s m^2 respectively. This means that the transfer coefficient deviates from the ideal case most at a water mass velocity of 4.485 kg/s m^2. Kranc (1993) correlated the percentage deviation of the transfer coefficient from the ideal case with the Christiansen coefficient. For the water mass velocity of 4.485 kg/s m^2 case the deviation is approximately 99.56 %. This means that the water is distributed close to ideal.

2.3.2   Fill region

The purpose of the fill region is to house the fill to be tested (17, Fig. 2-2). The overall height of the test facility which include fill, spray and rain zone height can be extended to 5 m. The test facility can be used with reasonable accuracy to test film, trickle and to a lesser degree of accuracy splash packs Bertrand (2011). The water migration effect is the water that runs along the wall bypassing the fill region. The water will thus partially bypass the fill region under predicting the fill's performance. Tim Bertrand (2011) tested various fills and fill heights found that the maximum deviation for film fill (the conventional fill used for experiments in this thesis) to be 15% of the average water flow rate. The lowest Christiansen coefficient was found to be 0.903 for a film fill height of 1.83 m and water mass velocity of 2.98 kg/s m^2. This Christiansen coefficient predicts a 99 % under prediction of the ideal performance.

2.3.3   Water collecting troughs

The water collecting troughs (Figure 2-4) collect the water falling from the fill region and drain it to the outlet piping to a collecting sump from where the water is pumped back to the hot water reservoir. The system consists of two levels of troughs directly below one another orientated at 90° to minimize water losses and allow air to pass through it. A deflector plate, shown in Figure 2-4b, was added to further reduce water losses passing through.

a Water collecting troughs

b Trough with deflector plate
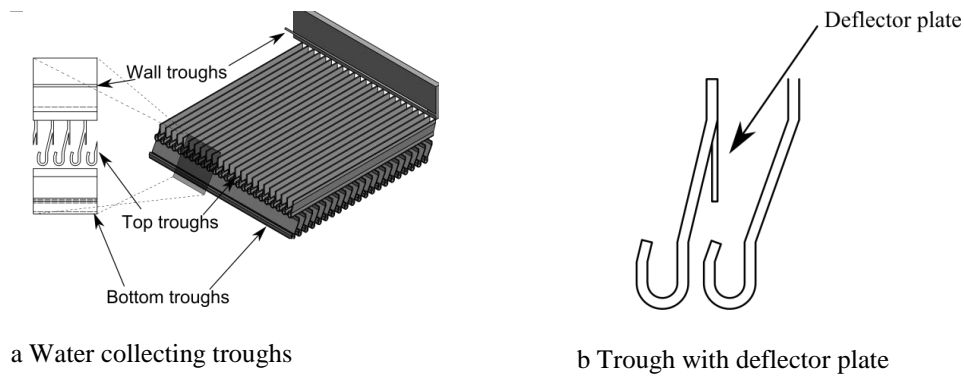
Figure 2-4: Two layer water collecting troughs

2.3.4 Description of grid

A description of the grid used for the experimental work is shown in this section.

A splash type grid of which a photograph is shown in Figure 2-5 was built for placing below a conventional film fill to reduce the Sauter mean rain zone drop diameter. The design was based on the research conducted by Steenmans (2010). The main criteria for designing the grid were to reduce the drop size below the fill to 2 mm with a minimal pressure drop. Steenmans tested various parameters to determine the optimum grid placement. The grid below was designed such that the drop is cut and not disintegrating when impacting the wire. This means the wire size must be smaller but comparable to the drop size resulting in a 1 mm wire size. Two rows of wires are placed 2 mm apart in a staggered pattern as shown in Figure 2-5a to reduce the size of the drop to 2 mm. The wires were placed at an angle of 20° since Steenmans found the smaller drops as a result of the cutting of the drop deflects by 20° after impact. This would ensure that even if the drop size after impact is larger than 2 mm can still reduce its size.
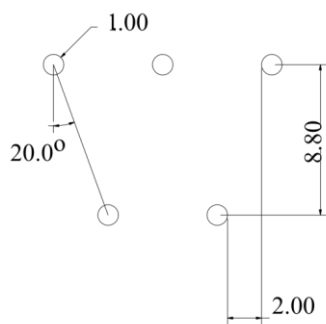
a.   Grid wire configuration

b.   Photograph of grid

Figure 2-5: Grid design

19

2.4   Measurement techniques and instrumentation

The instrumentation used for measuring the temperature, pressure and water flow rate is covered in this section.

2.4.1   Temperature

There are eight aspirated psychrometers (5, Fig. 2-1) and (9, Fig. 2-1), each containing two T-type T/C's, one for the wetbulb temperature and the other for the drybulb temperature (schematic drawing figure 2.6).There are three water inlet and six water outlet T-type T/C's fitted on the test facility (10, Fig. 2-1 and 15 Fig. 2-1 respectively) measuring the inlet and outlet water temperature respectively.

Four of the eight aspirated psychrometers measure the temperatures before the flow nozzles for air mass flow rate calculations. The remaining four measure the temperatures for performance characteristics calculations of the counterflow test section. The wet bulb temperature is a crucial component for determining performance characteristics. It is therefore measured according to ANSI ANSI/ASHRAE 41.1 − 1986, *Standard method for temperature measurement* standard which states:

For dry/wet bulb temperature measurements the T/C's must be shielded from radiant heat by fitting it with a metal sleeve. A continuous constant air velocity of between 4.8 m/s and 5.3 m/s must flow across the T/C's to ensure the air surrounding it does not become saturated with water vapour. The T/C's measuring the wetbulb temperature must be fitted with a wick covering at least 25.4 mm of the temperature sensitive part of the thermocouple. Distilled or demineralized water must be fed to the wick from a reservoir. The temperature of the reservoir must be at the wetbulb temperature which is practically achievable by allowing sufficient ventilation across the wick. The wick must also be kept clean from any contaminants that may influence its wettability or the water's partial pressure.
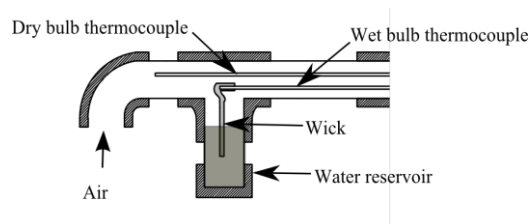
Figure 2-6: Schematic drawing of an aspirated psychrometer

The calibration details of the T/C's can be found in appendix A.

2.4.2   Pressure

There are three Endress and Hauser Deltbar S PMD75 pressure transducers (Figure 2-7) two measuring the pressure drop across the fill and one across the flow nozzles. The two pressure transducers measuring the pressure drop across the

fill are connected to a total of eight H-taps. Clear tubing is used to connect the H-taps to the pressure transducers making it possible to observe any water or condensation that may occur in the line. The range and calibration for each pressure transducer can be found in appendix A.
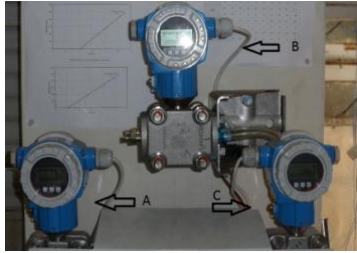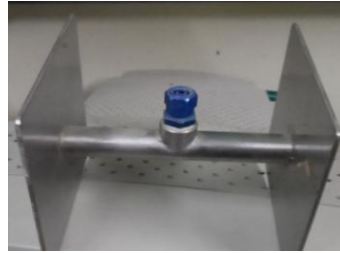
| a. Pressure transducers | b. H-tap |

Figure 2-7: Pressure transducers and H-tap

2.4.3   Air mass flow rate

The pressure drop across five ASHRAE 51-75 elliptical nozzles (Figure 2-8) is measured to calculate the air mass flow rate (calculation details can be found in appendix B). These nozzles can be closed to achieve the required Reynolds number for a given flow rate.
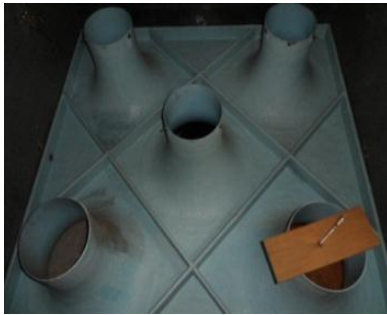
| a)   Picture of nozzles | b)   Schematic drawing of nozzles |
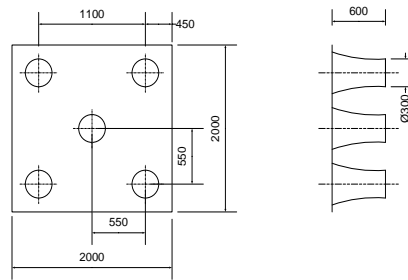
Figure 2-8: Elliptical nozzles

2.4.4   Water flow rate

An Endress and Hauser Promag 10W electromagnetic flow meter (Figure 2-9) is used to measure the flow rate of water to the counter flow test section. The flow meter is installed between the water reservoir and the test section and is installed vertically to avoid air to become trapped and lead to erroneous results.

21

Figure 2-9: Electromagnetic flow meter

2.5   Experimental procedure

This section provides the procedure used for conducting the experiments. Three procedures are covered for the different stages of a specific test. These procedures include the heating of the process water, test facility preparation and the performance test. The procedure for each of these stages is given below.

2.5.1   *Heating of process water*

This section provides the procedure for the heating of the process water to the required temperature for testing.

Before opening any valves the water level in the tank must be sufficient to avoid the cavitation of the pumps. Sufficient water level is also required to ensure that the amount of water loss during the tests, through leaks and evaporation have a negligible effect on the water flow rate to the test facility.

There are two pumps located in the system as seen in Figure 2-10. One of the pumps is used for circulating process water through the boiler and the other to supply process water to the counterflow test facility. Both pumps can however be used to deliver the process water to the test facility if a higher flow rate is required. The pump can therefore run in series or parallel.

The inlet valve to pump A is configured to be fully opened, while the outlet valve is slightly open for start-up of the pumps. Pump A is switched on and the outlet valve is slowly opened until fully opened. Water is now fed to the boiler. There is a pressure gauge on the water supply line to the boiler to ensure there is water flowing to the boiler.

With the water supply to the boiler opened the diesel tank level can be checked to ensure there is enough diesel to heat the water to the required temperature. Once checked and filled to the required level the diesel supply valve can be opened. The boiler may be started when the diesel supply line is open. A diesel pump to the boiler ensures that the diesel enters the boiler at the correct pressure for ignition. Before the diesel is fed to the boiler, the boiler is automatically purged to rid it of any volatiles that might ignite. After the system is purged the diesel is ignited and the water heated. The rate at which the water is heated is approximately 1.5 ^{o}C per

hour. The water should be heated to approximately 3 ^{o}C above the desired temperature to negate heat losses to the environment during start-up of the counter flow test facility

The shutdown of the boiler takes place in reverse order. This means the boiler is switched off first, followed by the diesel supply and finally the water supply. The water supply should be turned off 15 minutes after the boiler has been switched off to cool down the boiler.
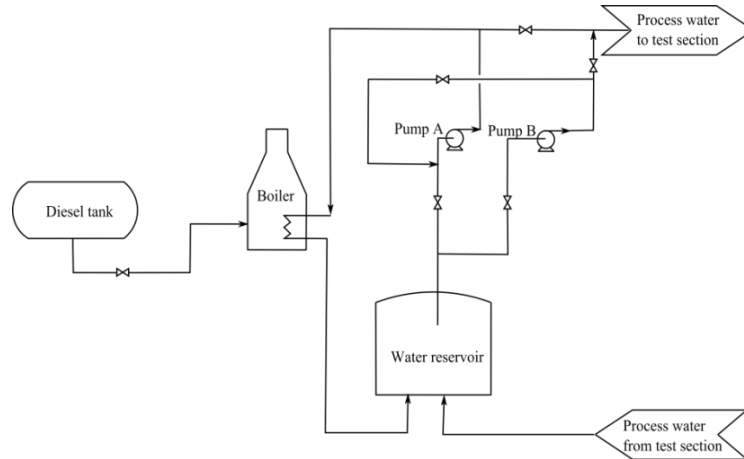
Figure 2-10: Process water heating flow diagram

2.5.2   Test facility preparation

Preparation starts with heating the process water to the desired temperature at a heating rate of approximately 1.5 ^{o}C per hour. It may take several hours before the desired temperature is achieved. The installation of the fill is done while the water is being heated. In addition blocked holes on the spray frame must be unblocked, the pressure lines connecting the H-taps and pressure transducers cleared to ensure a clear path for the air, the water inlet filter must be cleaned and all T/C's calibrated. The calibration details can be found in appendix A.

2.5.3   Performance Testing

Tests are conducted during the early morning hours approximately three hours before sunrise. The atmospheric conditions are most stable at this time of the day. It takes approximately 2h30 to complete one test when conducting the extensive test matrix. The extensive test matrix includes water mass velocities ranging from 1.5 to 4.5 kg/s m^2 in increments of 1.5 kg/s m^2. The air mass velocities are 1, 2, 3 and 3.5 kg/s m^2. It takes approximately 2 minutes for the system to stabilize after a test condition has been changed. Stabilization in this case refers to a constant: pressure drop across the fill, mass flow rate, wet- and dry bulb temperatures and outlet water temperature. In addition the pressure drop as measured by the pressure transducers must not deviate more than 2 N/m^2 from the average pressure drop across the fill.

The dry- and wet bulb temperature are measured with only the psychrometric fans running. The dry- and wet bulb temperatures are checked and recorded. As soon as the temperatures are within 0.2 ^{o}C from the average dry- and wet bulb temperature the performance test can commence.

The atmospheric pressure is measured before each test using a mercury barometer. The test starts by adjusting the water flow to the required flow rate. This is followed by adjusting the air flow rate accordingly. Four air flow rates are evaluated at a specified water flow rate. Once the system has stabilized at the specified flow rates, readings are taken for 1 minute. This is repeated until the test matrix is completed.

The shutdown of the test facility includes switching off the water supply pump and after the level in the collecting sump has dropped to an acceptable level the recirculation pump is switched off. Both the main fan and the psychrometric fans are switched off.

2.5.4   Data logging

An Agilent 34972 A unit connected to a laptop via a USB cable was used for data logging and recording of measured parameters. An Excel macro given in the Agilent 34972 A user guide was adapted to create the user interface, output measured and processed data. The output included the measured data on the test facility and processed data. Computer programs were written in Excel to calculate the calibrated values from the measured data, the air mass flow rate, the water- and air mass velocities, transfer- and loss coefficient using the Merkel method. The output for these parameters is given in Excel tabular and graphical form as can be seen in Figure 2-11, Figure 2-12 and Figure 2-13. It should be mentioned that the same hardware setup was used for calibration of T/C's and pressure transducers.
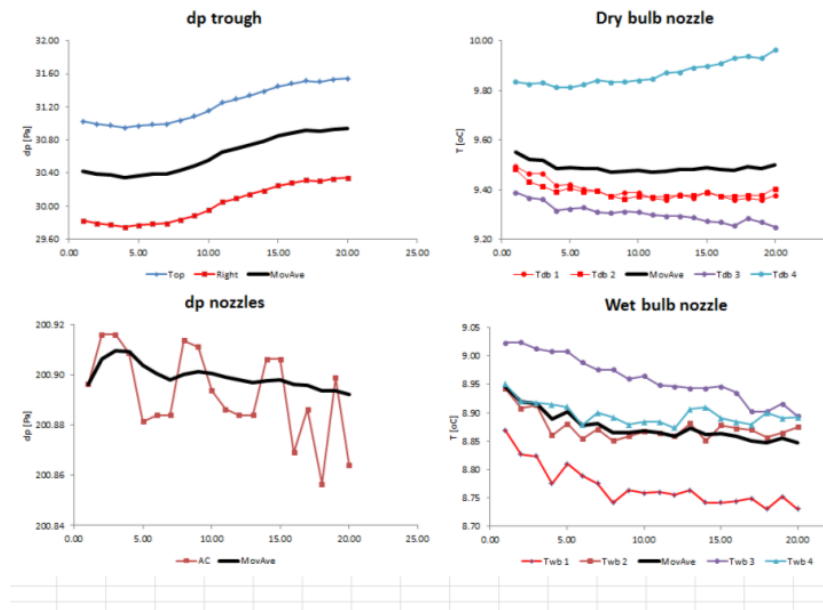
Figure 2-11: Excel graphical output for the experimentally measured pressure drop across the fill and nozzles, wet- and dry bulb temperatures at the air flow measuring nozzles
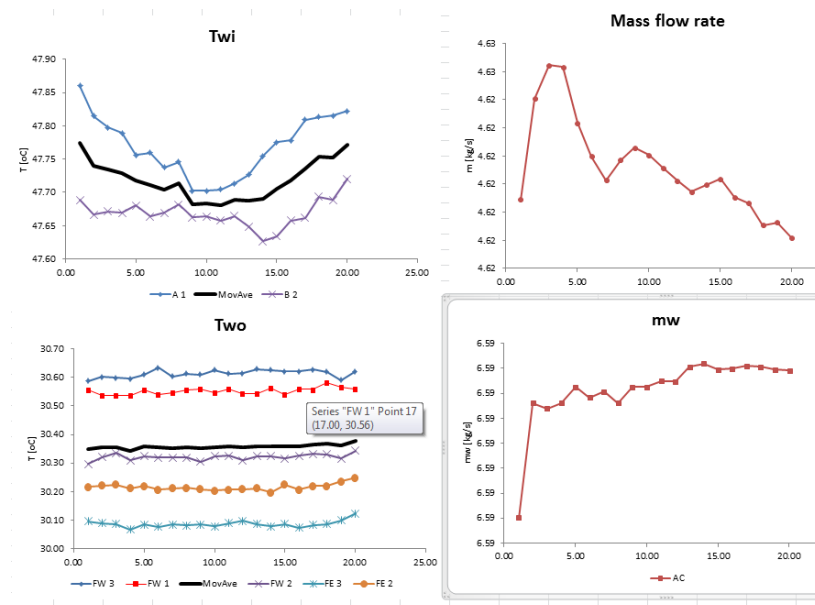
Figure 2-12: Excel graphical output for the experimentally measured inlet- and outlet water temperatures and air- and water mass flow rate

Start Time															
Channel	dpNozzles	dptrough	Twb [oC]	Tdb [oC]	vTdb [oC]	vTwb [oC]	A [oC]	F [oC]	ma [kg/s]	Dens [kg/	Vw [dm3/	mw	Ga	Gw	Me
1.00	200.00	30.42	8.95	9.55	9.81	8.97	47.77	30.35	4.62	989.14	6.66	6.59	2.05	2.93	0.87
2.00	200.91	30.39	8.92	9.52	9.81	8.96	47.74	30.35	4.62	989.16	6.66	6.59	2.06	2.93	0.87
3.00	200.91	30.37	8.92	9.52	9.81	8.96	47.73	30.36	4.63	989.16	6.66	6.59	2.06	2.93	0.87
4.00	200.91	30.35	8.89	9.48	9.81	8.96	47.73	30.34	4.63	989.16	6.66	6.59	2.06	2.93	0.87
5.00	200.90	30.37	8.90	9.49	9.80	8.94	47.72	30.36	4.62	989.17	6.66	6.59	2.06	2.93	0.87
6.00	200.90	30.39	8.88	9.49	9.80	8.94	47.71	30.35	4.62	989.17	6.66	6.59	2.05	2.93	0.87
7.00	200.90	30.39	8.88	9.48	9.78	8.94	47.70	30.35	4.62	989.17	6.66	6.59	2.05	2.93	0.87
8.00	200.90	30.44	8.87	9.47	9.80	8.93	47.71	30.36	4.62	989.17	6.66	6.59	2.05	2.93	0.87
9	200.90	30.49	8.87	9.47	9.79	8.93	47.68	30.35	4.62	989.18	6.66	6.59	2.05	2.93	0.87
10	200.90	30.55	8.87	9.48	9.79	8.92	47.68	30.36	4.62	989.18	6.66	6.59	2.05	2.93	0.87
11	200.90	30.65	8.86	9.47	9.79	8.93	47.68	30.36	4.62	989.18	6.66	6.59	2.05	2.93	0.87
12	200.90	30.69	8.86	9.47	9.78	8.90	47.69	30.35	4.62	989.18	6.66	6.59	2.05	2.93	0.87
13	200.90	30.74	8.87	9.48	9.77	8.90	47.69	30.36	4.62	989.18	6.66	6.59	2.05	2.93	0.87
14	200.90	30.79	8.86	9.48	9.77	8.90	47.69	30.36	4.62	989.18	6.66	6.59	2.05	2.93	0.87
15	200.90	30.85	8.86	9.49	9.77	8.90	47.70	30.36	4.62	989.17	6.66	6.59	2.05	2.93	0.87
16	200.90	30.88	8.86	9.48	9.76	8.89	47.72	30.36	4.62	989.17	6.66	6.59	2.05	2.93	0.87
17	200.90	30.92	8.85	9.48	9.76	8.90	47.74	30.36	4.62	989.16	6.66	6.59	2.05	2.93	0.87
18	200.89	30.90	8.85	9.49	9.77	8.91	47.75	30.37	4.62	989.15	6.66	6.59	2.05	2.93	0.87
19	200.89	30.93	8.86	9.48	9.79	8.92	47.75	30.36	4.62	989.15	6.66	6.59	2.05	2.93	0.87
20	200.89	30.94	8.85	9.50	9.80	8.92	47.77	30.38	4.62	989.14	6.66	6.59	2.05	2.93	0.87

Figure 2-13: Typical measured, calibrated and processed data output including Merkel number and loss coefficient

In the graphical output window (shown in Figure 2-11 and Figure 2-12) the temperature of the inlet- and outlet water and wet- and dry bulb temperatures have to be within 0.2 ^{o}C from the average temperature thereby indicating the system is stable. In addition the pressure drop across the fill should be within 2 N/m^2 from the average pressure drop. The minimum and maximum are shown on these graphs. The thermocouple and pressure transducer measurements should be within these boundaries before data is logged.

CHAPTER 3 EVALUATION OF THE EFFECT OF A GRID ON THE PERFORMANCE OF THE RAIN ZONE

The aim of this section is to evaluate the effect of introducing a grid below a conventional cross fluted film fill, to reduce the size of the drops leaving the fill as well as the effect of different fill/grid configurations on the performance characteristics of the rain zone.

The transfer- and loss coefficient values, determined experimentally using the Merkel method (appendix C) for several fill/grid configurations, are presented in this section. The effect of introducing a grid below conventional film fill on the rain zone performance characteristics is also presented here. Factors regarding the configuration of the grid below the fill including the distance between the grid and fill, the introduction of a second grid, rain zone height and the angle of the grid with the horizontal plane and its effect on the rain zone performance characteristics are also presented. The transfer- and loss coefficient of the rain zone below a conventional film fill is used as the reference case for comparing the rain zone's performance below other fill configurations.

This section comprise of a procedure for isolating the rain zone performance characteristics from the overall performance characteristics, the fill configurations tested as well as the experimental results.

3.1   Procedure for determining the rain zone performance characteristics

The process of determining the rain zone performance characteristics is described in the following section.

In each test conducted, the overall transfer coefficient also known as the Merkel number and loss coefficient are determined, which include the contribution of the spray-, fill-, rain- and water catchment zones. It becomes apparent that in order to isolate the performance characteristics of the rain zone from the overall performance characteristics, the performance characteristics of the spray-, fill-and water catchment zones (configuration 1 in Table 3-1) have to be determined as shown in Figure 3-1 and equation 3-1. This is subtracted from the overall performance characteristics of the other tests to isolate the specific test's rain zone's performance characteristics.

To be able to subtract the performance of the spray- fill- and water catchment zones (configuration 1) from the other tests, it is necessary that these tests be conducted in the exact same process conditions the aforementioned test was conducted in. It is difficult to recreate the exact same conditions of configuration1, however it is possible to create a power curve which is used to correlate the transfer- and loss coefficient of the 300 mm spray zone, 608 mm fill, 280 mm rain zone and troughs (configuration 1 in Table 3-1).

Several tests are performed to determine the effect of various fill configurations. These configurations summarised in Figure 3-2 and Table 3-1 include fill with: no rain zone, rain zone, grid and rain zone, two grids and rain zone, extended rain zone, grid and extended rain zone, two grids and extended rain zone and grid at an angle and extended rain zone.
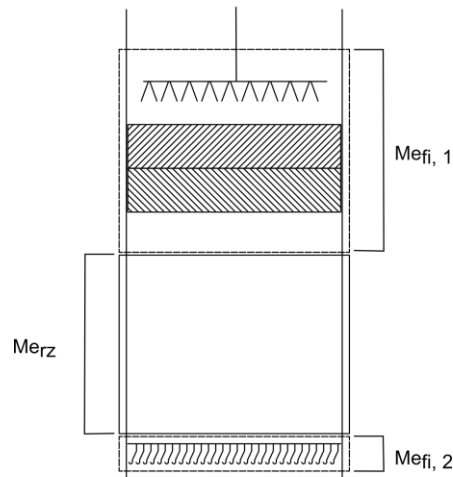
Figure 3-1: Illustration for the isolation of the rain zone Merkel number

$$Me_{overall} = Me_{fi} + Me_{rz} \qquad\qquad 3\text{-}1$$
where $Me_{fi} = Me_{fi,1} + Me_{fi,2}$
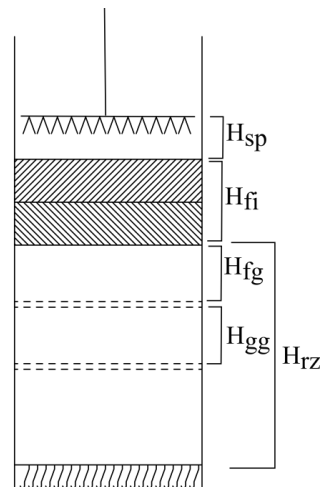
Figure 3-2: Notated vertical tower test section

Table 3-1 provides the configuration name and specification for the various tests conducted.

28

Table 3-1: Specification for the various test configurations

Configuration	Test description	Dimensions					Number of grids used
		H_{sp} [mm]	H_{fi} [mm]	H_{fg} [mm]	H_{gg} [mm]	H_{rz} [mm]	
1	Fill	300	608	N/A	N/A	280	0
2	Fill rain zone	300	608	N/A	N/A	2105	0
3	Grid 200	300	608	200	N/A	1905	1
4	Grid 300	300	608	300	N/A	1905	1
5	Grid 400	300	608	400	N/A	2105	1
6	Additional grid 400	300	608	400	400	1905	2
7	Additional grid 800	300	608	400	800	1905	2
8	Fill extended rain zone	300	608	N/A	N/A	4168	0
9	Grid 400 extended rain zone	300	608	400	N/A	4168	1
10	Additional grid 800 extended rain zone	300	608	400	800	4168	2
11	Diagonal grid extended rain zone	300	608	400-450	N/A	4168	1

These tests are necessary to determine the effect of various fill/grid configurations on the rain zone performance characteristics.

3.2 Performance characteristics of a cross fluted film fill

The experimental results for the fill (configuration 1 in Table 3-1) are presented in this section and the data can be found in appendix E. The configuration of the setup and notations are shown in Figure 3-2.

The purpose of this test is to determine the performance characteristics of this film fill. A power curve is fitted through the data for both the transfer- and loss coefficient. This power curve is later used to deduct the contribution of the film fill from the overall performance characteristics leaving only the rain zone performance characteristics as described in section 3.1. These rain zones are used for comparative studies.

The experimental results and power curve fit for the transfer- and loss coefficient of configuration 1 are shown in Figure 3-3 and Figure 3-4 respectively. The correlation plotted in Figure 3-3 is given by equation 3-2 and the correlation for the data shown in Figure 3-4 by equation 3-3.

It is imperative that the power curve fits the data well across a wide temperature, water and air flow rate range. The deviation, $\delta Me = \dfrac{Me_{,\,exp}-Me_{,\,calc}}{Me_{,exp}}$ and $\delta K_{fdm,x} = \dfrac{K_{fdm,Exp}-K_{fdm,\,Calc}}{K_{fdm,\,Exp}}$, are presented in Figure 3-5 and Figure 3-6 respectively.

a) $T_{wi} = 46\ ^oC - 39\ ^oC$

b) $T_{wi} = 38\ ^oC - 36\ ^oC$

c) $T_{wi} = 36\ ^oC - 28\ ^oC$
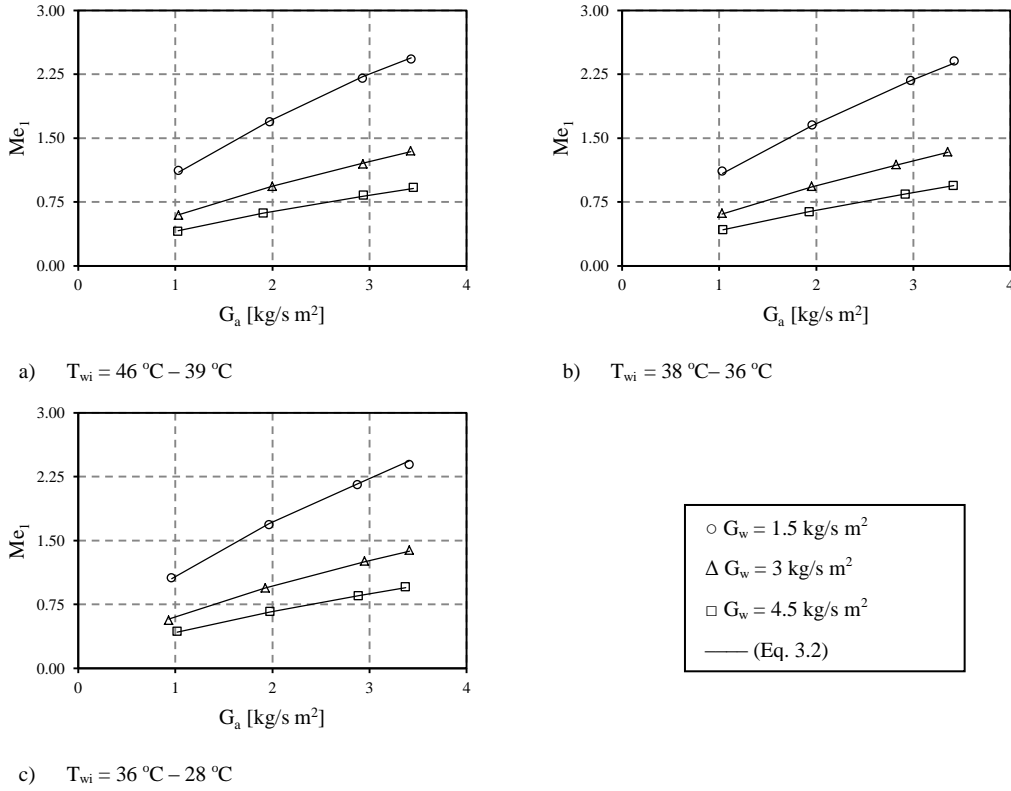
Figure 3-3: Transfer coefficient and correlation for configuration 1

$Me_{fi} = 2.4899 T_{wi}^{-0.1325} G_a^{0.6630} G_w^{-0.8582}$	$R^2 = 0.974$	3-2
$K_{fdm} = 16.579 G_a^{-0.259} G_w^{0.160}$	$R^2 = 0.949$	3-3

The maximum deviation for the transfer coefficient correlation given by equation 3-2 was found to be 3 %. The maximum deviation for the loss coefficient correlation given by equation 3-3 was found to be 8 %.

30

a) $T_{wi} = 46\ ^{\circ}C - 39\ ^{\circ}C$

b) $T_{wi} = 38\ ^{\circ}C - 36\ ^{\circ}C$

c) $T_{wi} = 36\ ^{\circ}C - 28\ ^{\circ}C$
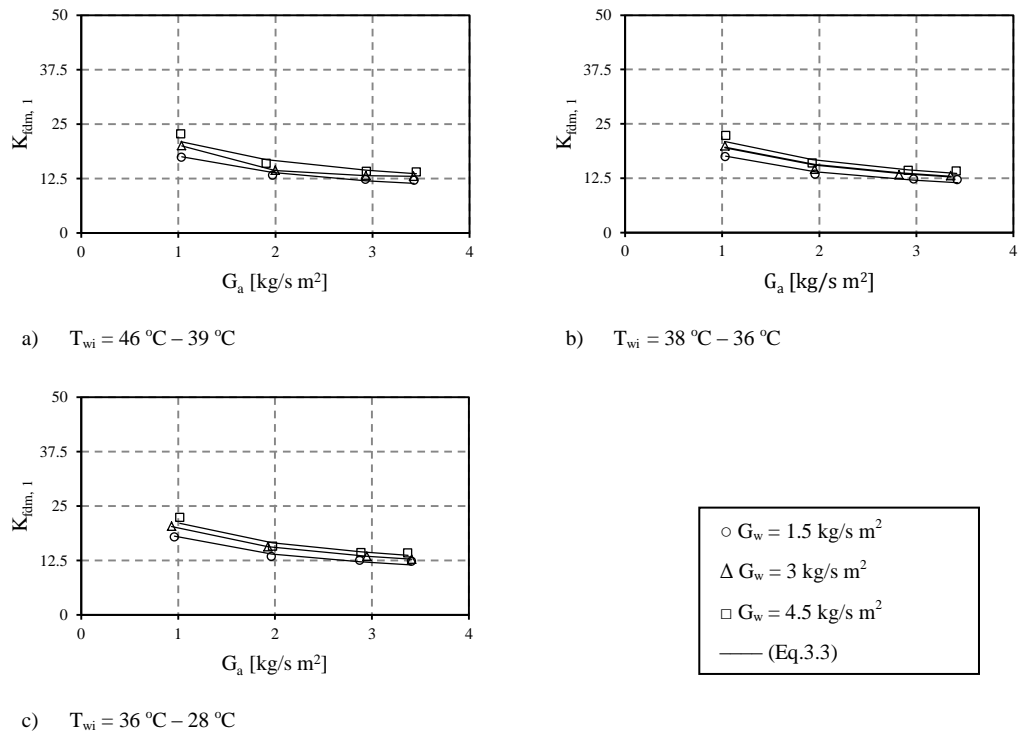
Figure 3-4: Loss coefficient and correlation for configuration 1

a) $T_{wi} = 46\ ^{\circ}C - 39\ ^{\circ}C$

b) $T_{wi} = 38\ ^{\circ}C - 36\ ^{\circ}C$

c) $T_{wi} = 36\ ^{\circ}C - 28\ ^{\circ}C$
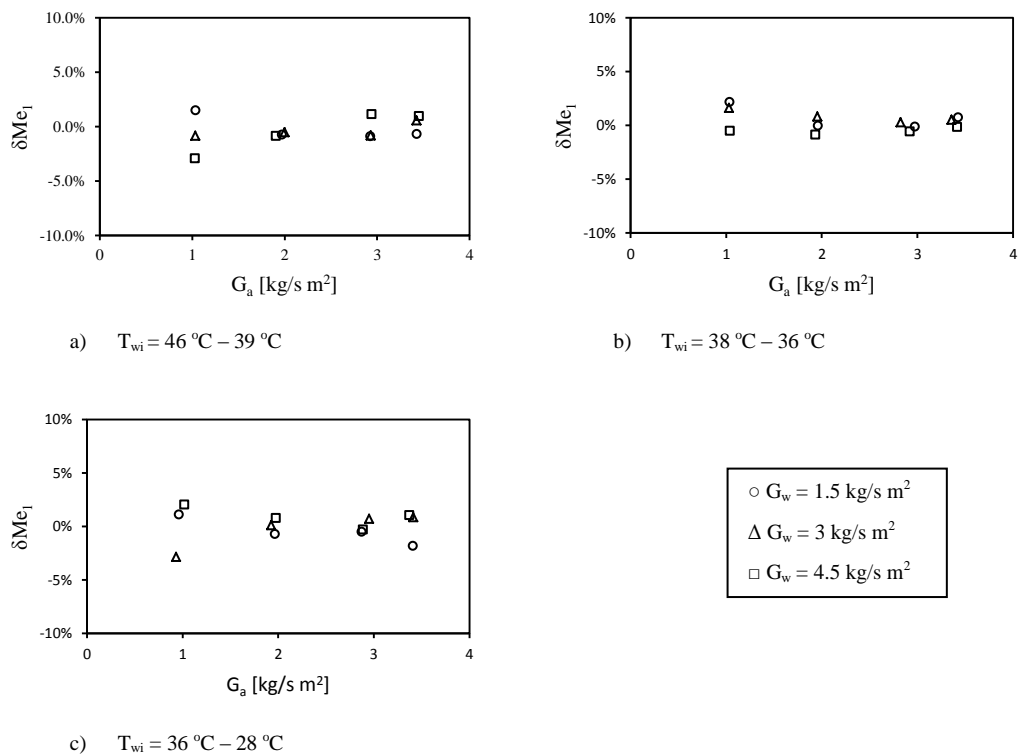
Figure 3-5: Transfer coefficient deviation plot for configuration 1

a) $T_{wi} = 46\ ^{\circ}C - 39\ ^{\circ}C$

b) $T_{wi} = 38\ ^{\circ}C - 36\ ^{\circ}C$

c)   Me $T_{wi} = 36\ ^{\circ}C - 28\ ^{\circ}C$
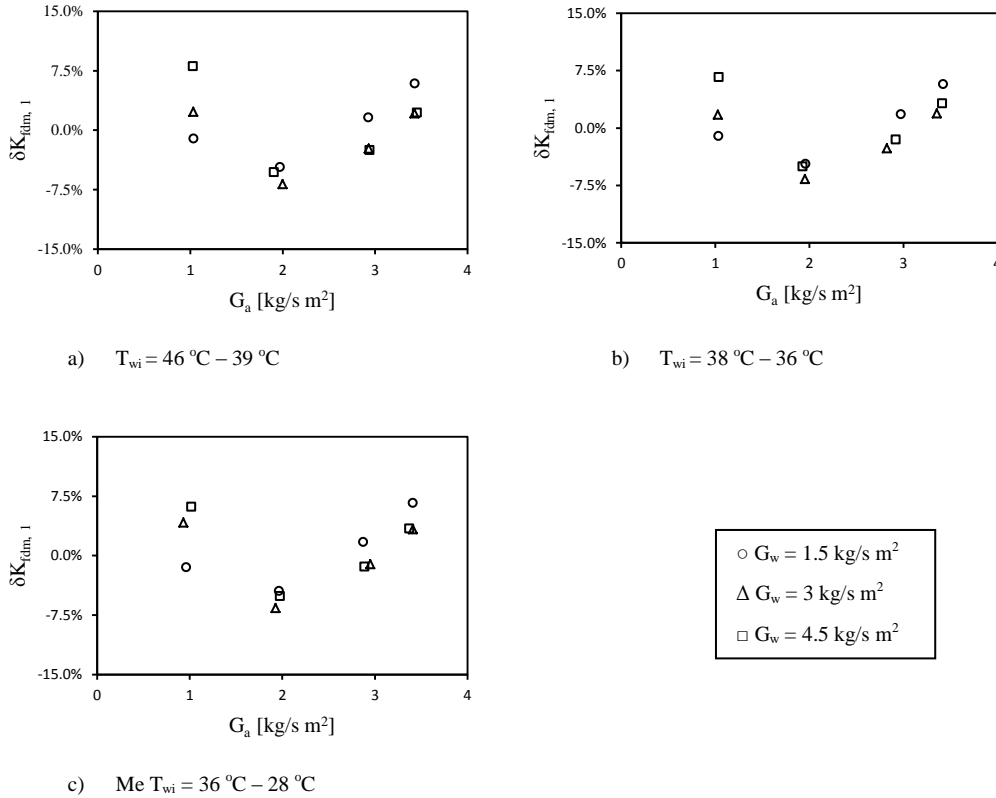
Figure 3-6: Loss coefficient deviation plot for configuration 1

3.3   Performance characteristics of a rain zone below configuration 2

The performance of a rain zone below a chemically bonded cross fluted film fill is characterised by determining the total performance characteristics and subtracting the characteristics of the film fill (configuration 1) presented in section 3.2. The process of isolating the rain zone performance characteristics are described in section 3.1.

Test configuration 2 as shown in Table 3-1 will serve as basis for comparing the performance of other configurations since this is how a typical natural draught wet cooling tower is configured i.e. conventional fill with a rain zone below it. A correlation is used for this purpose. Only the isolated performance of the rain zone will be compared to the other configurations.

The experimental results for the transfer-and loss coefficient of configuration 2 are shown in Figure 3-7 and Figure 3-8 respectively. The correlations fitted through the data shown in Figure 3-7 and Figure 3-8 are given by equation 3-4 and 3-5 respectively.
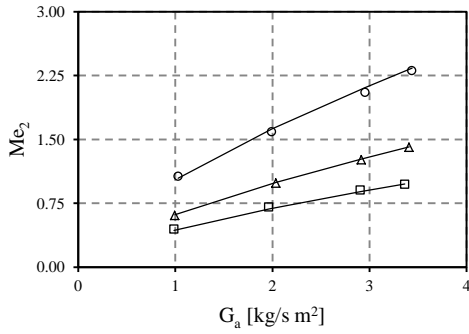
a) T_{wi} = 49 $^{\circ}$C – 40 $^{\circ}$C
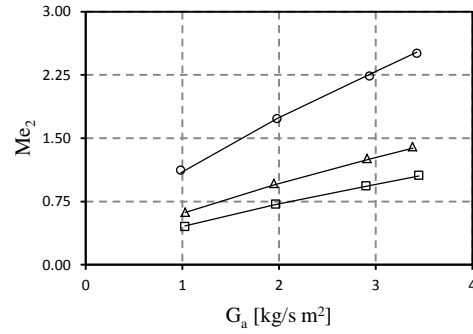
b) T_{wi} = 39 $^{\circ}$C – 34 $^{\circ}$C
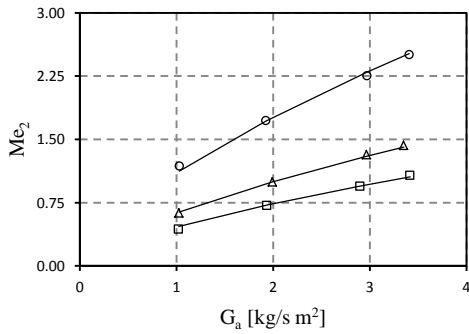
c) T_{wi} = 33 $^{\circ}$C – 29 $^{\circ}$C
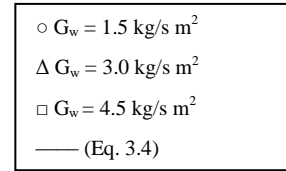
Figure 3-7: Transfer coefficient and correlation for configuration 2

$$Me_{fi,rz}=2.3080T_{wi}^{-0.1012}G_a^{0.6684}G_w^{-0.8480} \qquad\qquad R^2=0.9981 \qquad\qquad 3\text{-}4$$

The deviation plot of the experimental data in Figure 3-7 and correlation presented by equation 3-4 for the transfer coefficient of configuration 2 are shown in Figure 3-9. Similarly the deviation plot for the loss coefficient of configuration 2 i.e. experimental data from Figure 3-8 and correlation as given in equation 3-5 are shown in Figure 3-10.

$$K_{fdm,\,rz}=20.6922G_a^{-0.5657}G_w^{0.2908} \qquad\qquad R^2=0.9581 \qquad\qquad 3\text{-}5$$

33

a) T_{WI} = 49 °C– 40 °C

b) T_{wi} = 39 °C – 34 °C

c) T_{wi} = 33 °C – 29 °C
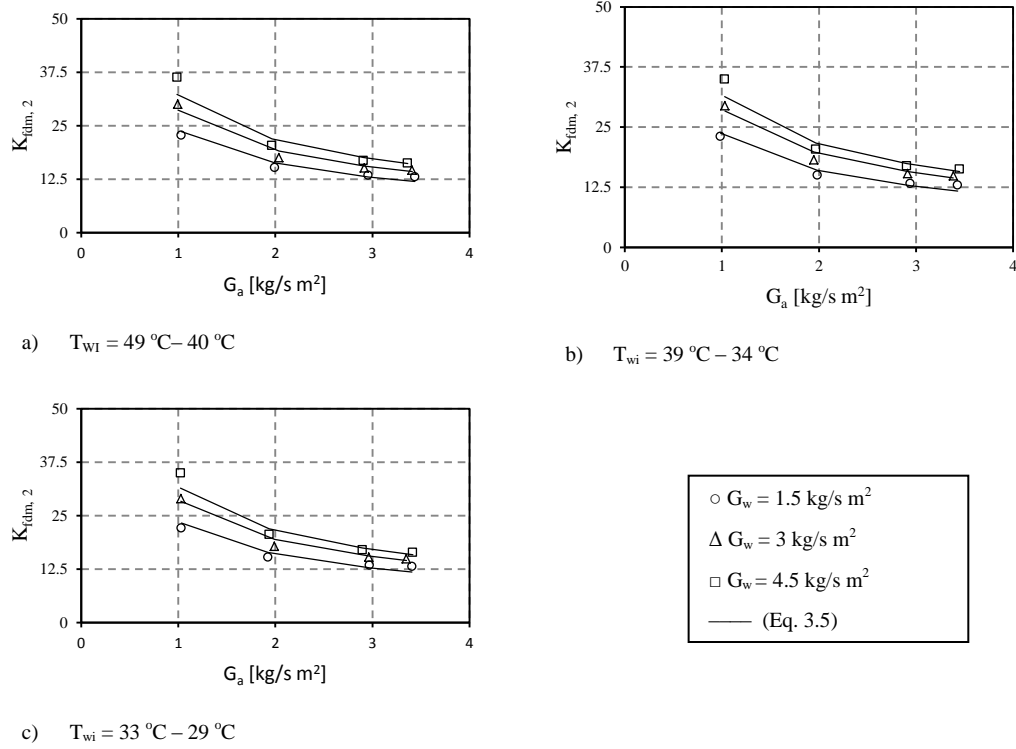
Figure 3-8: Loss coefficient and correlation for configuration 2

a) T_{WI} = 49 °C – 40 °C

b) T_{wi} = 39 °C – 34 °C

c) T_{wi} = 33 °C – 29 °C
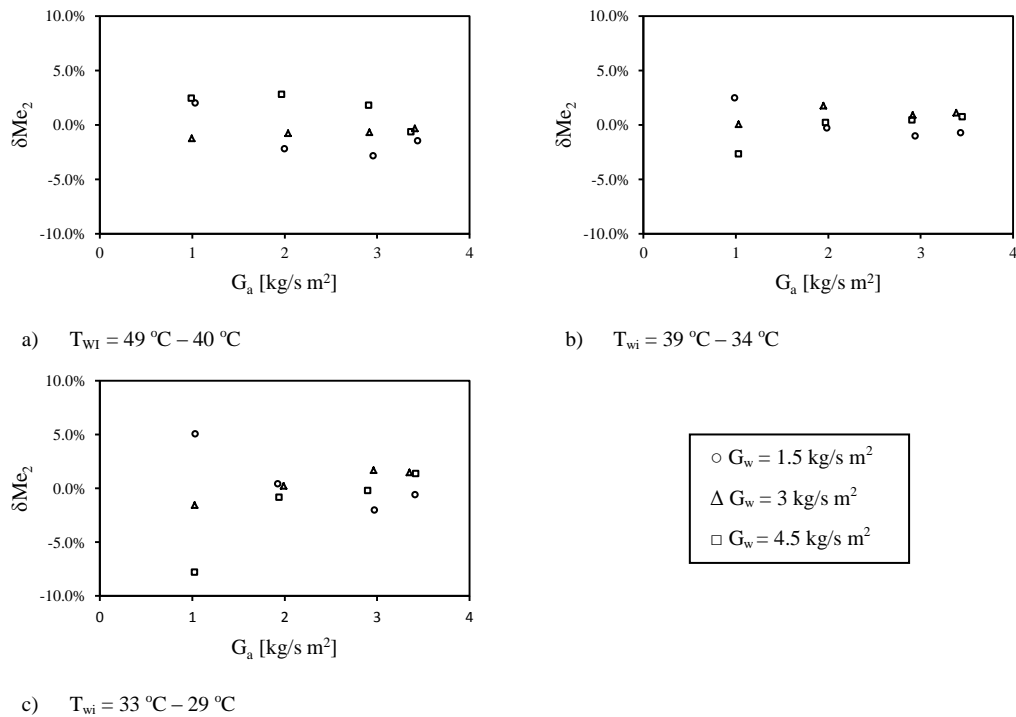
Figure 3-9: Transfer coefficient deviation plot for configuration 2

a) $T_{WI} = 49 \,^{\circ}\text{C} - 40 \,^{\circ}\text{C}$

b) $T_{wi} = 39 \,^{\circ}\text{C} - 34 \,^{\circ}\text{C}$

○ $G_w = 1.5$ kg/s m^2

Δ $G_w = 3$ kg/s m^2

□ $G_w = 4.5$ kg/s m^2

c) $T_{wi} = 33 \,^{\circ}\text{C} - 29 \,^{\circ}\text{C}$
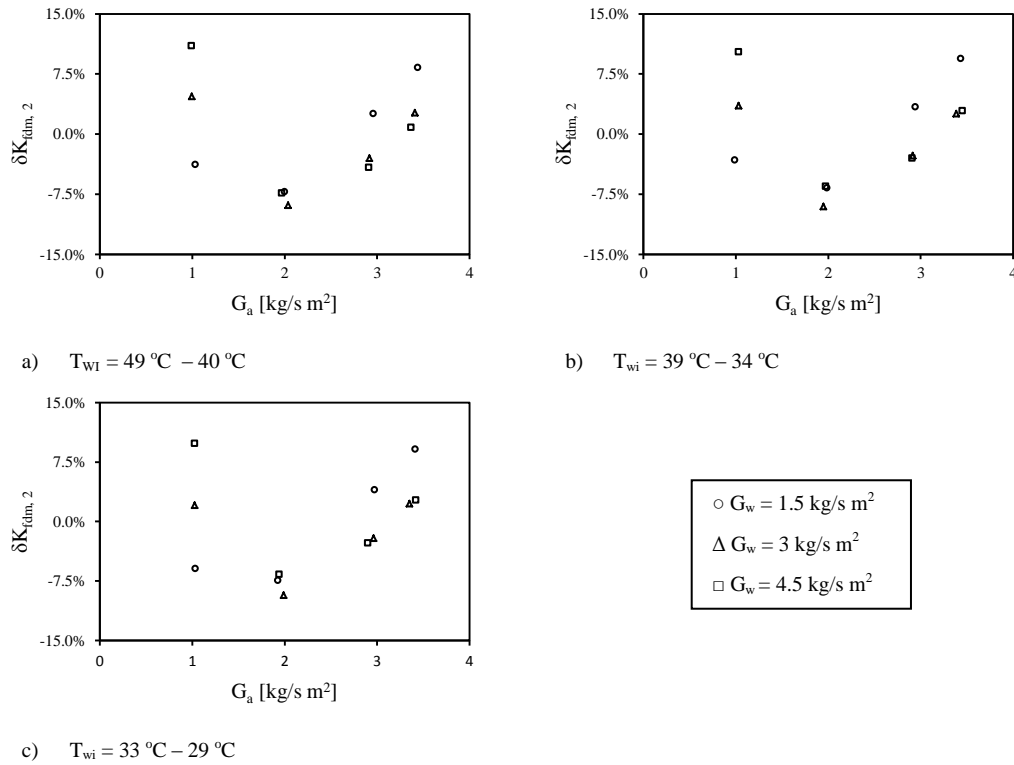
Figure 3-10: Loss coefficient deviation plot for configuration 2

The maximum deviation for the transfer- and loss coefficient was found to be 8 % and 11 % respectively.

3.4 The effect of installing a grid below a conventional film fill on the rain zone performance characteristics

The effect of placing a grid (refer to 2.3.4 for a description of the grid) underneath the fill (configuration 5 in Table 3-1) is investigated in this section.

The experimental results for the transfer- and loss coefficient of configuration 5 are shown in Figure 3-11 and Figure 3-12 respectively.

The rain zone transfer coefficient below the grid per meter rain zone below the grid as well as the correlation as given by equation 3-6 which was fitted through the data in Figure 3-13 is shown in Figure 3-13.

a) T_{wi} = 50 °C – 43 °C

b) T_{wi} = 43 °C – 37 °C

c) T_{wi} = 36 °C – 32 °C
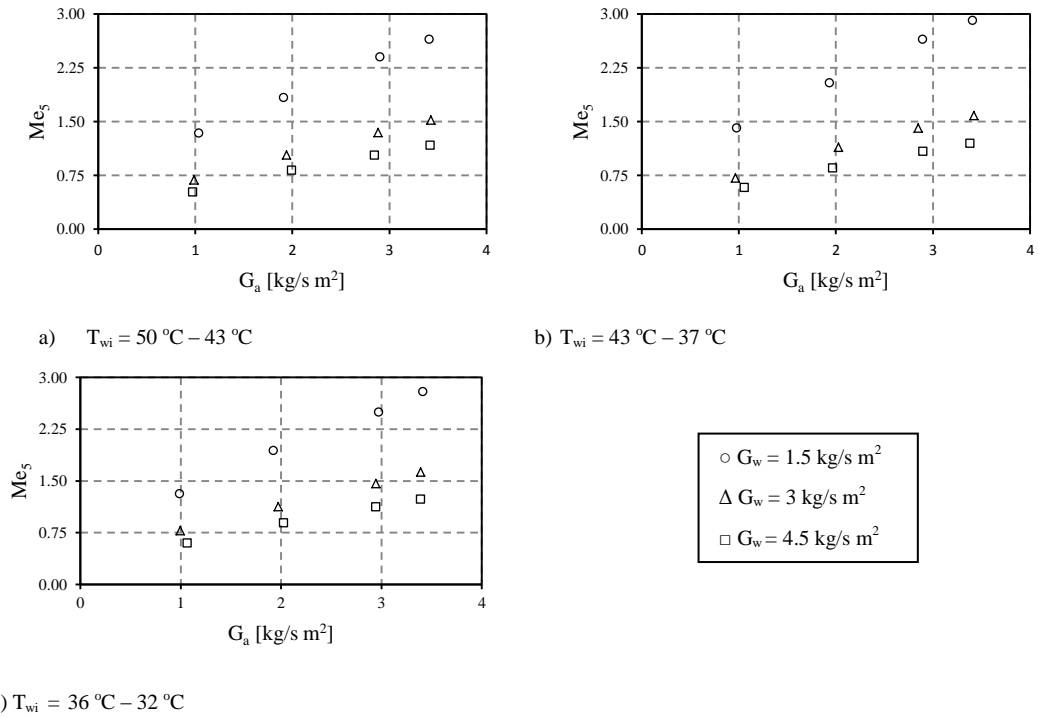
Figure 3-11: Transfer coefficient for configuration 5

a) T_{wi} = 50 °C – 43 °C

b) T_{wi} = 43 °C – 37 °C

c) T_{wi} = 36 °C – 32 °C
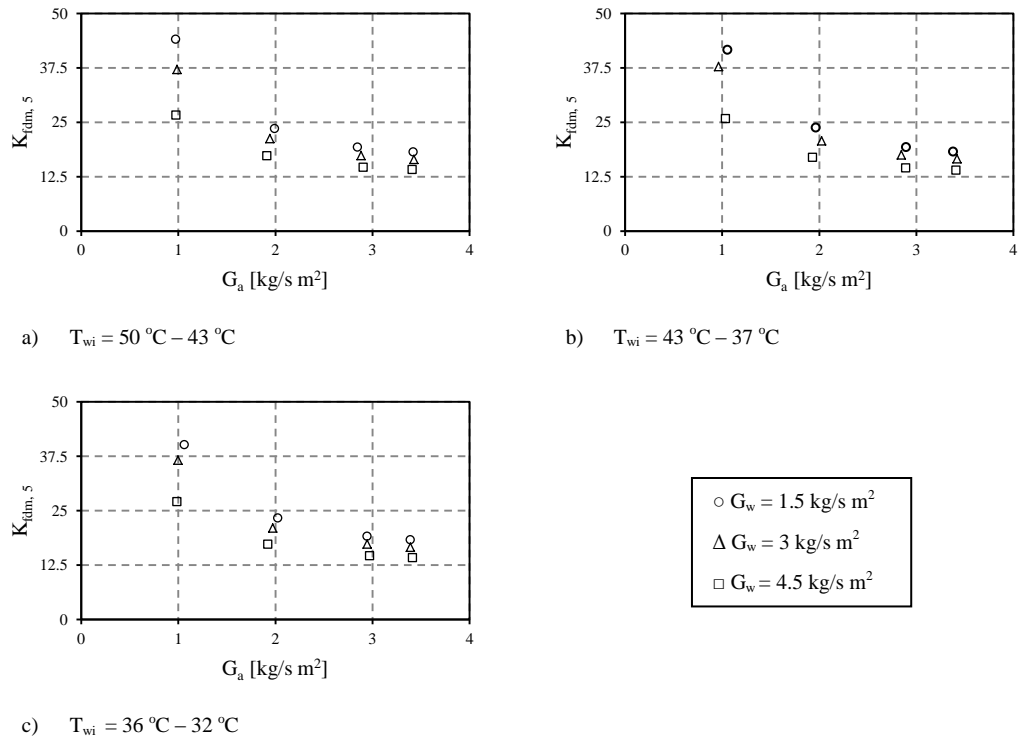
Figure 3-12: Loss coefficient for configuration 5

36

a) T_{wi} = 50 $^{\circ}$C – 43 $^{\circ}$C

b) T_{wi} = 43 $^{\circ}$C – 37 $^{\circ}$C

○ G_w = 1.5 kg/s m^2

Δ G_w = 3 kg/s m^2

□ G_w = 4.5 kg/s m^2

—— (Eq. 3.8)

c) T_{wi} = 36 $^{\circ}$C – 32 $^{\circ}$C
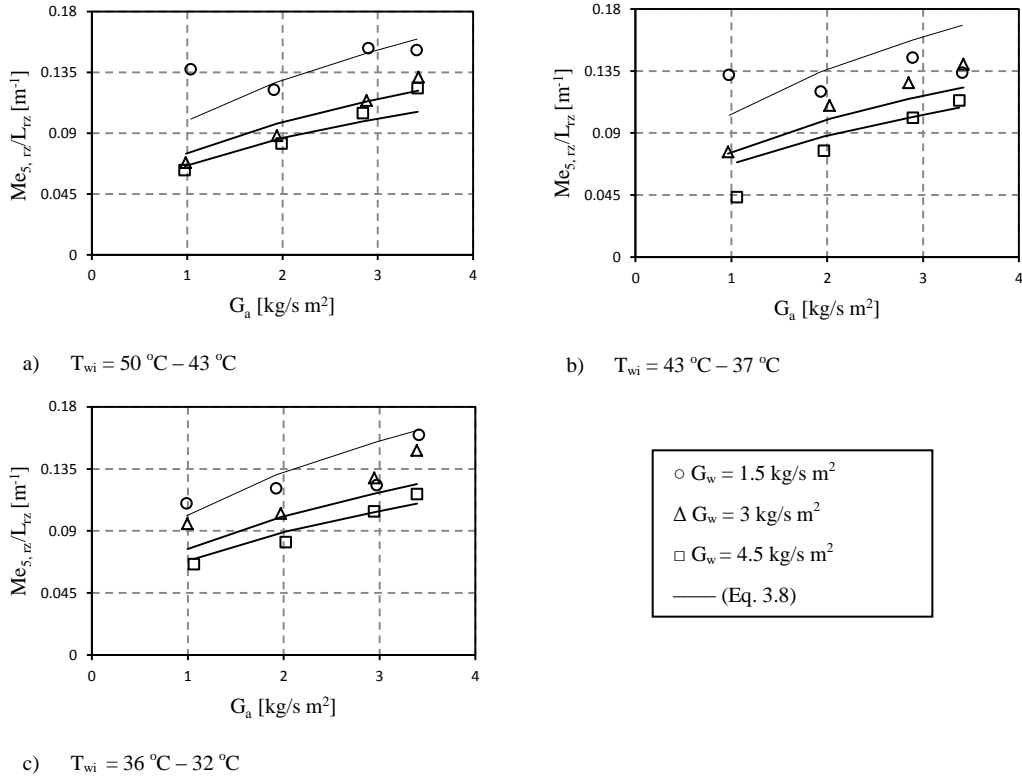
Figure 3-13: Rain zone transfer coefficient per meter rain zone for configuration 5

$$\frac{Me_{5,rz}}{L_{rz}} = 0.1436 G_a^{0.3884} G_w^{-0.3773} T_{wi}^{-0.0537}$$ 3-6

The transfer coefficient ratio for configuration 5 and configuration 2 rain zone is shown in Figure 3-14. This ratio was calculated using the equation shown in equation 3-7..

$$\frac{Me_{5,rzr}}{Me_{2,rz}} = \frac{Me_{5rz}\text{-}Me_1}{Me_2\text{-}Me_1}$$ 3-7

From Figure 3-14 it can be seen that the introduction of the grid increased the rain zone performance by a factor of approximately 4.5. A similar process was followed to determine the effect of the grid on the rain zone loss coefficient as can be seen in Figure 3-15. The loss coefficient increased by a factor of approximately 1.5 with the introduction of the grid below the fill.

There is thus a significant increase in the transfer coefficient with a minor increase in the loss coefficient.

a) T_{wi} = 50 °C – 43 °C

b) T_{wi} = 43 °C – 37 °C

c) T_{wi} = 36 °C – 32 °C
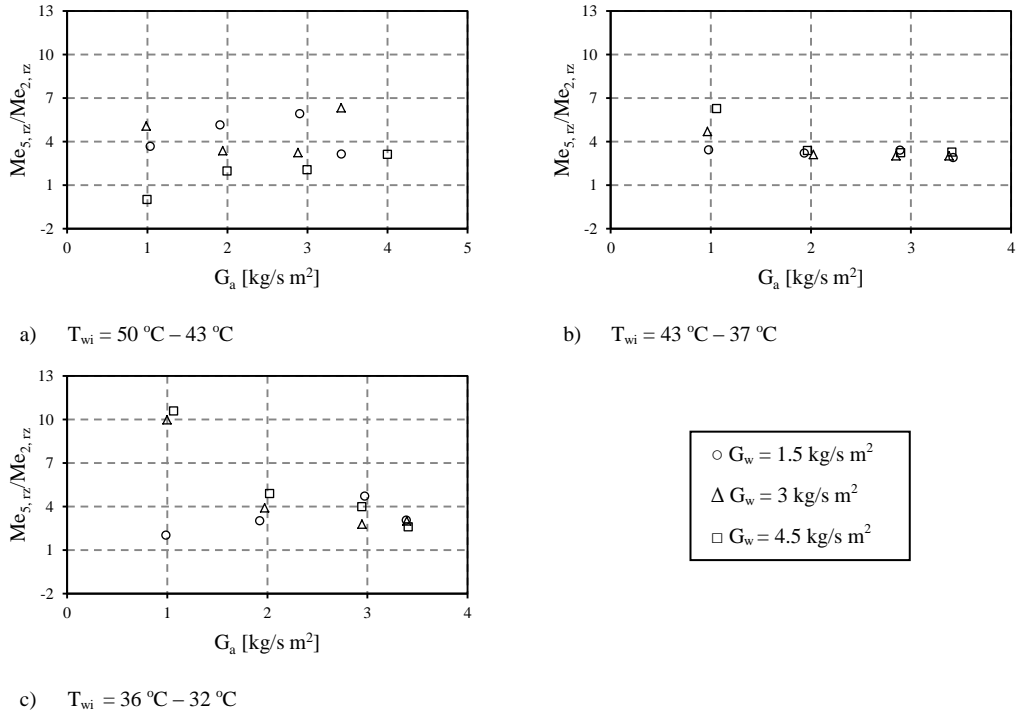
Figure 3-14: Ratio of rain zone transfer coefficient for configuration 5 and 2

a) T_{wi} = 50 °C – 43 °C

b) T_{wi} = 43 °C – 37 °C

c) T_{wi} = 36 °C – 32 °C
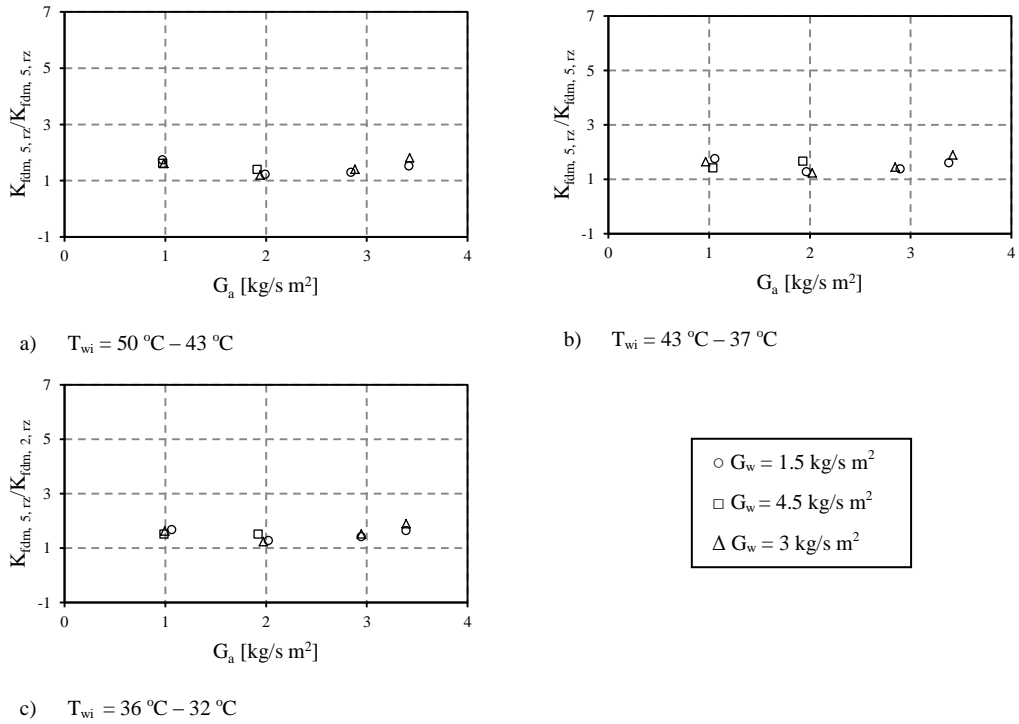
Figure 3-15: Ratio of rain zone loss coefficient for configuration 5 and 2

3.5   The effect of drop falling height before impact on the rain zone performance characteristics

The effect of the placement of the grid at 200 (configuration 3)- and 300 mm (configuration 4) below the fill is considered in this section. A reduced test matrix is used for experiments. This reduced test matrix is sufficient to determine the effect of air (G_a)- and water (G_w) mass velocities as well as water inlet temperature (T_{wi}) on the performance characteristics, however is insufficient test data to generated a correlation as was the case in the previous sections. Correlations are however not necessary for this and the sections that follows.

The heights were chosen based on the results as found by Steenmans (2010) with the results given in the figure below.
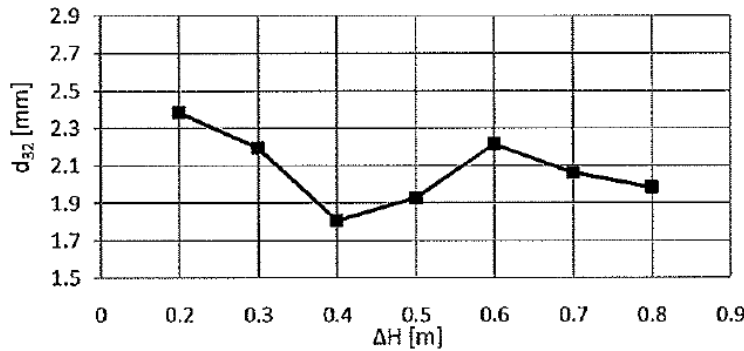
Figure 3-16: Drop falling height before impact (Steenmans, 2010)

Steenmans found the smallest drop diameter for a drop falling height before impact of 400 mm. The other heights tested include 200-and 300 mm. The rest of the heights in Figure 3-16 were not considered due to the restriction in height of the counter flow test facility.

The transfer coefficient ratio, which is calculated using the following expression, $\frac{Me_{3(4),rz}}{Me_{2,rz}} = \frac{Me_{3(4)}-Me_1}{Me_2-Me_1}$, for configuration 3 and 4 as well as the test conditions are given in Figure 3-17, Figure 3-18, Table 3-2 and Table 3-3 respectively. The loss coefficient ratio calculated using the following expression, $\frac{K_{fdm,3(4),rz}}{K_{fdm,2,rz}} = \frac{K_{fdm,3(4)}-K_{fdm,1}}{K_{fdm,2}-K_{fdm,1}}$ for configuration 3 and 4 is given in Figure 3-19. The transfer-and loss coefficient for the rain zone below the grid was calculated using correlation shown in equation 3-6. It should be mentioned that the results of test 7 and 8 were omitted from the calculation for determining the average loss coefficient ratio. The difference between the fill (configuration 1) and fill/rain zone (configuration 2) total loss coefficient is negligible leading to a small rain zone loss coefficient. This small rain zone loss coefficient increases the rain zone loss coefficient ratio to above 8 for tests 7 and 8 in most cases much higher than the rest of the tests. This suggests the loss coefficient for the unaltered rain zone, which is present in

the denominator, might be negligible at this water- and air mass velocities as per test 7 and 8. It is expected that the loss coefficient increases with increasing water mass velocity and decreasing air mass velocity. The rain zone loss coefficient is expected to be more dependent on the air mass velocity since the drop size, which causes the losses in the rain zone, does not differ much with water mass velocity. If this is the case then the smallest loss coefficient should be for test 8 conditions. This was found to be the case with a configuration 2 rain zone loss coefficient of $K_{fdm,\,2,}rz$ = -0.061 compared to the loss coefficient for test 7 $K_{fdm,\,2,\,rz}$ = 0.297. For all the test conditions these two were found to be the smallest.

The average transfer coefficient ratio for the tests was found to be 3.63 and 4.45 for configuration 3 and 4 respectively, while for the loss coefficient it was found to be 1.460 and 1.494 respectively.

Figure 3-17: Ratio of rain zone transfer coefficient for configuration 3 and 2

Table 3-2: Test parameters for configuration 3

Test	T_{wi} [^{o}C]	G_a [kg/s m^2]	G_w [kg/s m^2]
1	39.94	2.01	1.49
2	39.81	2.00	3.09
3	38.37	1.99	4.44
4	38.37	1.99	3.07
5	37.96	1.03	3.07
6	37.56	2.05	3.06
7	37.23	2.96	3.06
8	36.86	3.41	3.07
9	36.26	2.02	3.04

Figure 3-18: Ratio of rain zone transfer coefficient for configuration 4 and 2

Table 3-3: Test parameters for configuration 4

Test	T_{wi} [^{o}C]	G_a [kg/s m^2]	G_w [kg/s m^2]
1	31.22	1.96	1.57
2	30.84	1.95	3.11
3	30.44	1.93	4.40
4	29.27	2.00	2.86
5	29.19	1.06	2.87
6	29.01	2.03	2.87
7	28.89	3.02	2.87
8	28.73	3.40	2.86
9	28.39	2.00	2.84

a) Configuration 3   b) Configuration 4
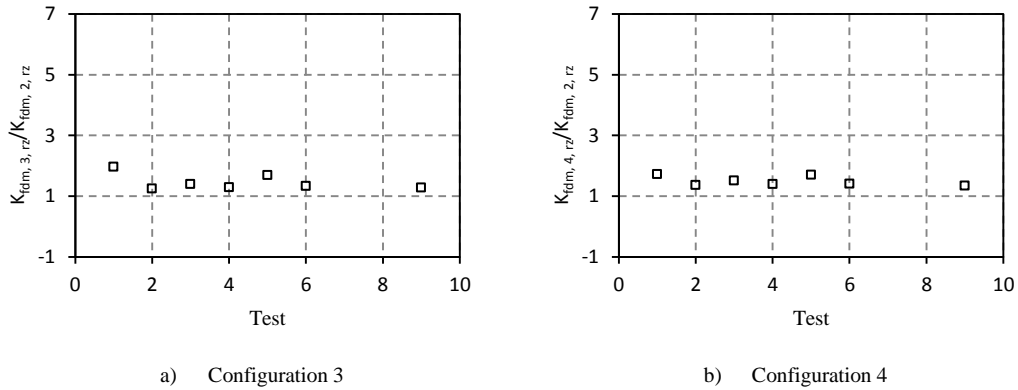
Figure 3-19: Ratio of rain zone transfer coeffcient for configuration 3 / 4 and 2

It can be seen from Fig. 3-17 that a slightly negative transfer coefficient was obtained for test one of configuration 3. The same was found for test one configuration 8. In both cases the transfer coefficient for configuration 1 was found to be greater than the transfer coefficient for configuration 3 and 8 at test 1 test conditions (G_a, G_w) (refer to table 3-2 and 3-6 respectively). This is however highly unlikely that this could actually be the case since both of these configurations have a rain zone beneath, while configuration 1 does not. Configuration 3 also has a rain zone modification making it even more unlikely that configuration 1 has a greater transfer coefficient. In addition if this was truly the case ($Me_1 > Me_{3/8}$) it would be more pronounced for configuration 2's rain zone transfer coefficient. This is however not the case as is evident from figure 3-13.

It is interesting to note that in both cases the negative transfer coefficient ratio is for test 1 which has approximately the same process parameters. It could be that the transfer coefficient for configuration 1 is over predicted for these process parameters. If this was the case all other tests would also indicate negative or close to zero transfer coefficient ratios. This is however not the case. It should be mentioned that both configuration 3 and 8 were the first configurations tested and system might not have reached "steady state" for the first test. As a result test one for these configurations were omitted when calculating the average transfer coefficient ratio.

The configuration achieving the highest transfer coefficient ratio was configuration 4 when comparing configuration 3 and 4. This is however slightly less than configuration 5 (transfer coefficient ratio of 4.5) similar to the results given in Steenmans (2010) where the smallest average drop size was achieved for the configuration 5 followed by configuration 4.

3.6 The effect of an additional grid on the rain zone performance characteristics

In the preceding section the effect of introducing a grid to the performance characteristics were considered. The effect of an additional grid is considered in this section. Steenmans (2010) found that there is a relationship between drop size

prior to impact and drop size after impact. This means that the additional grid would further reduce the size of the drop in the rain zone which can result in the increase of the transfer coefficient in this zone. Two drop falling heights before impact between the grids are considered in this section. The first is the drop falling height of 400 mm found to produce the highest rain zone transfer coefficient in section 3.4 and 3.5. The second drop falling height before impact considered is 800 mm. This was found according to Terblanche et al. (2009) to be the height producing the smallest Sauter mean diameter drop size after impact, although the design of the grid used in his experiments differs from the grid used here. The higher distance results in a higher drop impact speed causing the drop to be more likely to split and not drip compared to shorter distances. The effect of the double grid configuration (configuration 6 and 7) on the transfer-and loss coefficient is given in Figure 3-20, Figure 3-21 and Figure 3-22 and the test parameters in Table 3-4 and Table 3-5. As mentioned in section 3.5 test 7 and 8 is omitted due to the very small loss coefficient achieved for the rain zone below configuration 2 at their test conditions. The following expressions are used to calculate the rain zone ratio, $\frac{Me_{6(7),rz}}{Me_{2,rz}} = \frac{Me_{6(7)} - Me_1}{Me_2 - Me_1}$ and for the loss coefficient ratio, $\frac{K_{fdm,6(7),rz}}{K_{fdm,6(7),rz}} = \frac{K_{fdm,6(7)} - K_{fdm,1}}{K_{fdm,2} - K_{fdm1}}$
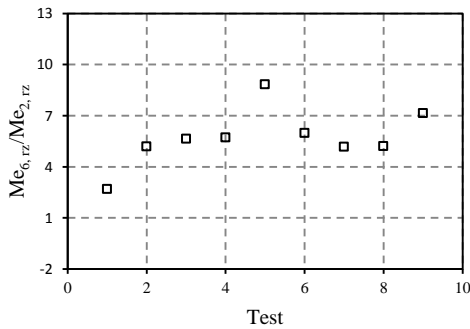
Figure 3-20: Ratio of rain zone transfer coefficient for configuration 6 and 2

Table 3-4: Test parameters for configuration 6

Test	T_{wi} [°C]	G_a [kg/s m²]	G_w [kg/s m²]
1	42.53	2.02	1.64
2	42.02	2.00	3.14
3	40.73	1.98	4.33
4	40.09	1.98	3.09
5	39.64	1.00	3.09
6	39.38	1.95	3.07
7	39.09	2.90	3.08
8	38.81	3.39	3.09
9	37.95	1.99	3.06
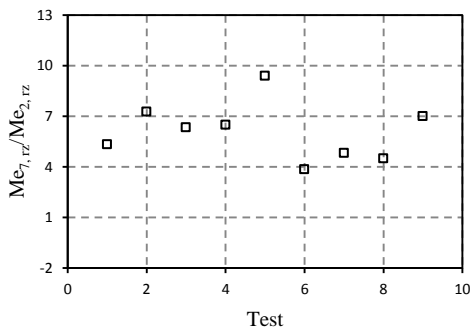
Figure 3-21 Ratio of rain zone transfer coefficient for configuration 7 and 2

Table 3-5 Test parameters for configuration 7

Test	T_{wi} [°C]	G_a [kg/s m²]	G_w [kg/s m²]
1	36.8	1.96	1.53
2	36.41	1.94	3.07
3	36.41	1.93	4.32
4	36.29	1.94	3.08
5	35.98	1.01	3.07
6	35.82	2.00	3.08
7	35.80	2.96	3.06
8	35.47	3.42	3.06
9	34.76	1.96	3.07

The average transfer coefficient ratio is found to be 5.729 and 6.097 for configuration 6 and 7 respectively. The corresponding average ratio for the loss

coefficient was found to be 2.227 and 2.291 for configuration 6 and 7 respectively.

a) Configuration 6
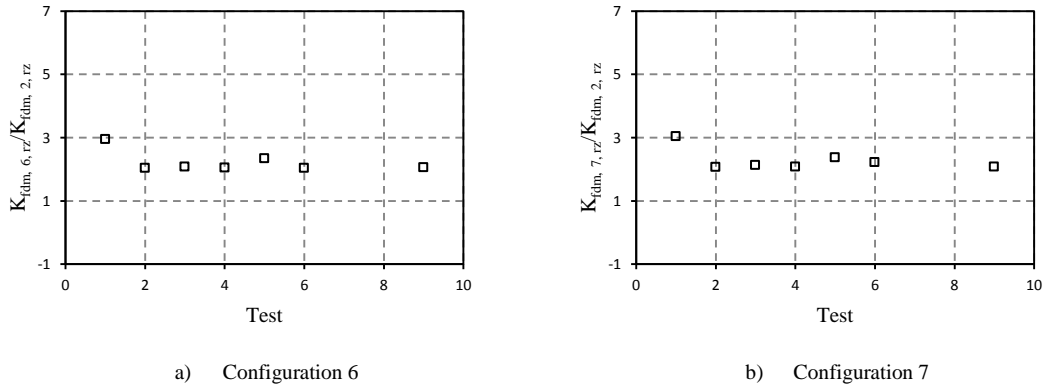
b) Configuration 7

Figure 3-22: Ratio of rain zone loss coefficient for configuration 6/7 and 2

It should be mentioned that although there is an increase in the transfer coefficient of the rain zone there is also an increase in the loss coefficient. The increase in the loss coefficient could possibly negate the increase in the transfer coefficient in a natural draught wet cooling tower. This means this type of configuration will not necessarily give the best performance in a cooling tower.

3.7 Effect of extending the rain zone below configuration 2, 5 and 7 on the rain zone performance characteristics

The effect of rain zone height on the performance characteristics are investigated in this section. The rain zone below configurations 2, 5 and 7 is extended and results presented here. The results are for configurations 8, 9 and 10. As mentioned in section 3.5 and 3.6 test 7 and 8 are omitted when calculating the loss coefficient ratio. The transfer coefficient ratio were calculated using the following expression, $\frac{Me_{8(9,10),rz}}{Me_{2,rz}} = \frac{Me_{8(9,10)} - Me_1}{Me_2 - Me_1}$ and for the loss coefficient ratio, $\frac{K_{fdm,8(9,10),rz}}{K_{fdm,2,rz}} = \frac{K_{fdm,8(9,10)} - K_{fdm,1}}{K_{fdm,2} - K_{fdm,1}}$.

The rain zone height was increased from 2105 mm to 4168 mm representing an almost 2 fold increase. The performance characteristics for configuration 8 (extended rain zone below configuration 2) is shown in the Fig. 3-23 and 3-24.

43
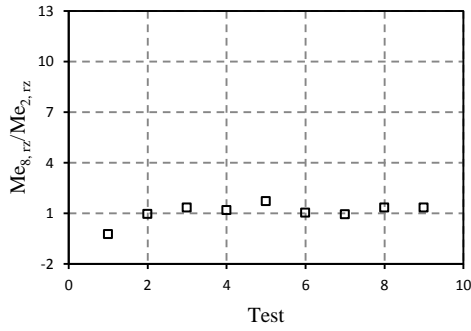
Table 3-6: Test parameters for configuration 8

| Test	T_{wi} [^{o}C]	G_a [kg/s m^2]	G_w [kg/s m^2]
1	47.19	2.02	1.62
2	46.98	2.00	3.04
3	46.78	2.02	4.55
4	46.40	2.04	2.99
5	46.27	1.06	3.00
6	46.02	2.02	2.98
7	45.97	3.02	2.98
8	45.85	3.44	2.98
9	44.40	2.02	3.00

Figure 3-23: Ratio of rain zone transfer coefficient for configuration 8 and 2
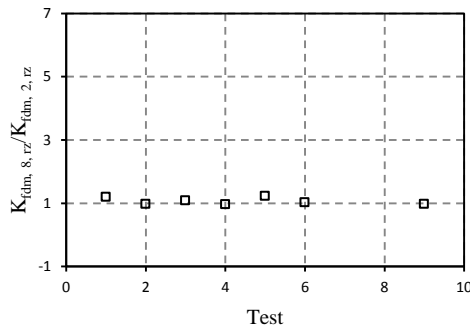
Figure 3-24: Ratio of rain zone loss coefficient for configuration 8 and 2

There is a slight increase of transfer coefficient with increasing rain zone height amounting to a factor of approximately 1.06. The loss coefficient also increases with a factor of approximately 1.224. However the increases are not significant and indicate that the rain zone height has a negligible effect on the transfer or loss coefficient for configuration 2.

The performance characteristics for configuration 9 (extended rain zone below a single grid configuration) are shown in Figure 3-25 and Figure 3-26 and the test parameters in Table 3-7. The transfer coefficient increases by a factor of 2.89 and the loss coefficient by 1.56 compared to the rain zone below configuration 2. The loss coefficient does not show a significant change, however the transfer coefficient for extended section indicates a decrease in performance where the average ratio decrease from 4.5 for configuration 5 to 2.893 for the extended rain zone configuration, configuration 9. The transfer coefficient decreases down the length of the rain zone as a result of a decrease in residence time per meter rain zone as the drop accelerates through the rain zone (assuming the drop diameter stays approximately constant and the drop size distribution remains unchanged throughout the rain zone). This decrease in residence time is more evident for smaller drops. This is why the decrease in transfer coefficient is less obvious for configuration 8 due to the larger drop sizes (less air-water interfacial area). A similar decreasing trend for the transfer coefficient ratio is found for configuration

44

10 (shown in Figure 3-27 for the transfer coefficient and Figure 3-28 for the loss coefficient), where the average transfer coefficient ratio decreased from 6.097 to 3.388 for configuration 7 and 10 respectively. It can also be seen that the average loss coefficient ratio is approximately constant when comparing configuration 5 (1.500) and configuration 9 (1.560). The same is valid for configuration 7 (2.317) and 10 (2.017). This corresponds to the modelling done by Reuter (2010), which indicates that loss coefficient stays approximately constant for drop path lengths of greater than two meters.
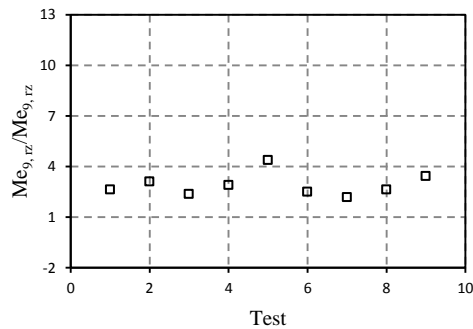
Table 3-7: Test parameters for configuration 9

Test	T_{wi} [^{o}C]	G_a [kg/s m^2]	G_w [kg/s m^2]
1	40.65	2.05	1.40
2	38.43	2.02	2.92
3	38.27	2.00	4.59
4	36.29	1.97	2.97
5	35.94	1.05	2.96
6	35.90	2.01	2.96
7	35.70	2.96	2.96
8	35.38	3.42	2.95
9	34.66	1.95	2.95

Figure 3-25: Ratio of rain zone transfer coefficient for Configuration 9 and 2
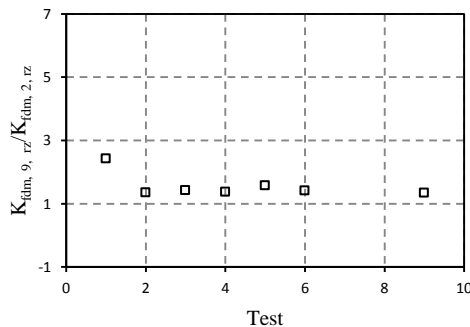
Figure 3-26: Ratio of rain zone loss coefficient for configuration 9 and 2

45
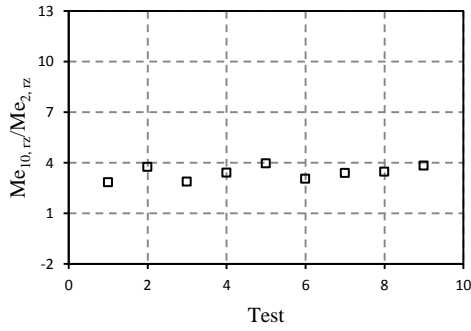
Table 3-8: Test parameters for configuration 10

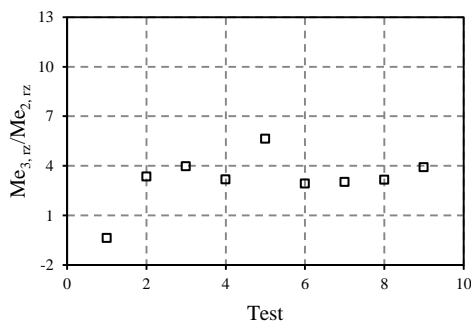| Test	T_{wi} [^{o}C]	G_a [kg/s m^2]	G_w [kg/s m^2]
1	43.22	1.97	1.49
2	43.11	1.95	2.95
3	43.10	1.98	4.41
4	43.07	2.00	3.01
5	43.03	1.05	2.99
6	42.97	2.01	2.99
7	42.96	2.98	2.98
8	42.88	3.39	2.97
9	42.18	1.99	2.97

Figure 3-27: Ratio of rain zone transfer coefficient for configuration 10 and 2
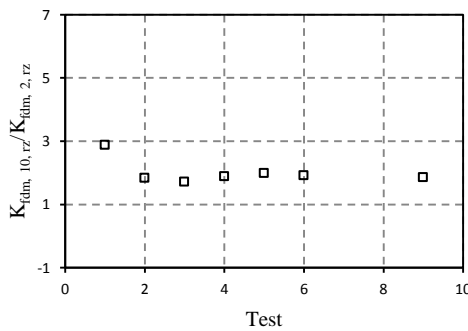
Figure 3-28: Ratio of rain zone loss coefficient for configuration 10 and 2

3.8 Effect of placing the grid diagonally on the rain zone performance characteristics

The effect of placing a grid diagonally below a fill on the rain zone's performance characteristics is shown in Figure 3-29 and Figure 3-30 for the transfer-and loss coefficient ratios respectively. The ratios were calculated according to $\frac{Me_{11,rz}}{Me_{2,rz}} = \frac{Me_{11}-Me_1}{Me_2-Me_1}$ and $\frac{K_{fdm,11,rz}}{K_{fdm,2,rz}} = \frac{K_{fdm,11}-K_{fdm,1}}{K_{fdm,2}-K_{fdm,1}}$ for the transfer- and loss coefficient respectively.

Placing the grid at an angle of 2° has a negligible effect on the performance of the rain zone as is evident when comparing configuration 9 and configuration 11 where the average transfer coefficient ratio is found to be 2.893 and 2.514 respectively. The average loss coefficient ratio was found to be 1.427
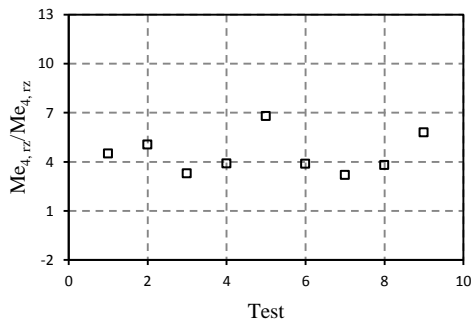
46

Figure 3-29: Ratio of rain zone transfer coefficient for configuration 11 and 2
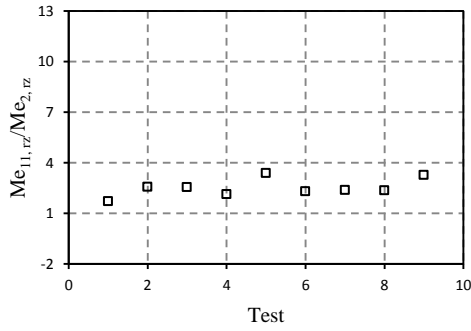
Table 3-9: Test parameters for configuration 11

Test	T_{wi} [°C]	G_a [kg/s m^2]	G_w [kg/s m^2]
1	42.32	2.02	1.38
2	41.88	2.00	3.11
3	40.59	1.98	4.40
4	39.26	2.01	3.07
5	37.99	0.96	3.05
6	36.99	1.96	3.06
7	35.91	2.91	3.05
8	35.44	3.45	3.05
9	34.73	1.93	3.08
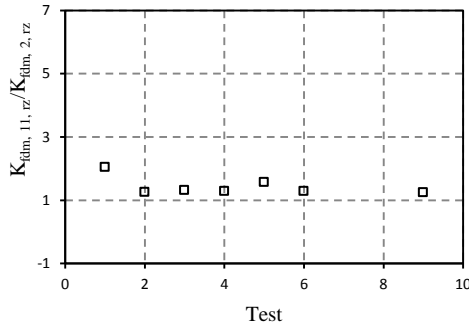
Figure 3-30: Ratio of rain zone loss coefficient for configuration 11 and 2

3.9   Conclusion

The introduction of the grid below the conventional film fill had a significant effect on this zone's transfer coefficient, increasing it by a factor of approximately 4.5, while it had less of an effect on this zone's loss coefficient increasing it by a factor of approximately 1.5 compared to an unaltered rain zone (rain zone below configuration 2).

The drop falling height for a single grid configuration producing the highest rain zone transfer coefficient was found to be 400 mm or configuration 5.

The double grid configuration achieved the highest transfer coefficient compared to the other configurations however also had the highest loss coefficient as a result of the additional grid and smaller average rain zone drop sizes. This could possibly negate the higher transfer coefficient in a natural draught wet cooling tower.

Increasing the rain zone height had a negligible effect on the loss coefficient, however showed a decrease in rain zone transfer coefficient. This decrease was attributed to the decrease in drop residence time in the rain zone with increasing rain zone drop path length.

Lastly the placement of the grid at an angle of 2° was also investigated and was found to have a negligible effect on the performance of the rain zone. Table 3-10 gives a summary of the results presented in chapter 3.

Table 3-10: Average rain zone transfer-and loss coefficient ratios for the different configurations

Configuration x	Description	$\dfrac{Me_x - Me_1}{Me_2 - Me_1}$	$\dfrac{K_{fdm,x} - K_{fdm,1}}{K_{fdm,2} - K_{fdm,1}}$
3	Grid 200	3.18	1.73
4	Grid 300	4.45	2.12
5	Grid 400	4.5	1.5
6	Additional grid 400	5.73	2.63
7	Additional grid 800	6.097	2.85
8	Fill extended rain zone	1.06	1.06
9	Grid 400 extended rain zone	2.89	1.86
10	Additional grid 800 extended rain zone	3.39	2.51
11	Diagonal grid extended rain zone	2.51	1.62

48

CHAPTER 4 RAIN ZONE DROP SIZE

The effect of the introducing a grid below a conventional film fill on the rain zone Sauter mean diameter (drop size) is presented in this section. The drop size is inferred from the rain zone's transfer coefficient according to the algorithm shown in Fig. 4.1. The purely counterflow one dimensional rain zone model referred to in the algorithm can be found Kröger (2004). A sample calculation can be found in Appendix D. The purpose of calculating the Sauter mean drop diameter is to be able to utilize the experimental data from chapter 3 in the De Villiers and Kröger (1997) one dimensional NDWCT rain zone model as presented in chapter 5 to determine the effect of the rain zone modification on cooling tower performance.
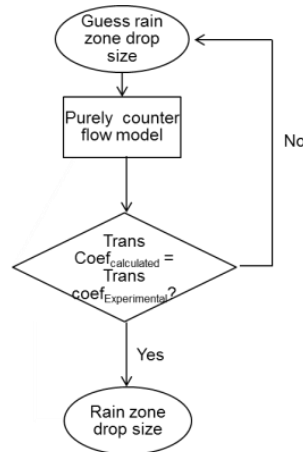
Figure 4-1: Rain zone Sauter mean drop diameter algorithm

The Sauter mean drop diameter for several configurations is given in this section. This includes Sauter mean drop diameter below configuration 2, 3, 4, 5, 7 and 11.

4.1   Rain zone drop size below a conventional fill (configuration 2)

The rain zone Sauter mean drop diameter below configuration 2 is shown in this section. More configuration details can be found in chapter 3. The rain zone Sauter mean diameter drop diameter in the 2105 mm rain zone for three different water inlet temperature ranges and water mass velocities using the Kröger purely counter flow transfer coefficient correlation is shown in Figure 4-2. Terblanche et al. (2009) found that the mass velocities for both water and air had a minimal effect on the Sauter mean drop diameter below the fill and is mostly a function of the fill used. This is confirmed in the figures below. Thus an overall Sauter mean drop diameter will be calculated for a specific configuration. There are a number of outliers as a result of a small rain zone transfer coefficient.

The rain zone Sauter mean drop diameter below configuration 2 for the three tests shown in Figure 4-2 was found to be 6.527 mm (including the outliers). Terblanche et al. (2009) found that it is uncommon to find a drop diameter larger

than 10 mm in the rain zone. These sized drops are often unstable and usually breaks into smaller drops. By omitting the drops larger than 10 mm the rain zone Sauter mean drop diameter was found to be 6.08 mm. Terblanche et al. (2009) found a typical rain zone Sauter mean drop size distribution between 5 and 6 mm below cross fluted film fills.

a) $T_{wi} = 46\ ^oC - 39\ ^oC$

b) $T_{wi} = 38\ ^oC - 36^oC$

c) $T_{wi} = 36\ ^oC - 28\ ^oC$
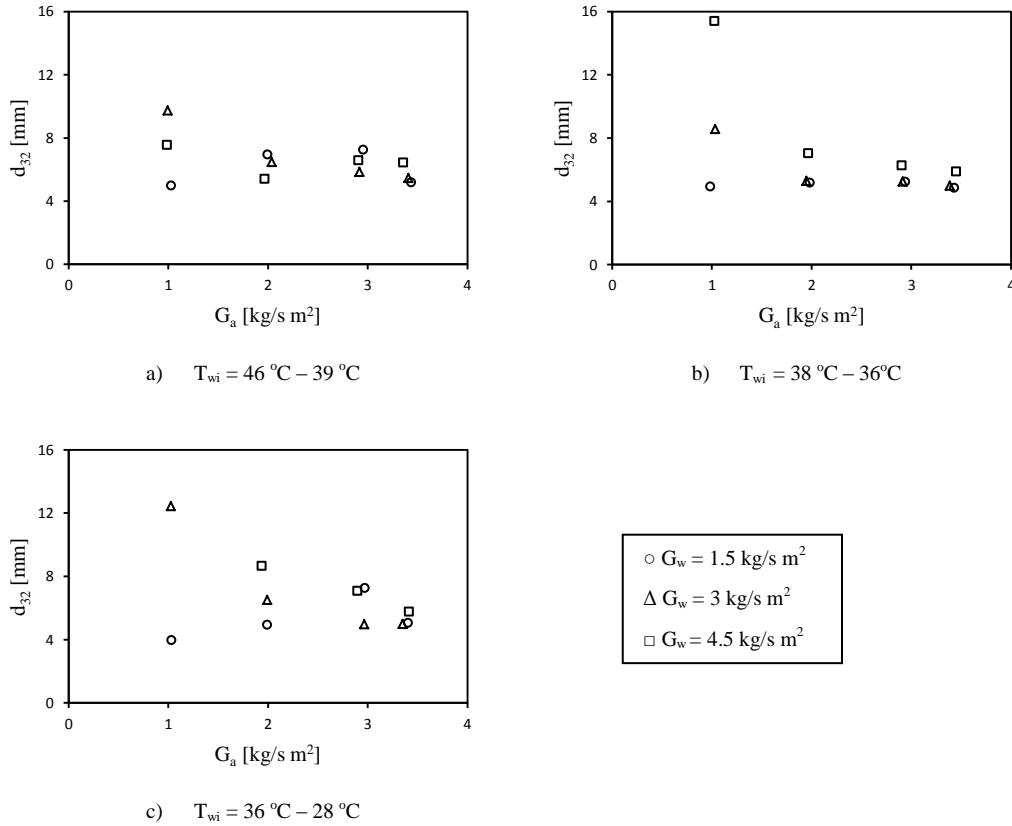
Figure 4-2: Rain zone Sauter mean drop diameter below configuration 2

4.2   Rain zone drop size below a single grid

This section presents the rain zone Sauter mean drop diameter below configuration 5. These configurations consist of a spray zone, fill zone, rain zone between fill and grid and rain zone below the grid. Subtracting the fill performance, as determined in chapter 3, would result in a rain zone above and below the grid, however only the drop size below the grid is of importance. The rain zone height above the grid is approximately 120 mm and the drop size is known from section 4.1, since this is the drop size exiting the fill. In order to isolate the rain zone below the grid it is necessary to determine the correlation for the transfer coefficient per meter rain zone above the grid. The correlation was determined in section 3.3. By substituting the conditions (i.e. T_{wi}, G_a, G_w) for the test considered here the transfer coefficient for the small rain zone above the grid per meter rain zone is determined. In order to deduct this value from the combined transfer coefficient it must be multiplied with the height of the small rain zone

(i.e. 0.12 mm). The resulting transfer coefficient below the grid is then found. The newly determined transfer coefficient and height below the grid is the parameters to use in calculating the rain zone Sauter mean drop diameter.

The resulting Sauter mean drop diameter is shown in Fig. 4-3. The rain zone Sauter mean drop diameter was found to be 2.56 mm

a) $T_{wi} = 50\ ^{o}C - 43\ ^{o}C$ b) $T_{wi} = 43\ ^{o}C - 37\ ^{o}C$

c) $T_{wi} = 36\ ^{o}C - 32\ ^{o}C$
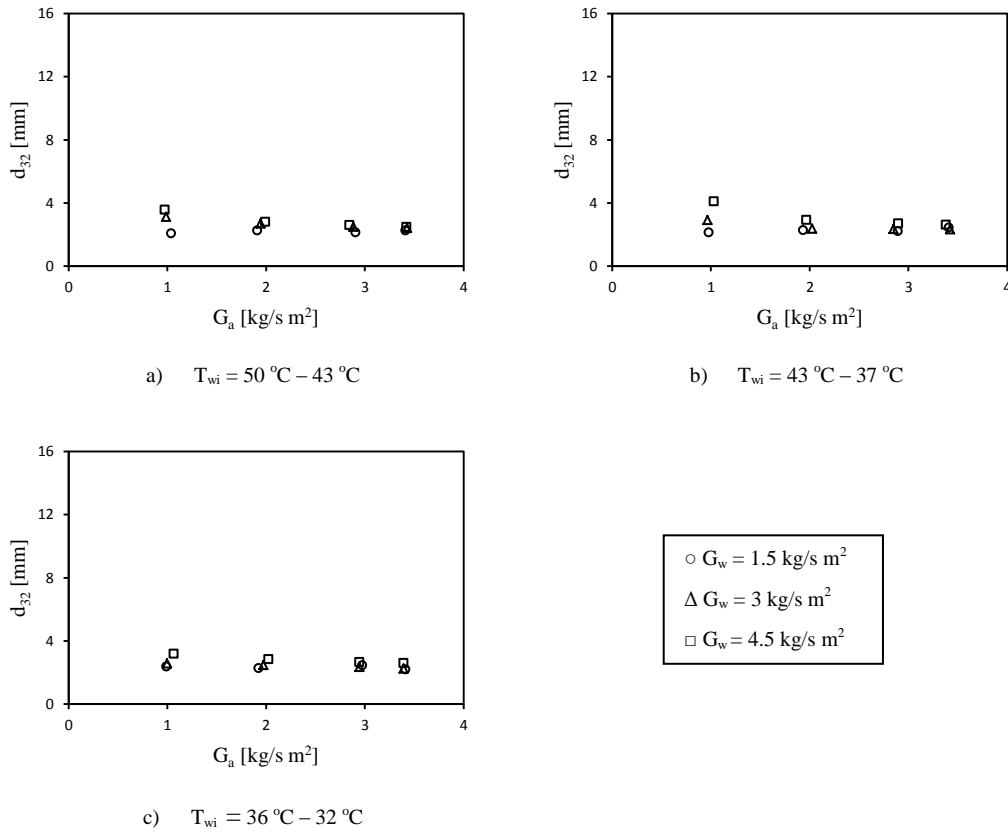
Figure 4-3: Rain zone Sauter mean drop diameter below configuration 5

4.3   Effect of drop falling height before impact on rain zone Sauter mean drop diameter

The rain zone Sauter mean drop diameter for the rain zone below configurations 3 and 4 is presented in this section. Steenmans (2010) found the smallest drop size for a drop falling height of 400 mm. This was followed by the 300 mm and 200 mm configuration respectively.

The rain zone Sauter mean drop diameter for configuration 3 is calculated by subtracting configuration 1's transfer coefficient from configuration 3's transfer coefficient. Configuration 1's performance test rain zone height was 280 mm, which is higher than the distance between the fill and grid for configuration 3. This means the performance of the configuration 3's rain zone is underestimated since an additional 80 mm of rain zone below the fill is deducted from this configuration's performance. This additional performance must be added to

51

configuration 3's rain zone transfer coefficient to obtain the true transfer coefficient below the grid. The rain zone Sauter mean drop diameter for this configuration is shown in Figure 4-4. The test conditions can be found in Table 3-2.
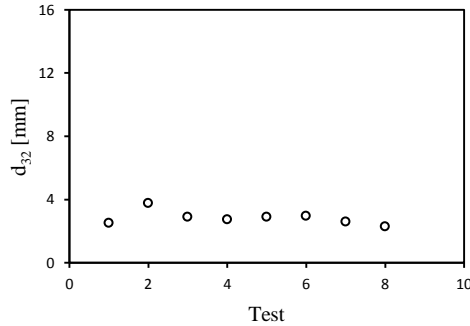
Figure 4-4: Rain zone Sauter mean drop diameter below configuration 3

The rain zone Sauter mean drop diameter for configuration 3 was found to be 2.956 mm.

The rain zone Sauter mean drop diameter for configuration 4 is shown in Figure 4-5 and test conditions in Table 3-3. In this case the additional 20 mm of rain zone above the grid is deducted in a similar process as in configuration 3..
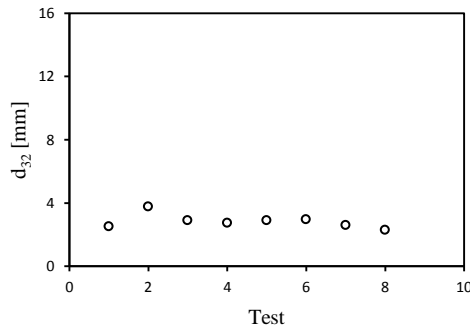
Figure 4-5: Rain zone Sauter mean drop diameter for configuration 4

The rain zone Sauter mean drop diameter for configuration 4 was found to be 2.83 mm. The rain zone Sauter mean drop diameter for configuration 3, 4 and 5 is summarized in Table 4-1.

Table 4-1: Rain zone Satuer mean drop diameter for configuration 3, 4 and 5

Configuration	d_{32} [mm]
5	2.56
4	2.83
3	2.96

It can be seen from Table 4-1 there is a decrease in rain zone Sauter mean drop diameter with an increase in drop falling height before impact. A similar trend was found by Steenmans (2010).

4.4   Rain zone Sauter mean drop diameter for configuration 6

The effect of a double grid configuration on the rain zone Sauter mean drop diameter are presented here. It is expected that two grids will decrease the Sauter mean drop diameter. The first grid below the fill will break the drop as before, however this changes the drop size before impact to the second grid which can result in a smaller drop size below the second grid. In order to isolate the transfer coefficient below the second grid it is important to know the transfer coefficient per meter rain zone for the rain zone exactly below the fill (i.e. above the first grid) and exiting the first grid (below the first grid). The correlation for this is given in section 3.3 and 3.4. This is deducted from the overall rain zone transfer coefficient for this configuration and as a result isolating the rain zone transfer coefficient below the second grid. The resulting drop size associated with the transfer coefficient below the second grid for configuration 6 is given in Figure 4-6 with the test conditions given in Table 3-7.
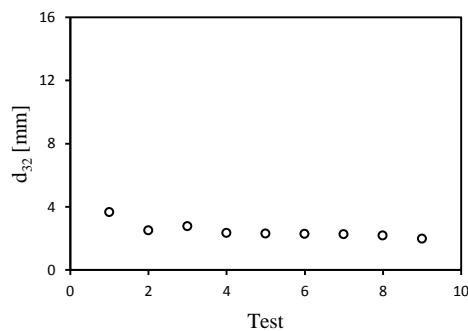
Figure 4-6: Rain zone Sauter mean drop diameter below the second grid for configuration 6

The rain zone Sauter mean drop diameter below the second grid for configuration 6 was found to be 2.31 mm.

The same procedure was followed for determining the rain zone Sauter mean drop diameter below the second grid for configuration 7 with the test conditions given in Table 3-8 and is presented in Figure 4-7.
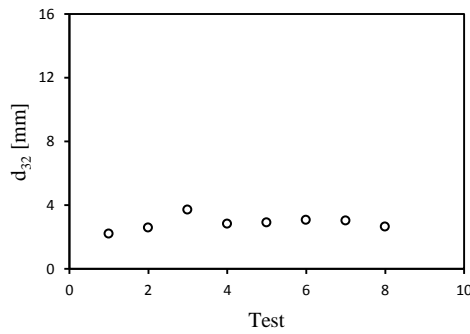
Figure 4-7: Rain zone Sauter mean drop diameter below the second grid for configuration 7

The rain zone Sauter mean drop diameter below the second grid of configuration 7 was found to be 2.68 mm.

4.5   Conclusion

The smallest rain zone Sauter mean drop diameter after impact for the single grid configurations i.e. configurations 3, 4 and 5 was found to be 2.56 mm for a drop falling height before impact of 400 mm (configuration 5) and 2.31 mm for the double grid configuration drop falling height before impact between the first and second grid of 400 mm for configuration 6. Table 4-2 provides a summary of the results.

Table 4-2: Rain zone Sauter mean drop diameter for configurations 3, 4, 5, 6, 7

Configuration	d_{32} [mm]
3	2.96
4	2.83
5	2.56
6	2.31
7	2.68

54

CHAPTER 5 THE EFFECT OF DIFFFERENT FILL CONFIGURATIONS ON THE PERFORMANCE OF A NDWCT

The NDWCT performance in this section is modelled using a one dimensional model employing the Merkel method for performance evaluation. Fig. 5-1 gives a labelled drawing of a typical NDWCT. The model is solved by following an iterative method that satisfies both the draught equation and energy balance across the NDWCT.
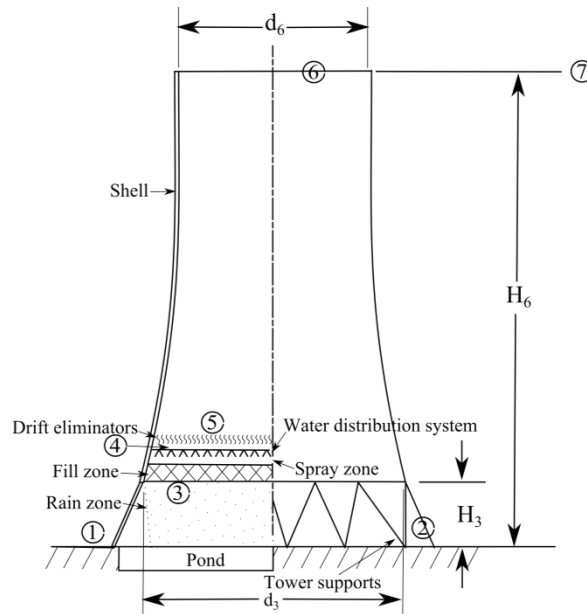
Figure 5-1: Labelled drawing of a typical NDWCT

5.1   Cooling tower model

The one dimensional NDWCT model as given in Kröger (2004) is used for modelling a NDWCT located at a South African power utility, Eskom, coal fired power station.

Table 5-1 shown below contains the iteration parameters for a converged solution, the Reuter iteration parameters and the difference between these values both based on example 7.3.2 Kröger (2004). A sample calculation, input and output parameters are given in appendix E

Table 5-1: NDWCT one dimensional iteration parameters

Iteration parameter	Symbol	Michaels	Reuter	Difference
Air-vapour mass flow rate through fill	m_{av15}	16 808.98 kg/s	16 810.89 kg/s	0.011 %
Air pressure after drift eliminators	p_{a5}	83 937.72 N/m^2	83 937.7 N/m^2	0.000 %
Temperature after drift eliminators	T_{a5}	26.438 ^{o}C	26.437 ^{o}C	0.005 %
Air pressure at tower outlet	p_{a6}	82 650.58	82 650.6	0.000 %
Water outlet temperature	T_{wo}	21.39 ^{o}C	21.39 ^{o}C	0.062 %

Table 5-3 shows the design data for the cooling tower. A natural draught wet cooling tower fitted with asbestos cement flat sheet film fill, containing drift eliminators, water distribution system, spray zone, fill zone and rain zone is investigated in this section. The correlation for the transfer-and loss coefficient of which the form is given in equations (5-1) and (5-2) respectively was obtained by linear extrapolation using the coefficients for asbestos flat sheets as given in Kröger (2004) and presented in Table 5-2.

$$Me_{fi}\left(G_w, G_a, L_{fi}\right) = a_d \left(\frac{G_w}{G_a}\right)^{-b_d} L_{fi} \qquad\qquad 5\text{-}1$$

$$K_{fdm1}\left(G_w, G_a, L_{fi}\right) = (a_p \left(\frac{G_w}{G_a}\right) + b_p) L_{fi} \qquad\qquad 5\text{-}2$$

Table 5-2: Asbestos flat sheet film fill performance characteristics for different sheet spacing

Asbestos flat sheet spacing [mm]	44.4	38.1	31.8	25.4	22.5 (tower 1)
Transfer coefficient					
a_d	0.2887	0.361	0.94	0.459	0.4823
b_d	0.7	0.72	0.76	0.73	0.7539
Loss coefficient					
a_p	0.725	0.936	0.77	0.89	0.8949
b_p	1.37	1.3	1.7	1.7	1.7902

The fill currently installed in the cooling towers that are investigated is asbestos cement flat sheets. The height of the installed fill in the cooling tower is 2.4 m. The thickness of the Asbestos flat sheets are 4 mm and spacing of the flat sheets is 22.5 mm on the periphery of the tower and 25.4 mm in the centre of the tower with frontal area (A_{fr}) of 6 500 m^2. The fill with the 22.5 mm spacing constitutes 38 % of the fill wetted surface area and the fill with the 25 mm 62 %.The one dimensional model can however not model variation in fill characteristics. The weighted average of each fill's characteristic was used for the modelling of the variation in fill using the fill wetted surface area as the basis.

Table 5-4 gives the performance data as calculated using the one dimensional cooling tower model as found in Kröger (2004) and cooling tower 1 design data as

input parameters and compares it with the original design performance data. It was found that the one dimensional model compares well with the original design data for the re-cooled cooling water temperature.

The current performance of the cooling tower is considered below.

A performance test was conducted on cooling tower 1 in October 2002 following the cleaning and repairs of the water distribution system to determine how effective the cleaning was.

Table 5-5 shows the results for the performance test data as well as ambient conditions conducted in October 2002.

Table 5-3: Cooling tower design parameters

Water conditions:			
Water mass flow rate:	m_w	$=$	12 500 kg/s
Water inlet temperature:	T_{w5}	$=$	39.44 ^{o}C
Ambient conditions:			
Air temperature at ground level:	T_{a1}	$=$	15.45 ^{o}C
Wetbulb temperature at ground level:	T_{a1wb}	$=$	11.05 ^{o}C
Atmospheric pressure:	p_{a1}	$=$	84 100 N/m^2
Ambient temperature gradient:	dT_a/dz	$=$	-0.00975 K/m
Cooling tower specifications:			
Tower height:	H_6	$=$	126.7 m
Tower inlet height	H_3	$=$	7.157 m
Tower inlet diameter	d_3	$=$	85.6 m
Tower outlet diameter	d_6	$=$	51.821 m
Number of tower supports	n_{ts}	$=$	72
Length of tower supports	L_{ts}	$=$	8.5 m
Diameter of support	d_{ts}	$=$	0.76 m
Drag coefficient of tower support (round)	C_{Dts}	$=$	1.0
Shell thickness (inlet)	t_s	$=$	0.86 m
Fill specifications:			
Fill height	L_{fi}	$=$	2.4 m
Fill performance characteristics:			
Transfer coefficient:			

$$Me_{fi}(G_w,G_a,L_{fi})=(0.1848\left(\frac{G_w}{G_a}\right)^{-0.7529} + 0.2832\left(\frac{G_w}{G_a}\right)^{-0.73})L_{fi}$$

Loss coefficient:

57

$$K_{fdm1}(G_w, G_a, L_{fi}) = L_{fi}\left(0.3831\left(0.8949\left(\frac{G_w}{G_a}\right) + 1.7902\right) + 0.6169\left(0.89\left(\frac{G_w}{G_a}\right) + 1.7\right)\right)$$

Other specifications:

Frontal area of fill	A_{fr}	=	6 500 m^2
Depth of spray zone above fill	L_{sp}	=	1.0 m
Mean drop diameter in rain zone	d_d	=	0.005 m

Table 5-4: Performance comparative data for Kröger one dimensional model and original design data

Parameter	1 D model	Original design
Type of fill	Film	Film
Fill height, L_{fi} [mm]	2 400	2 400
L_{sp} [mm]	1 000	1 000
Outlet water temperature, T_{wo} [^{o}C]	22.51	22.5
Cooling tower range, ΔT_w [^{o}C]	16.93	16.94
Approach, ΔT_{app} [^{o}C]	11.46	11.45

Table 5-5: Cooling tower 1 latest performance test results

Water conditions:			
Water mass flow rate:	m_w	=	14857 kg/s
Water inlet temperature:	T_{w5}	=	44.61 ^{o}C
Ambient conditions:			
Air temperature at ground level:	T_{a1}	=	25.35 ^{o}C
Wetbulb temperature at ground level:	T_{a1wb}	=	15.98 ^{o}C
Atmospheric pressure:	p_{a1}	=	84 100 N/m^2
Ambient temperature gradient:	dT_a/dz	=	-0.00975 K/m
Results :			
Re-cooled water temperature	T_{wo}	=	29.09 ^{o}C
Cooling tower range	ΔT_r	=	15.52 ^{o}C

The current performance is modelled by using the data in

Table 5-5. As mention earlier the performance test was carried out after the cleaning and repairs of the water distribution system. This means that the current deterioration of the cooling tower performance is mostly attributed to the degradation of the fill. There are two factors that are currently responsible for the fill degradation, which include: missing/broken fill and fouling of fill. For the current cooling tower under investigation the latter is a major contributor to the degradation of the performance.

58

The fouling of fill will result in increase in the loss coefficient across the fill resulting in decrease in draught i.e. air mass flow rate through the cooling tower leading to decrease in cooling tower performance.

The fouling will be modelled as an increase in flow resistance as a result of the smaller spacing between the sheets. This increase is incorporated in the fill loss coefficient. Although the spacing between the fill sheets is different the correlation for the transfer coefficient will remain unchanged since the fill transfer area remains unchanged. The decrease in transfer coefficient is as a result of the decrease in air mass flow rate caused by the increase in flow resistance. The new loss coefficient correlation was found through an iterative process by changing the total loss coefficient until the re-cooled water outlet temperature as given in Table 5-5 is reached. The correlations for both the transfer-and loss coefficient are given in Table 5-6 and the results given in Table 5-7.

5.2   Cooling tower modelling

There are several performance enhancement methods investigated in this section. These include replacing the current fill with new types of modern fill and introduction of a grid below a conventional fill to reduce rain zone Sauter mean diameter. Four different fills are investigated in this section. These include three different film fills, including the current fill installed and one trickle fill. All fills would have to use the existing tower configurations which results in the fill height being limited to 2 400 mm as this is the current maximum height. The spray zone height of the cooling tower will remain constant at $L_{sp} = 1\,000$ mm, while the fill height L_{fi} can vary to achieve the optimum height for the specific fill limited to a height of 2 400 mm and finally the rain zone height which can vary as well depending on the fill height, however it has a minimum height of $H_{rz} = 7\,157$ mm. It should also be noted that the effect of the air flow at the cooling tower inlet as a result of the change in rain zone height was not modelled.

Table 5-6.shows the performance characteristics of the different fills used. It should be mentioned all performance characteristics were determined using the Merkel method. Some of the correlations parameters were given in imperial units, which are converted directly in the correlation. The current characteristics of the installed fill including the effect of fouling is also given in the table below. It should however be noted that only the correlation for the loss coefficient is different from the clean installed fill and the current condition of the fill, which was discussed earlier in this section.

59

Table 5-6: Performance characteristics for different fills

Fill	
Transfer coefficient	
Asbestos flat sheet (clean and fouled):	$Me_{fi}(G_w,G_a,L_{fi})=(0.1848\left(\dfrac{G_w}{G_a}\right)^{-0.7529}+0.2832\left(\dfrac{G_w}{G_a}\right)^{-0.73})L_{fi}$
High performance Fill:	$Me_{fi}=2.746G_w^{-0.984}G_a^{0.73}T_{wi}^{-0.104}L_{fi}^{-0.085}$
Anti-fouling film fill:	$Me_{fi}=0.1744\left(\dfrac{G_a}{G_w}\right)^{0.64362}\left(\dfrac{60v_a}{0.3048}\right)^{0.18373}\left(\dfrac{L_{fi}}{0.3048}\right)^{0.69676}$
Trickle fill:	$Me_{fi}=3.931G_w^{-0.857}G_a^{0.644}T_{wi}^{-0.285}L_{fi}^{-0.294}$
Loss coefficient	
Asbestos flat sheet (clean):	$K_{fdm1}(G_w,G_a,L_{fi})=L_{fi}(0.3831\left(0.8949\left(\dfrac{G_w}{G_a}\right)+1.7902\right)$ $+0.6169(0.89\left(\dfrac{G_w}{G_a}\right)+1.7)$
Asbestos flat sheet (Fouled):	$K_{fdm1}(G_w,G_a,L_{fi})=L_{fi}(3.9065\left(\dfrac{G_w}{G_a}\right)+7.5974)$
High performance Fill:	$K_{fdm}=\left(4.499G_w^{0.359}G_a^{-1.122}+9.577G_w^{0.028}G_a^{0.056}\right)L_{fi}^{-0.043}$
Anti-fouling film fill:	$K_{fdm}=498.1778\Delta p_{fill}\rho_{av15}\left(\dfrac{A_{fr}}{m_{av15}}\right)^2$ $=498.1778\rho_{av15}\left(\dfrac{A_{fr}}{m_{av15}}\right)^2(0.13257\times10^{-6}\left(\dfrac{60v_a}{0.3048}\right)^{1.9965}$ $+(1.472513G_w)(0.60829\times10^{-3}+0.79793\times10^{-8}$ $\times\left(\dfrac{60v_a}{0.3048}\right)^2))\left(\dfrac{L_{fi}}{0.3048}\right)(0.06243\rho_{av15})/0.07$
Trickle fill:	$K_{fdm}=\left(3.402G_w^{0.067}G_a^{-0.022}+1.324G_w^{0.798}G_a^{-1.777}\right)L_{fi}^{0.055}$

5.3 Effect of changing the fill on NDWCT performance

Table 5-7 and 5-8 below shows the performance results when installing different fill in the cooling tower. The optimum height for the different fill is not necessarily the same height as the current installed fill leaving room for an additional rain zone. Tables 5-7 and 5-8 below shows the effect of leaving the rain zone height at the original height and the other is to increase it.

Table 5-7: Cooling tower one performance results constant inlet temperature

Parameter		Units	Asbestos flat sheet (clean)	Asbestos flat sheet (fouled)	High perform-ance film fill	Anti-fouling film fill	Trickle fill
Type of fill			Film	Film	Film	Film	Trickle
Fill height	L_{fi}	mm	2 400	2 400	1 220	1 660	1 220
Spray zone height	L_{sp}	mm	1 000	1 000	1 000	1 000	1 000
Rain zone height	H_{rz}	mm	7.157	7.157	7.157	7.157	7 157
Rain zone drop size	d_d	mm	5	5	5	5	5
Air mass flow rate	m_{av15}	kg/s	11 898	9954	11 640	11 522	12 154
Inlet water temperature	T_{w5}	^{o}C	39.44	39.44	39.44	39.44	39.44
Outlet water temperature	T_{wo}	^{o}C	22.51	23.88	21.22	20.98	22.29
Dry bulb temperature above drift eliminators	T_{a5}	^{o}C	29.45	30.66	30.68	30.99	29.34
Pressure above drift eliminators	p_{a5}	N/m^2	83 959	83 949	83 958	83 954	83 967
Pressure at tower outlet	p_{a6}	N/m^2	82 849	82 849	82 651	82 849	82 849
Cooling tower range	ΔT_w	^{o}C	16.93	15.56	18.21	18.46	17.15
Approach	ΔT_{app}	^{o}C	11.46	12.83	10.18	9.93	11.24

Table 5-8 shows the effect of adjusting the rain zone to the available height after installing new fill at the new fill's optimum or recommended height.

The best performing fill according to the one dimensional model based on the lowest outlet water temperature (T_{wo}), cooling tower range (ΔT_w) and approach (ΔT_{app}) for both the original rain zone height (as shown in Table 5-7) and adjusted rain zone height based on the optimum or recommended fill height (as shown in Table 5-8) was found to be for the anti-fouling film fill. It should be mentioned that the effect of changing the inlet conditions by increasing the rain zone height was not taken into account. The increase in rain zone height was taken into account by including the increase in the rain zone transfer-and loss coefficient correlations. Based on these results the recommended fill would be the anti-fouling film fill. It should however be mentioned that the fill chosen should not be purely based on the re-cooled outlet water temperature and should other factors also be considered including fouling rate.

Table 5-8: Cooling tower one performance results with variable rain zone height

Parameter	Units	Asbestos flat sheet (clean)	Asbestos flat sheet (fouled)	High performance film fill	Anti-fouling film fill	Trickle pack
Type of fill		Film	Film	Film	Film	Trickle
Fill height, L_{fi}	mm	2 400	2 400	1 220	1 660	1 220
L_{sp}	mm	1 000	1 000	1 000	1 000	1 000
Rain zone height, H_{rz}	mm	7 157	7.157	8.337	7.897	8.337
Rain zone droplet size, d_d	mm	5	5	5	5	5
Air mass flow rate, m_{av15}	kg/s	11 898	9954	12 008	11 759	12 684
Inlet water temperature, T_{w5}	^{o}C	39.44	39.44	39.44	39.44	39.44
Outlet water temperature, T_{wo}	^{o}C	22.51	23.88	20.92	20.77	21.91
Dry bulb temperat-ure above drift eliminators, T_{a5}	^{o}C	29.45	30.66	30.49	30.87	29.08
Pressure above drift eliminators, p_{a5}	N/m^2	83 959	83 949	83 949	83 949	83 959
Pressure at tower outlet, p_{a6}	N/m^2	82 849	82 849	82 848	82 849	82 849
Cooling tower range, ΔT_w	^{o}C	16.93	15.56	18.52	18.67	17.53
Approach, ΔT_{app}	^{o}C	11.46	12.83	9.87	9.72	10.86

5.4   Introduction of a splash grid to reduce rain zone drop size

The effect of introducing a splash pack grid (referred to as grid in the text) below a conventional fill is modelled using the one dimensional model and its effect on the performance of the cooling tower where performance is measured in terms of cooling water range, approach and water outlet temperature.

The effect of a single grid and double grid below a conventional fill on the performance is modelled. In this case there are two conventional fills considered. This include asbestos cement flat sheet film fill (currently installed in the cooling tower) and anti-fouling film fill, which was found to be the best performing fill

from parametric study. Both a clean and fouled asbestos cement film fill is modelled

Figure 5-2 below shows a schematic of the proposed configuration of the grid below the conventional fill installed at an angle of two degrees from the horizontal plane in the cooling tower.
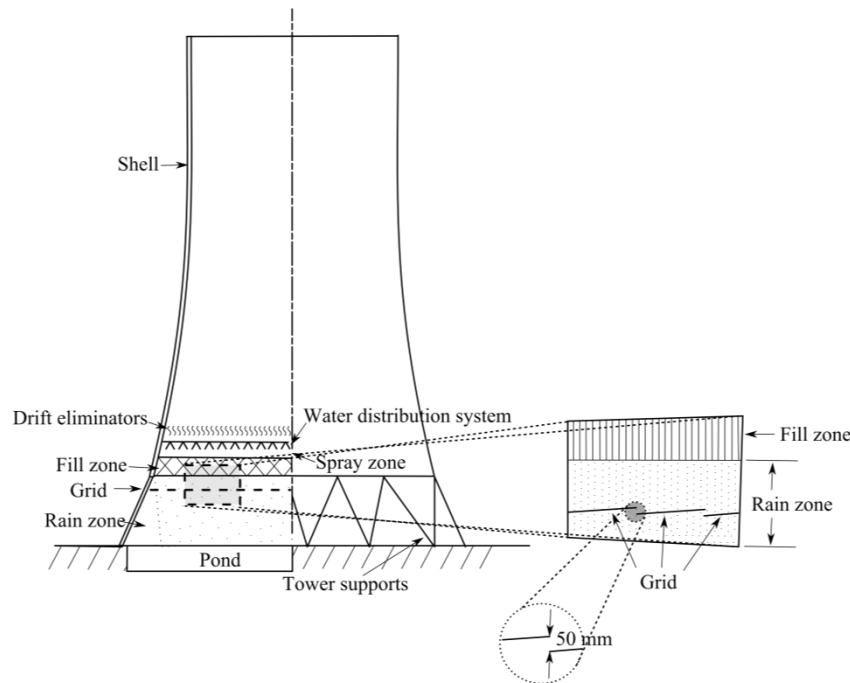
Figure 5-2: Proposed grid placement below the fill zone in a typical NDWCT

The angle is necessary to reduce the surface area occupied by the frame of the grid.. Fig. 5-2 is a sketch illustrating the reduction in surface area compared to placing the grid horizontally adjacent and placing it at an angle.
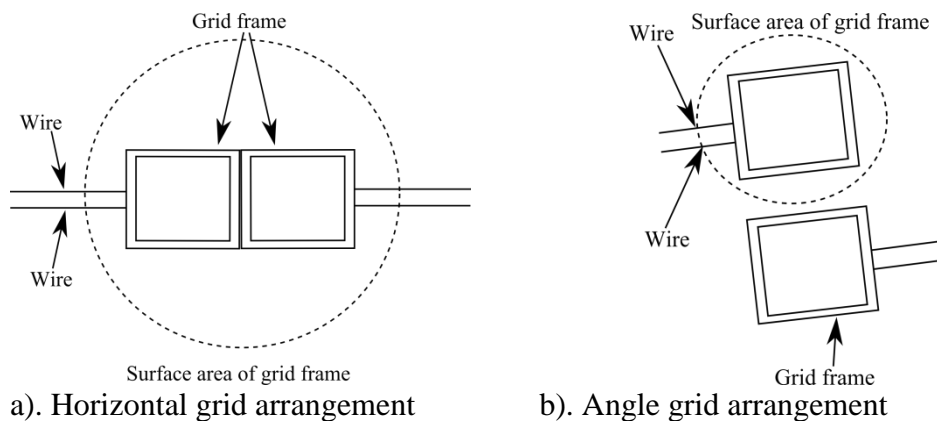
a). Horizontal grid arrangement   b). Angle grid arrangement
Figure 5-3: Grid frame surface area comparison

The design data for the modelling of the cooling tower with the addition of the grid is similar to what is given in Table 5-3 with the exception of rain zone drop size and rain zone height, although the total rain zone height remains the same it is

divided into two (three in the double grid configuration) different rain zones based on rain zone drop size. These two rain zones would be referred to as rain zone above the grid and rain zone below the grid (below the second grid in a double grid configuration). The results for the grid modelling are given in Table 5-11 to Table 5-15. The grid was modelled as a screen. It is necessary to add the loss coefficient of the screens since the rain zone loss coefficient correlation accounts for the rain zone drops and not the screen. The correlation to be used is based on the screen Reynolds number as given below.

$$Re_s = \frac{\rho v d_s}{\beta_s \mu}$$ 5-3

Where:

The properties shown in equation 5-3 are determined at the mean free stream condition of the fluid flowing across the screen.

And $\beta_s = \frac{Area\ of\ holes}{Total\ area} = \left(1 - \frac{d_s}{P_s}\right)^2$

The screen loss coefficient for $60 < Re_s < 1000$ as given in Kröger (2004) is shown in the correlation below.

$$K_s = 6(1 - \beta_s)\beta_s^{-2} Re_s^{-0.333}$$ 5-4

The input parameters for calculating the screen loss coefficient is given in Table 5-9.

Table 5-9: Input parameters for calculation screen loss coefficient according to equation 5-4

Description	Symbol	Value
Porosity of the screen (β_s)		
Wire diameter	d_s	1 mm
Screen pitch	P_s	3 mm
Porosity of screen	β_s	0.4444
Screen Reynolds number (Re_s)		
Mean density of air flowing across screen	ρ_{av15}	0.9859 kg/m^3
Mean air velocity across screen	v_{av15}	1.8067 m/s
Mean air viscosity across screen	μ_{av15}	1.84×10^{-5} kg/ms
Screen Reynolds number	Re_s	217.83

The resulting screen loss coefficient was found according to equation 5-4 to be $K_s = 2.8104$

The rain zone above the grid ($H_{rz,\ above\ grid}$), which is around 400 mm, cannot be modelled using the correlation proposed by De Villiers and Kröger (1997), equation **Error! Reference source not found.**, since it is only valid for rain zone heights of greater than 4 m. To account for the performance characteristics of such small rain zones a correlation for both the transfer-and loss coefficient was experimentally determined for a rain zone below a conventional film fill in section

64

5.3. Terblanche et al. (2008) found that the rain zone Sauter mean drop diameter for most film-and trickle fill ranges between 5-6 mm, which subsequently means that the aforementioned correlation can be used in most film and trickle fill cases. The correlations as determined in section 3.3 will thus be used for both the asbestos flat sheet as well as the anti-fouling fill. Similar correlations were determined in section 3.4 for the rain zone below the grid, which is used for the rain zone between grids in a double grid configuration. The rest of the rain zone i.e. the rain zone exiting the grid configuration can be modelled using the De Villiers and Kröger correlation for the transfer-and loss coefficient since the rain zone height is greater than 4 m. The correlations for the transfer-and loss coefficients of a rain zone below a conventional fill and below a single grid are given below in Table 5-10.

Table 5-10: Rain zone transfer-and loss coefficient correlations

Rain zone performance characteristics below conventional film fill	
$Me_{rz}/L_{rz} = 0.0284 T_{wi}^{0.011} G_a^{0.6234} G_w^{-0.4412}$	5-5
$\dfrac{K_{rz}}{L_{rz}} = 0.3095 G_a^{-3.2407} G_w^{2.5950}$	5-6
Rain zone performance characteristics below the splash grid	
$\dfrac{Me_{rz}}{L_{rz}} = 0.3348 T_{wi}^{-0.0879} G_a^{0.3988} G_w^{-0.3816}$	5-7
$\dfrac{K_{rz}}{L_{rz}} = 2.5725 G_a^{-1.4663} G_w^{0.9803}$	5-8

The results of the effect of the grid and double grid configurations for both the current installed fill as well as anti-fouling film fill on the re-cooled water outlet temperature, range and approach are shown in Tables 11, 12 and 13.

It is clear from Table 5-11 above that clean current asbestos cement film fill with a single grid installed below it gives a better performance with a re-cooled water outlet temperature of 21.59 °C compared to 22.51 °C of an unaltered rain zone. The double grid configuration was however expected to give the best performance due to its smaller rain zone Sauter mean drop diameter. The double grid configuration however only achieved a re-cooled cooling water outlet temperature of 21.70 °C compared to the single grid's 22.51 °C. The additional grid as well as the smaller drop size increases the flow losses throughout the cooling tower as is evident from the lower air flow rate as can be seen in the Table 5-11 above. This means the additional heat-and mass transfer as a result of the smaller rain zone drop size is partially negated by the additional flow resistances due to the additional grid and smaller Sauter mean drop diameter.

Table 5-11: Cooling tower 1 performance results for current clean film fill, film fill with single grid and film fill with double grid configuration

Parameter	Units	Asbestos flat sheet (clean)	Asbestos flat sheet (clean) + single grid	Asbestos flat sheet (clean) + double grid
Type of fill		Film	Film/splash	Film/splash
Fill height, L_{fi}	mm	2 400	2 400	2 400
L_{sp}	mm	1 000	1 000	1 000
Rain zone height, H_{rz}	mm	7 157	7 157	7 157
Rain zone height above first grid, $H_{rz, first}$	mm	N/A	400	400
Rain zone height above second grid, $H_{rz, second}$	mm	N/A	N/A	400
Rain zone height below last grid, $H_{rz, below}$	mm	N/A	6 757	6 326
Rain zone drop size, d_d	mm	5	N/A	N/A
Rain zone drop size above grid, $d_{d, above}$	mm	N/A	5	5
Rain zone drop size below first grid, $d_{d, first}$	mm	N/A	2.56	2.56
Rain zone drop size below second grid, $d_{d, second}$	mm	N/A	N/A	2.31
Air mass flow rate, m_{av15}	kg/s	11 898	11 352	10 860
Inlet water temperature, T_{w5}	^{o}C	39.44	39.44	39.44
Outlet water temperature, T_{wo}	^{o}C	22.51	21.59	21.70
Dry bulb temperature above drift eliminators, T_{a5}	^{o}C	29.45	30.74	31.25
Pressure above drift eliminators, p_{a5}	N/m^2	83 959	83 960	83 964
Pressure at tower outlet, p_{a6}	N/m^2	82 849	82 849	82 849
Cooling tower range, ΔT_w	^{o}C	16.93	17.84	17.74
Approach, ΔT_{app}	^{o}C	11.45	10.55	10.65

Table 5-12 shows the effect of the single-and double grid configuration if installed below the fouled asbestos cement film fill.

Table 5-12: Cooling tower 1 performance results for current fouled film fill, fouled film fill with single grid and fouled film fill with double grid configuration

Parameter	Units	Asbestos flat sheet (fouled)	Asbestos flat sheet (fouled) + single grid	Asbestos flat sheet (fouled) + double grid
Type of fill		Film	Film/splash	Film/splash
Fill height, L_{fi}	mm	2 400	2 400	2 400
L_{sp}	mm	1 000	1 000	1 000
Rain zone height, H_{rz}	mm	7 157	7 157	7 157
Rain zone height above first grid, $H_{rz, first}$	mm	N/A	400	400
Rain zone height above second grid, $H_{rz, second}$	mm	N/A	N/A	400
Rain zone height below last grid, $H_{rz, below}$	mm	N/A	6 757	6 326
Rain zone drop size, d_d	mm	5	N/A	N/A
Rain zone drop size above grid, $d_{d, above}$	mm	N/A	5	5
Rain zone drop size below first grid, $d_{d, first}$	mm	N/A	2.56	2.56
Rain zone drop size below second grid, $d_{d, second}$	mm	N/A	N/A	2.31
Air mass flow rate, m_{av15}	kg/s	9 954	9 685	9 393
Inlet water temperature, T_{w5}	^{o}C	39.44	39.44	39.44
Outlet water temperature, T_{wo}	^{o}C	23.88	22.81	22.82
Dry bulb temperature above drift eliminators, T_{a5}	^{o}C	30.66	31.92	32.33
Pressure above drift eliminators, p_{a5}	N/m^2	83 948	83 948	83 952
Pressure at tower outlet, p_{a6}	N/m^2	82 849	82 849	82 849
Cooling tower range, ΔT_w	^{o}C	15.56	16.63	16.62
Approach, ΔT_{app}	^{o}C	12.83	11.76	11.77

It can be seen from Table 5-12 above that the difference between the single-and double grid configuration is marginal with the single grid giving a slight better performance compared to the double grid configuration. In this case the contribution of the rain zone's loss coefficient to the overall cooling tower loss coefficient is less. This is due to the increase in flow resistance in the fill zone.

From Table 5-13 it can be seen that the effect of the additional grid becomes more evident when considering the difference in cooling tower range for the single grid configuration and the double grid configuration. This is due to the larger contribution of the rain zone loss coefficient to the overall loss coefficient.

A similar process is followed to calculate the effect of the addition of the single grid to the overall performance of the cooling tower, however the range is kept constant at 16.94 ^{o}C and varying the cooling tower inlet water temperature. Cooling towers provide a constant range for given conditions. This will reduce the re-cooled water temperature. The results are shown in Table 5-14.

67

Table 5-13: Cooling tower 1 performance results for anti-fouling film fill, anti-fouling film fill with single grid and anti-fouling film fill with double grid configuration

Parameter	Units	Anti-fouling film fill	Anti-fouling film fill + single grid	Asbestos flat sheet (fouled) + double grid
Type of fill		Film	Film/splash	Film/splash
Fill height, L_{fi}	mm	2 400	2 400	2 400
L_{sp}	mm	1 000	1 000	1 000
Rain zone height, H_{rz}	mm	7 897	7 897	7 897
Rain zone height above first grid, $H_{rz, first}$	mm	N/A	400	400
Rain zone height above second grid, $H_{rz, second}$	mm	N/A	N/A	400
Rain zone height below last grid, $H_{rz, below}$	mm	N/A	7 497	7 097
Rain zone drop size, d_d	mm	5	N/A	N/A
Rain zone drop size above grid, $d_{d, above}$	mm	N/A	5	5
Rain zone drop size below first grid, $d_{d, first}$	mm	N/A	2.56	2.56
Rain zone drop size below second grid, $d_{d, second}$	mm	N/A	N/A	2.31
Air mass flow rate, m_{av15}	kg/s	11 759	10 852	10 511
Inlet water temperature, T_{w5}	^{o}C	39.44	39.44	39.44
Outlet water temperature, T_{wo}	^{o}C	20.77	19.71	19.87
Dry bulb temperature above drift eliminators, T_{a5}	^{o}C	30.87	32.71	33.04
Pressure above drift eliminators, p_{a5}	N/m^2	83 949	83 941	83 946
Pressure at tower outlet, p_{a6}	N/m^2	82 849	82 848	82 848
Cooling tower range, ΔT_w	^{o}C	18.67	19.73	19.57
Approach, ΔT_{app}	^{o}C	9.72	8.66	8.82

The re-cooled water outlet temperature for a constant range was found to be 22.51 ^{o}C, 24.05 ^{o}C and 20.71 ^{o}C for the clean asbestos cement, fouled asbestos cement and anti-fouling film fill respectively. The result for the addition of a grid below the fill for a constant range is shown in the table below. The re-cooled outlet water temperature for this configuration was found to be 21.27 ^{o}C, 22.84 ^{o}C and 19.73 ^{o}C for the clean asbestos cement, fouled asbestos cement and anti-fouling film fill respectively.

Table 5-14: Cooling tower 1 performance results for asbestos cement film fill (clean), asbestos cement film fill (fouled) and anti-fouling film fill at constant cooling range

Parameter	Units	Asbestos cement flat sheet (clean)	Asbestos cement flat sheet (fouled)	Anti-fouling film fill
Type of fill		Film	Film	Film
Fill height, L_{fi}	mm	2 400	2 400	2 400
L_{sp}	mm	1 000	1 000	1 000
Rain zone height, H_{rz}	mm	7 157	7 157	7 897
Rain zone height above first grid, $H_{rz, first}$	mm	N/A	N/A	N/A
Rain zone height above second grid, $H_{rz, second}$	mm	N/A	N/A	N/A
Rain zone height below last grid, $H_{rz, below}$	mm	N/A	N/A	N/A
Rain zone drop size, d_d	mm	5	5	5
Rain zone drop size above grid, $d_{d, above}$	mm	N/A	N/A	N/A
Rain zone drop size below first grid, $d_{d, first}$	mm	N/A	N/A	N/A
Rain zone drop size below second grid, $d_{d, second}$	mm	N/A	N/A	N/A
Air mass flow rate, m_{av15}	kg/s	11 900	10 229	11 404
Inlet water temperature, T_{w5}	^{o}C	39.45	40.99	37.65
Outlet water temperature, T_{wo}	^{o}C	22.51	24.05	20.71
Dry bulb temperature above drift eliminators, T_{a5}	^{o}C	29.45	31.43	30.00
Pressure above drift eliminators, p_{a5}	N/m^2	83 960	83 945	83 952
Pressure at tower outlet, p_{a6}	N/m^2	82 849	82 849	82 849
Cooling tower range, ΔT_w	^{o}C	16.94	16.94	16.94
Approach, ΔT_{app}	^{o}C	11.46	13.00	9.66

Table 5-15: Cooling tower 1 performance results for asbestos cement film fill (clean + single grid), asbestos cement film fill (fouled + single grid) and anti-fouling film fill (single grid) at constant range

Parameter	Units	Asbestos cement flat sheet (clean + single grid)	Asbestos cement flat sheet (fouled + single grid)	Anti-fouling film fill (single grid)
Type of fill		Film	Film	Film
Fill height, L_{fi}	mm	2 400	2 400	2 400
L_{sp}	mm	1 000	1 000	1 000
Rain zone height, H_{rz}	mm	7 157	7 157	7 897
Rain zone height above first grid, $H_{rz,\,first}$	mm	400	400	400
Rain zone height above second grid, $H_{rz,\,second}$	mm	N/A	N/A	N/A
Rain zone height below last grid, $H_{rz,\,below}$	mm	6 757	6 757	7 497
Rain zone drop size, d_d	mm	5	5	5
Rain zone drop size above grid, $d_{d,\,above}$	mm	5	5	5
Rain zone drop size below first grid, $d_{d,\,first}$	mm	2.56	2.56	2.56
Rain zone drop size below second grid, $d_{d,\,second}$	mm	N/A	N/A	N/A
Air mass flow rate, m_{av15}	kg/s	11 480	9 743	10 344
Inlet water temperature, T_{w5}	^{o}C	38.21	39.78	36.67
Outlet water temperature, T_{wo}	^{o}C	21.27	22.84	19.73
Dry bulb temperature above drift eliminators, T_{a5}	^{o}C	29.92	32.09	31.28
Pressure above drift eliminators, p_{a5}	N/m^2	83 965	83 948	83 947
Pressure at tower outlet, p_{a6}	N/m^2	82 849	82 849	82 849
Cooling tower range, ΔT_w	^{o}C	16.94	16.94	16.94
Approach, ΔT_{app}	^{o}C	10.22	11.79	8.68

5.5   Conclusion

The Kröger (2004) one dimensional NDWCT model was used to model a South African coal fired power station cooling tower. The performance of the tower as measured in October 2002 following the cleaning and repairs of the water distribution system. The system showed an increase of 1.2 ^{o}C in the re-cooled outlet water temperature compared to a clean tower. The deterioration of performance was largely attributed to the fouling of fill and was modelled as such.

Two different NDWCT performance enhancement methods were modelled, which include replacing of the fill with newer type fills and introducing a grid below the

fill. For the modelling of the fill four different fill were considered (five if the fouled fill is also considered as a separate fill). These fills include the current installed asbestos cement flat sheets-, high performance-, anti-fouling film fill and trickle fill. These fills were chosen based on either their high performance or anti-fouling combined with relatively high performance characteristics. The following results for the re-cooled water outlet temperature for the same tower design parameters and atmospheric conditions were obtained. The current installed fill if cleaned conditions are assumed achieved an outlet water temperature of 22.51 ^{o}C, while fouled fill achieved an outlet temperature of 23.88 ^{o}C. An improvement for the outlet temperature was achieved for both the high performance film-and trickle fill at 21.22 ^{o}C and 22.29 ^{o}C respectively, however the anti-fouling fill achieved the best performance for the fill considered achieving an outlet water temperature of 20.98 ^{o}C.

The rain zone height was also adjusted where the adjustment depended on the fill optimum or recommended height. In this case the anti-fouling fill achieved the best performance reaching a re-cooled outlet water temperature of 20.77 ^{o}C.

The introduction of a grid caused a significant increase in performance of the rain zone compared to the unaltered rain zone for both the single-and double grid configuration. For the clean asbestos cement film fill the unaltered outlet temperature of 22.51 ^{o}C was achieved compared to the single-and double grid outlet temperature of 21.59 ^{o}C and 21.70 ^{o}C respectively. The double grid configuration was expected to give the best performance, however this was not the case due to the increase in flow losses reducing the air mass flow rate through the tower. Similar results were achieved for the fouled fill which had a re-cooled outlet water temperature of 23.88 ^{o}C, 22.81 ^{o}C and 22.82 ^{o}C for the unaltered rain zone, single-and double grid configuration respectively. This was also the case for the anti-fouling film fill, which achieved a re-cooled water outlet temperature of 20.77 ^{o}C, 19.71 ^{o}C and 19.87 ^{o}C for the unaltered rain zone, single-and double grid configuration.

Similar modelling was done for a constant range across the cooling tower for the unaltered rain zone and single grid configuration for clean asbestos cement, fouled asbestos cement- and anti-fouling film fill. The re-cooled outlet water temperatures were found to be 22.51 ^{o}C, 24.05 ^{o}C and 20.71 ^{o}C for the clean asbestos cement-, fouled asbestos cement-and anti-fouling film fill respectively. The addition of the grid reduced the re-cooled outlet water temperature for a constant range to 21.27 ^{o}C, 22.84 ^{o}C and 19.73 ^{o}C for the clean asbestos cement-, fouled asbestos cement-and anti-fouling film fill respectively.

CHAPTER 6 CONCLUSION

Kröger (2004) found that the rain zone can contribute up to 20% of the overall cooling tower performance. The introduction of a grid below a film fill on the performance characteristics of a rain zone was investigated.

Several tests were conducted to determine the effect of the grid as well as the optimum placement below a conventional film fill.

It was found that the grid had a significant effect on the rain zone performance characteristics where an increase in the transfer-and loss coefficient of 4.5 and 1.5 respectively compared to an unaltered rain zone was achieved. This performance improvement was found for a drop falling height before impact of 400 mm.

The addition of a second grid was also investigated and found that it improved the performance characteristics by a factor of 6.097 and 2.85 for the transfer-and loss coefficient respectively. It should however be mentioned that the increase in transfer coefficient might be negated by the increase in the loss coefficient which would decrease the air mass flow rate through the tower.

A decrease in the transfer coefficient was found when extending the rain zone, while the loss coefficient stayed approximately constant. The decrease in the transfer coefficient is as a result of the decrease in the rain zone drop residence time with increase in drop path length.

The addition of the grid resulted in a drop size reduction from 6 mm to 2.56 mm and 2.31 mm below a single-and double grid configuration, which is also used in the modelling of the NDWCT.

A South African coal fired power station NDWCT is modelled using the one dimensional Kröger (2004) model. Two cooling tower performance enhancement methods are considered, which include replacing the current fill and the introduction of a grid below a conventional fill to reduce the rain zone drop size and subsequently increase the performance of the rain zone. There are four different fills considered which include the current installed asbestos cement-, high performance-, anti-fouling film fill and trickle fill. The current state of the asbestos cement film fill is also modelled. The current installed fill achieved a re-cooled water outlet temperature of approximately 22.51 $^{\circ}$C, while the current state of the installed fill achieved a temperature of 23.88 $^{\circ}$C. The best performing fill based on the re-cooled water outlet temperature is for the anti-fouling film fill achieving a temperature of 20.98 $^{\circ}$C. This result is achieved for a rain zone height of 7.157 m, however in certain cases the rain zone height is adjusted to the optimum or recommended fill height to achieve the best performance. The rain zone height is limited to 2.4 m, which is the rain zone of the current installed fill. The decrease in height for the fill is added to the rain zone height. The lowest re-cooled water outlet temperature for the anti-fouling fill is 20.77 $^{\circ}$C.

The modification of the rain zone by adding a single-or double grid below the fill increased the cooling tower performance. Clean-and fouled asbestos cement film fill as well as the best performing fill which was found to be the anti-fouling film fill were chosen as the conventional film fill. For the single grid configuration the outlet water temperature was 21.59 ^{o}C, 22.81 ^{o}C and 19.71 ^{o}C for the clean asbestos cement-, fouled asbestos cement-and anti-fouling film fill respectively. The same or slightly worse performance was achieved for the double grid configuration where the outlet temperature was found to be 21.7 ^{o}C, 22.82 ^{o}C and 19.87 ^{o}C for the clean asbestos cement-, fouled asbestos cement-and anti-fouling film fill respectively. The slight decrease in performance was attributed to the increase in flow losses in the tower due to the additional grid and smaller rain zone drop size. The modelling was however for a constant inlet re-cooled water temperature.

For a constant range across the cooling tower the re-cooled outlet water temperature for an unaltered rain zone was found to be 22.51 ^{o}C, 24.05 ^{o}C and 20.71 ^{o}C for clean asbestos cement-, fouled asbestos cement-and anti-fouling film fill respectively. The addition of the grid decreased the outlet water temperature further to 21.27 ^{o}C, 22.84 ^{o}C and 19.73 ^{o}C for the clean asbestos cement-, fouled asbestos cement- and anti-foiling film fill.

REFERENCES

Al-waked, R. and Behnia, M., 2000, *CFD simulation of wet cooling towers,* Applied thermal engineering, vol 26, pp. 382-395.

Benocci, C., Buchlin, J.M. and Weinacht, P., 1986, *Predicting the air-droplet interaction in the inlet section of a natural draft cooling tower*, Proceeding of the 5th IAHR cooling tower workshop, Monterey.

Benton, D.J. and Rehberg, R.L., 1986, *Mass transfer and pressure drop in sprays falling in a freestream of various angles*, Proceedings of the 5th IAHR cooling tower workshop, Monterey.

Bertrand, T.P., 2011, *Evaluation of 1.5x1.5 m^2 counter-flow fill performance test facility with a view to contributing to a fill performance standard*, MSc thesis, Stellenbosch University, Stellenbosch, South Africa.

De Villiers, E. and Kröger, D.G., *Analysis of heat, mass and momentum transfer in the rain zone of counterflow cooling towers,* proceedings of the 1997 IJPGC, vol. 2, PWR-vol. 32, pp. 141-149, Denver, November 1997.

De Villiers, E., Kröger, D.G., 1999, *Analysis of heat, mass and momentum transfer in the rain zone of counterflow cooling towers,* Journal of engineers for gas turbines and power, Vol. 121, pp. 1-5.

Dreyer, A.A., Erens, P.J., 1996, *Modelling of cooling tower splash pack*, International journal of heat and mass transfer, Vol. 39, No. 1, pp. 109-123.

Hollands, K.G.T., 1974, *An analysis of a counter flow spray cooling tower*, International journal of heat and mass transfer, Vol. 17, pp. 1227-1239.

Hung, L.S. and Yao, S.C., 2002, *Dripping phenomena of water droplets impacted on horizontal wire screens*, international journal of multiphase flow, Vol. 28, pp. 93-104.

Grobbelaar, P.J., 2012, *Experimental and numerical evaluation of anisotrpic fill performance characteristics in cross-and counterflow,* MSc thesis, Stellenbosch University, Stellenbosch, South Africa

Klimanek, A., 2013, *Numerical modelling of Natural draft wet-cooling towers,* Archives of computational method in engineering, vol 20, pp. 61-109.

Kranc, S.C.M., 1993, *Performance of counterflow cooling tower with structural packing and maldistribution water flow,* Numerical heat transfer, Part A, Vol. 23, pp.15-127.

Kröger, D.G., 2004, *Air-cooled heat exchangers and cooling towers, Thermal-flow performance evaluation and design,* Penwell Corp., Tulsa, Oklahoma.

Lowe, H.J. and Christie, D.G., 1961, *Heat transfer and pressure drop data on cooling tower packings and model studies of the resistance of natural draft towers to airflow*, Proc. Of the int. Heat transfer conf., Boulder, Colorado.

Majumdar, A.K. and Singhal, A.K., 1983, *VERA2D: Program for 2 D analysis of flow, heat and mass transfer in evaporative cooling towers*, EPRI report CS 2923.

Missimer, J.R. and Brochett, C.A., 1986, *Model tests of the rain zone of a counterflow natural cooling tower*, Proceedings of the 5th IAHR cooling tower workshop, Monterey.

Oosthuizen, H.R., 1995, *Enhancement of cooling tower performance by manipulating of rain zone drop size,* MSc. Eng dissertation, Stellenbosch University, Stellenbosch, South Africa.

Reuter, H.C.R., 2010, *Performance evaluation of a natural draught cooling towers with anisotropic fills,* PhD thesis, Stellenbosch University, Stellenbosch, South Africa.

Rish, R.F., 1961, *The design of a natural draught cooling tower*, Proceedings of the 2nd international heat transfer conference, Boulder, Colorado, USA.

Sedina, M., 1992, *Heat and mass transfer and pressure drop in the rain zone of cooling towers*, Proc. Of the 8th IAHR cooling tower and spraying pond symposium, Karlsruhe, Germany.

Steenmans, D.F., 2010, *Experimental investigation of water droplet impingement on various objects*, BEng (Mech) final year project, University Stellenbosch, Stellenbosch, South Africa.

Terblanche, R., 2008, *Investigation of performance enhancing devices for the rain zones of wet cooling towers,* MSc thesis, University Stellenbosch, Stellenbosch, South Africa.

Terblanche, R., Reuter, H.C.R., Kröger, D.G., 2009, *Drop size distribution below different wet-cooling tower fills,* International journal of applied thermal engineering, No. 29 (2009), pp. 1552-1560.

Williamson, N., Behnia, M. and Armfield, S., 2008, *Comparison of a 2D axisymmetric CFD model of a Natural draught wet cooling tower and a 1D model,* International journal of heat and mass transfer, vol 51, pp 2227-2236.

APPENDIX.A   CALIBRATION

This section contains the calibration details of the instrumentation on the test facility, which include the flow meter, pressure transducers and thermocouples.

A.1 Water flow meter

An Endress and Hauser Promag 10 W electromagnetic flow meter measures the process water flow rate to the counter flow fill performance test section. The current output ranging from 4-20 mA direct current is measured against various flow rates. The flow to the counter flow test section is diverted to a tank next to the test section. The volume of the tank was calibrated by measuring the weight of water that filled the tank. The temperature of the water was also measured to determine the density since it is used for the conversion from mass to volume. The current against flow rate is shown in figure A-1 and the equation describing the curve in equation A-1.
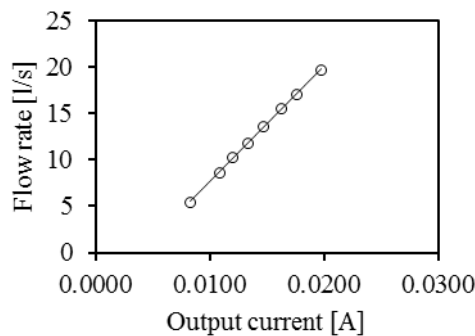
Figure A-1: Calibration curve for flow meter

$\dot{V}=1250.8383I-4.9082, l/s$ $\hspace{4cm}$ $R^2=0.9997$ $\hspace{2cm}$ A-1

A.2 Air flow rate pressure transducer

The air flow rate is calculated from the pressure drop across ASHRAE 51-75 elliptical converging nozzles. This pressure drop is converted to a voltage by an Endress and Hauser Deltbar S PMD75 pressure transducer. A Betz manometer is used for calibrating the pressure transducer. A known pressure output is plotted against a corresponding voltage output and is shown in figure A-2 and calibration curve in equation A-2.

A-1
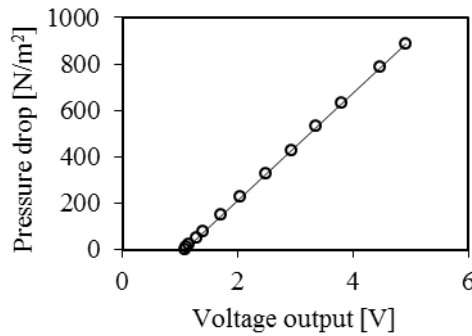
Figure A-2: Calibration curve for 0-10 000 N/m^2 pressure transducer

$$\Delta p_{noz} = 231.5065V - 248.7281 \qquad\qquad R^2 = 0.9999 \qquad\qquad \text{A-2}$$

A.3 Fill pressure drop pressure transducer

Pressure drop across the fill is measured using eight H-taps connected to two Endress and Hauser Deltabar S PMD75 pressure transducers. It is calibrated using a Betz manometer where the pressure drop is plotted against the voltage output. This is shown in figure A-3 a and b and the equation describing the calibration curve shown in equations A.3 and A.4
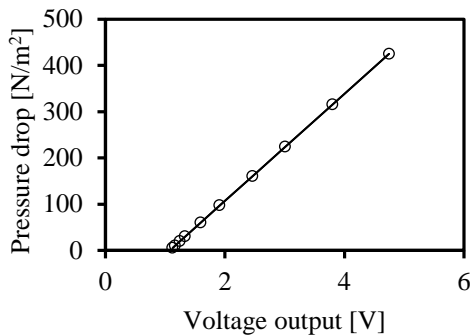
a. 0-1000 N/m^2 pressure transducer   b. 0- 2500 N/m^2 pressure transducer
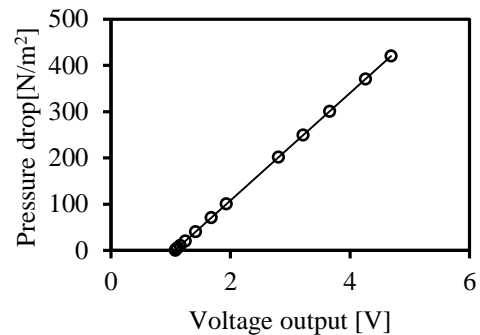
Figure A-3: Calibration curve for pressure transducers outputting pressure drop across fill

$$\Delta p_a = 115.7668V - 124.6738 \qquad\qquad R^2 = 1.0000 \qquad\qquad \text{A-3}$$

$$\Delta p_a = 116.1259V - 124.7574 \qquad\qquad R^2 = 1.0000 \qquad\qquad \text{A-4}$$

A.4 Thermocouple

There are 17 T-type thermocouples used for measuring the water inlet temperature, water outlet temperature, wet-and dry bulb temperature upstream of nozzle and wet-and dry bulb temperature of vertical test section.. Each was calibrated by placing it along with a reference platinum resistance thermometer, in a Fluke 9142 field metrology metal well. The thermocouples were calibrated between 10 and 60 ^{o}C in intervals of 10 ^{o}C and the measured temperature of each thermocouple and resistance as measured by the platinum resistance thermometer recorded. The resistance as measured by the platinum resistance thermometer is converted to a temperature according to a calibration curve and this serves as the reference temperature to which the thermocouples are adjusted to. A linear relationship exists between the reference thermometer and thermocouples according to:

$$T_{ref}=mT_{meas}+c$$

The thermocouples were calibrated within 0.1 ^{o}C from the reference thermometer. The calibration constants are shown in Table A-1

Table A-1: Thermocouple calibration curve constants

Thermocouple	m	c
Water side		
A 1	0.9981	0.7186
A 2	0.9953	0.7742
A 3	1.0008	0.7188
FE 1	1.0152	-0.3270
FE 2	0.9987	0.1780
FE 3	1.0012	0.0973
FW 1	0.9964	0.4946
FW 2	0.9969	0.1860
FW 3	0.9973	0.5994
Air side		
ATn 1	0.9904	1.0947
ATn 1 wb	0.9915	0.9469
ATn 2	0.9900	0.9765
ATn 2 wb	0.9920	0.8380
ATn 3	0.9887	0.7648
ATn 3 wb	0.9892	0.7013
ATn 4	0.9939	0.5972
ATn 4 wb	0.9951	0.6032
AT 1	0.9986	-0.0729
AT 1 wb	1.0009	- 0.0783
AT 2	1.0023	- 0.0924
AT 2 wb	0.9998	- 0.0582
AT 3	1.0055	-0.0839
AT 3 wb	1.0018	0.0928
AT 4	1.0054	0.1927
AT 4 wb	0.9973	0.4999

The deviation of the counter flow test section air side thermocouples before and after calibration is shown in figure A-4
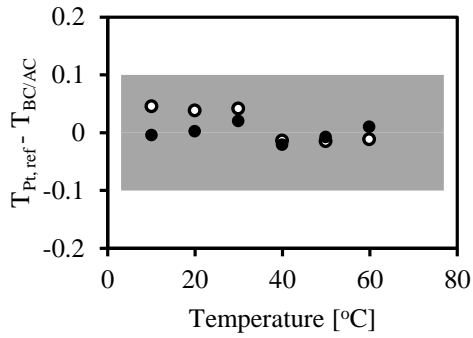
a.   AT 1
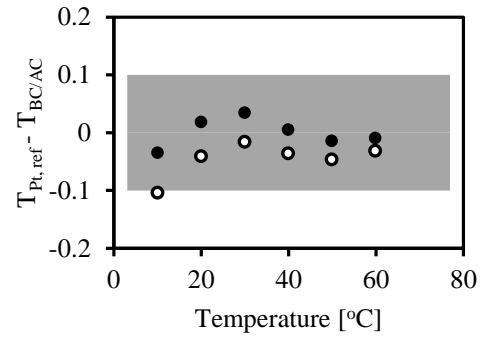
b.   AT 1 wb
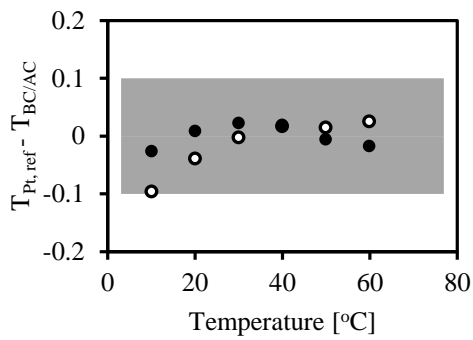
c.   AT 2
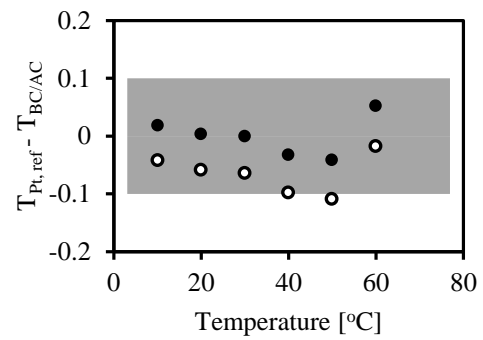
d.   AT 2 wb
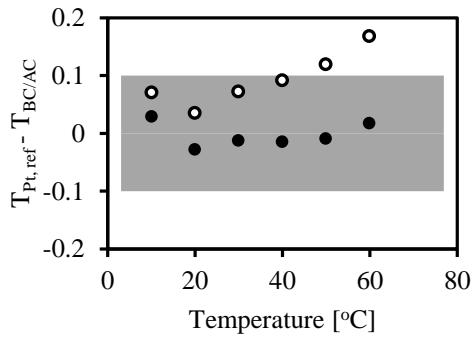
e.   AT 3
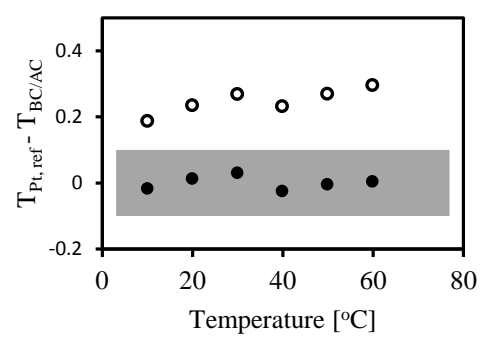
f.   AT 3 wb
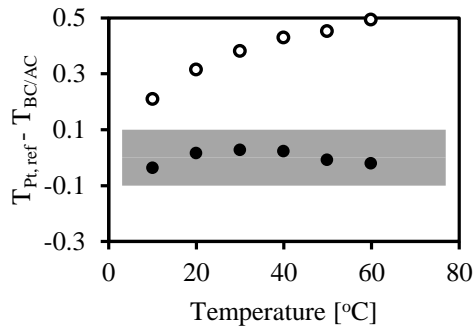
g.   AT 4
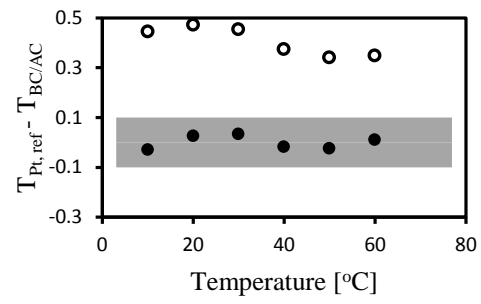
h.   AT 4 wb

Figure A-4: Before and after calibration deviation from the reference temperature for the counter flow test section airside thermocouples

APPENDIX.B   SAMPLE CALCULATION AIR MASS FLOW RATE

The method for determining the air mass flow rate from the pressure drop across the nozzles is covered in this section. An iterative method is utilized to obtain the air mass flow rate from pressure drop across nozzles.

Test conditions:

Atmospheric pressure	p_a =	100 410 N/m^2
Pressure drop across nozzle	dp_{noz} =	48.73 N/m^2
Wetbulb temperature upstream from nozzle	T_{wb} =	13.2 ^{o}C
Dry bulb temperature upstream from nozzle	T_{ai} =	17.55 ^{o}C

Nozzle and system specifications:

Nozzle diameter	d_n =	0.3 m
Nozzle area	A_n =	0.071 m^2
Area upstream from nozzle	A_{tus} =	4 m^2
Number of nozzles	$\#Nozzles$ =	3

The iterative method for calculating the mass flow rate requires the specification of an initial mass flow rate. An initial mass flow rate is calculated using Bernoulli. This is shown below.

Thermophysical properties:

Vapour pressure	p_{vap} =	1515 N/m^2
Humidity ratio	w =	0.011
Air-vapour density	ρ_{av} =	1.195 kg/m^3

The air mass flow rate is calculated from Bernoulli, equation B-1 shown below

$$\dot{m}_{Bernoulli} = \#\,nozzles \left(\frac{\left(2\left(\frac{dp_{noz}}{\rho_{av}}\right)^{0.5}\right)}{\left[\left(\frac{1}{A_n^2}-\frac{1}{A_{tus}^2}\right)^{0.5}\left(\frac{1}{\rho_{av}}\right)\right]} \right) \qquad \text{B-1}$$

= 2.289 kg/s

As mentioned before the mass flow rate calculated using equation B-1 serves only as an initial guess. There are two underlying assumptions made leading to inaccuracies by using equation 1-1 the iterative method does not make. These assumptions include constant fluid properties before and after the nozzle and a flat

velocity profile. This value calculated using the Bernoulli equation does however serve as a good initial guess. The iterative method is shown below.

The parameters shown in equation B-2 are calculated below.

$$m_{avn} = C_n \phi_g Y A_n \left(2\rho_{avn} dp_n\right)^{0.5} \qquad \text{B-2}$$

The nozzle discharge coefficient, C_n, is a function of Reynolds number according to:

For $3 \times 10^4 < Re_n < 10^5$

$$C_n = 0.954803 + 6.37817 \times 10^{-7} Re_n - 4.65394 \times 10^{-12} Re_n^2 + 1.3351 \times 10^{-17} Re_n^3 \qquad \text{B-3}$$

For $10^5 < Re_n < 3.5 \times 10^5$

$$C_n = 0.9758 + 1.08 \times 10^{-7} Re_n - 1.6 \times 10^{-13} Re_n^2 \qquad \text{B-4}$$

For $Re_n > 3.5 \times 10^5$

$$C_n = 0.994 \qquad \text{B-5}$$

Where $Re_n = \frac{(m_{avn} d_n)}{\mu_{avn} A_n}$.

The gas expansion factor, according to Kröger (2004)

$$\phi_g = 1 - 3\left(\frac{dp_{noz}}{4p_{ai}1.4}\right) \qquad \text{B-6}$$

The approach velocity, as given by Kröger (2004)

$$Y = 1 + 0.5\left(\frac{A_n}{A_{up}}\right)^2 + 2\left(\frac{A_n}{A_{up}}\right)^2 \frac{dp_{noz}}{1.4p_{ai}} \qquad \text{B-7}$$

The inlet density is necessary for calculating the mass flow rate, however it is a function of the inlet pressure, which is given by:

$$p_{ai} = p_{atm} - p_{dyn} \qquad \text{B-8}$$

Where the dynamic pressure is given by

$$p_{dyn} = 0.5\rho_{avi} v_{ai}^2 \qquad \text{B-9}$$

Assuming the mass flow rate stays approximately constant through the nozzle the inlet velocity is given by

$$v_{ai} = \frac{m_{av}}{\rho_{avi}A_{fr}}$$ B-10

It can be seen from the relations above that the inlet pressure is a function of the dynamic pressure, which is a function of the inlet velocity, which is a function of the mass flow rate, which is in turn a function of the inlet pressure. It becomes apparent that an iterative solution is required. The mass flow rate was found to be:

$m_{avn} = 2.267$ kg/s

APPENDIX.C   SAMPLE CALCULATION MERKEL NUMBER AND LOSS COEFFICIENT

The sample calculation presented in this section illustrates the calculation of the Merkel number and loss coefficient using the Merkel method of analysis.

Test conditions:

Atmospheric pressure	p_a =	100 700 N/m^2
Air inlet temperature	T_{ai} =	8.08 ^{o}C
Wet bulb temperature	T_{wb} =	6.35 ^{o}C
Dry air mass flow rate	m_a =	4.44 kg/s
Pressure drop across fill	Δp_{fi} =	22.13 N/m^2
Water inlet temperature	T_{wi} =	39.61 ^{o}C
Water outlet temperature	T_{wo} =	20.16 ^{o}C
Water mass flow rate (in)	m_w =	3.36 kg/s
Gravitational acceleration	g =	9.81 m/s^2

Fill specifications:

Fill height	L_{fi} =	0.61 m
Fill frontal area	A_{fr} =	2.25 m^2

Merkel number

The Merkel number expression as shown in equation C-1

$$\frac{h_d a_{fi} L_{fi}}{G_w} = \int_{T_{wo}}^{T_{wi}} \frac{c_{pw}}{i_{masw} - i_{ma}} dT_w \qquad \text{C-1}$$

Chebyshev method is used to approximate the integral numerically as given by equation C-2

$$\int_a^b f(x)dx = \frac{b-a}{4}(f(x_1) + f(x_2) + f(x_3) + f(x_4)) \qquad \text{C-2}$$

The function is evaluated at intermediate position along the cooling tower height, x as shown below

$f(x_1)$ for $x_1 = a + 0.1(b-a)$

$f(x_2)$ for $x_2 = a + 0.4(b-a)$

$f(x_3)$ for $x_3 = a + 0.6(b-a)$

f(x₄) for x_4 = a + 0.9(b-a)

The Merkel number in the form of the Chebyshev numerical integral given in equation C-3

$$\int_{T_{wo}}^{T_{wi}} \frac{c_{pw}}{(i_{masw} - i_{ma})} dT_w = \frac{(T_{wi}-T_{wo})}{4}\left(\frac{c_{pw1}}{\Delta i_1} + \frac{c_{pw2}}{\Delta i_2} + \frac{c_{pw3}}{\Delta i_3} + \frac{c_{pw4}}{\Delta i_4}\right)$$ C-3

Assuming the specific heat of water between the inlet and outlet temperature stays approximately constant the Merkel number reduces to equation C-4

$$\frac{h_d a_{fi} L_{fi}}{G_w} = \frac{c_{pwm}(T_{wi}-T_{wo})}{4}\left(\frac{1}{\Delta i_1} + \frac{1}{\Delta i_2} + \frac{1}{\Delta i_3} + \frac{1}{\Delta i_4}\right)$$ C-4

The intermediate temperatures at which the enthalpy differentials in the Chebyshev integral are calculated at are shown below.

$T_{w1} = T_{wo} + 0.1(T_{wi} + T_{wo})$ $T_{w1} = 22.11^\circ$C

$T_{w2} = T_{wo} + 0.4(T_{wi} + T_{wo})$ $T_{w2} = 27.94^\circ$C

$T_{w3} = T_{wo} + 0.6(T_{wi} + T_{wo})$ $T_{w3} = 31.83^\circ$C

$T_{w4} = T_{wo} + 0.9(T_{wi} + T_{wo})$ $T_{w4} = 37.67^\circ$C

The mean specific heat of water evaluated at $T_{wm} = \frac{T_{wi}+T_{wo}}{2}$, $T_{wm} = 29.89^\circ$C

Heat capacity of water c_{pwm} =   4179 J/kg K

The entering air enthalpy is used to determine the enthalpy away from the air water interface. The entering air thermophysical properties for determining the inlet air enthalpy.

Entering air thermophysical properties:

Specific heat of dry air c_{pai} =   1006 J/kg K
Specific heat of water vapour c_{pvi} =   1866 J/kg K
Vapour pressure p_{vi} =   958.31 N/m²
Humidity ratio of entering air w_i =   0.005
Enthalpy of entering air i_{mai} =   2.502×10⁶ J/kg

Enthalpy differential 1 thermophysical properties

Specific heat of dry air c_{pa1} =   1007 J/kg K
Specific heat of water vapour c_{pv1} =   1872 J/kg K
Vapour pressure p_{v1} =   2662 N/m²
Humidity ratio of saturated air w_{s1} =   0.017

C-2

The enthalpy of saturated air at T_{w1}

$i_{masw1} = c_{pa1}(T_{w1}\text{-}273.15)+w_{s1}[i_{ifwo}+c_{pv1}(T_{w1}\text{-}273.15)]$

= 65 421 J/kg

$i_{ma1} = \dfrac{m_w c_{pwm}(T_{w1}\text{-}T_{wo})}{m_a}+i_{mai}$

= 27 616 J/kg K

Enthalpy of the air away from the air water interface at position $x = x_1$

With the enthalpy of the air at the air water interface and away from the air water interface known find the enthalpy differential at position $x = x_1$

$\Delta i_1 = (i_{masw1} - i_{ma1})$

= 37 880 J/kg K

Similarly for intermediate enthalpies for 2, 3 and 4

$\Delta i_2 = 44\ 231$ J/kg
$\Delta i_3 = 52\ 392$ J/kg
$\Delta i_4 = 72\ 403$ J/kg

The Merkel number is found to be

$Me = \dfrac{c_{pwm}(T_{wi}\text{-}T_{wo})}{4}\left(\dfrac{1}{\Delta i_1}+\dfrac{1}{\Delta i_2}+\dfrac{1}{\Delta i_3}+\dfrac{1}{\Delta i_4}\right)$

= 1.66

Loss coefficient

The pressure drop across the fill is due to frictional- and drag force and difference in momentum. The buoyancy effect due to the difference in density counteracts these losses, however loss still occurs since these forces don't balance out. The

$\Delta p_{fi} = \Delta p_{fd}+(\rho_{avo}v_{avo}^2\text{-}\rho_{avo}v_{avi}^2)\text{-}(\rho_{ava}\text{-}\rho_{avm})gL_{fi}$ C-5

equation shown below formulates this effect.

It is of interest to know frictional drag force (Δp_{fd}) since this is caused by the fill. This term can however not be determined directly. It is a function of the fill design and along with the Merkel number is a characteristic of the fill. It is normally expressed as a loss coefficient as shown in equation

$K_{fd} = \dfrac{2\Delta p_{fd}}{\rho v^2}$ C-6

Rearranging equation C-5 and substituting it in equation C-6 above gives the following expression for the loss coefficient:

$$K_{fd} = \frac{2\left[\Delta p_{fi} - (\rho_{avo}v_{avo}^2 - \rho_{avi}v_{avi}^2) + (\rho_{avi} - \rho_{avm})gL_{fi}\right]}{\rho v^2}$$
C-7

The loss coefficient is based upon mean vapour flow rate and density. Equation C-7 is substituted with the mean air vapour properties and the velocity, which is written in terms of mean mass flow rate, as shown in equation C-8

$$K_{fd} = \frac{2\left[\Delta p_{fi} - (\rho_{avo}v_{avo}^2 - \rho_{avi}v_{avi}^2) + (\rho_{avi} - \rho_{avm})gL_{fi}\right]\rho_{avm}A_{fr}^2}{m_{avm}^2}$$
C-8

The inlet air density is required for the calculation of the in air mass flow rate. The inlet air flow rate is found to be:

$$m_{avi} = ma + w_i m_a$$

$$= 4.45 \ \text{kg/s}$$

The inlet air velocity is then found to be

$$v_{avi} = \frac{m_{avi}}{\rho_{avi}A_{fr}}$$

$$= 1.64 \ \text{m/s}$$

From an energy balance it is known that the change in enthalpy for the air must be the same as the change in enthalpy for the water. This is shown below:

$$m_a(i_{mao} - i_{mai}) = m_w c_{pwm}(T_{wi} - T_{wo})$$

Rearranging the equation above to isolate the outlet air enthalpy (i_{mao}) the expression below is obtained.

$$i_{mao} = \frac{m_w c_{pwm}(T_{wi} - T_{wo})}{m_a} + i_{mai}$$

$$= 82\ 895 \ \text{J/kg}$$

It is also assumed that the air leaving the fill is saturated which means the condition of the outlet air is known and thus the following expression shown below can also be used to calculate the enthalpy at the outlet.

$$i_{ma} = c_{pa}(T - 273.15) + w[i_{fgwo} + c_{pv}(T - 273.15)]$$

All the properties used in the equation shown above are a function of the outlet temperature. This can be found through an iterative method by minimising the difference between the outlet enthalpies. $T_{ao} = 24.28 \ ^\circ\text{C}$ is taken as the initial guess. To assess the correctness of the iterative solution all the necessary thermophysical properties are determined at the final outlet temperature.

Entering air thermophysical properties

Specific heat of dry air	c_{pao}	=	1007 J/kg K
Specific heat of water vapour	c_{pvo}	=	1873 J/kg K
Vapour pressure	p_{vo}	=	3036 N/m^2
Humidity ratio of entering air	w_{si}	=	0.019
Enthalpy of entering air	i_{mao}	=	73 940 J/kg K

C-4

The outlet air mass flow rate is found to be

$$m_{avo} = m_a + w_{so}m_a$$

$$= 4.486 \ \text{kg/s}$$

And the outlet air velocity to be:

$$v_{avo} = \frac{m_{avo}}{\rho_{avo}A_{fr}}$$

$$= 1.73 \ \text{m/s}$$

The arithmetic mean mass flow rate through the fill

$$m_{avm} = \frac{m_{avi} + m_{avo}}{2}$$

$$= 4.486 \ \text{kg/s}$$

The harmonic mean density through the fill

$$\rho_{avm} = 2\left(\frac{1}{\rho_{avi}} + \frac{1}{\rho_{avo}}\right)^{-1}$$

$$= 1.185 \ \text{kg/m}^3$$

The loss coefficient is found to be

$$K_{fdm} = \frac{2\left[\Delta p_{fi} - (\rho_{avo}v_{avo}^2 - \rho_{avi}v_{avi}^2) + (\rho_{avi} - \rho_{avm})gL_{fi}\right]\rho_{avm}A_{fr}^2}{m_{avm}^2}$$

$$= 13.35$$

APPENDIX.D   SAMPLE CALCULATION RAIN ZONE DROP SIZE

The drop size in the rain zone below a cross fluted film fill is calculated from the Kröger purely counter flow model. The following conditions and parameters are used in calculating the rain zone's Merkel number.

Experimental conditions:

Atmospheric pressure	p_{atm}	=	101 460 N/m^2
Ambient temperature	T_{a1}	=	5.962 °C
Wetbulb temperature	T_{wb}	=	5.185 °C
Water outlet temperature	T_{wo}	=	16.767 °C
Air mass flow rate	m_a	=	4.605 kg/s
Air mass flow rate	m_{av1}	=	4.629 kg/s
Water vapour gas constant	R_v	=	461.5 J/kgK
Gravitational acceleration	g	=	9.8 m/s^2
Frontal area	A_{fr}	=	2.25 m^2
Drop diameter	d_d	=	0.0035 m
Rain zone height	H_{rz}	=	3.88 m

Thermophysical properties:

Inlet air humidity ratio	w_1	=	0.005
Inlet air density	ρ_{av1}	=	1.262, kg/m^3
Inlet air viscosity	μ_{av1}	=	1.744×10^{-5} kg/ms
Density of water	ρ_w	=	998.735, kg/m^3
Surface tension of water	σ_w	=	0.073, N/m
Humidity ratio of saturated air at outlet water conditions	w_{so}	=	0.012

The air outlet velocity

It is assumed that the air exiting the rain zone and entering the fill is at the same conditions as measured by the aspirated psychrometers. The resulting air velocity is thus found by the relation shown below.

$$v_{out} = m_{av1}/(\rho_{av1}A_{fr})$$

$= 1.630$ m/s

Schmidt number

$$Sc = \mu_{avl}/(\rho_{avl}D)$$

$=0.762$

The "a" coefficients

$$a_\rho = 998/\rho_w$$

$=0.999$

$$a_\mu = 3.061 \times 10^{-6} \left(\frac{\rho_w^4 g^9}{\sigma_w}\right)^{0.25}$$

$=0.999$

$$a_v = 73.298 \left(\frac{g^5 \sigma_w^3}{\rho_w^3}\right)^{0.25}$$

$=1.007$

$$a_L = 6.122 \left(\frac{g\sigma_w}{\rho_w}\right)^{0.25}$$

$=1.002$

The rain zone Merkel number using Kröger purely counterflow model

$$\frac{\square_{drz} a_{rz} H_i}{G_w} = 3.6 \left(\frac{p_{atm}}{R_v T_a \rho_w}\right) \left(\frac{D}{v_{out} d_d}\right) \left(\frac{H_i}{d_d}\right) Sc^{0.33} \left[\frac{\ln\left(\frac{w_s + 0.622}{w + 0.622}\right)}{w_s - w}\right]$$

$\times [5.01134 a_\rho \rho_a - 192121.7 a_\mu \mu_a - 2.57724$

$+23.61842\{0.2539(a_v v_{out})^{1.67} + 0.18\}$

$\times \{0.83666(a_L H_i)^{-0.5299} + 0.42\}\{43.0696(a_L d_d)^{0.7947}$

$+0.52\}]$

$=0.222$

The experimental rain zone Merkel number was however found to be

$$\left(\frac{\square_{drz} a_{rz} H_i}{G_w}\right)_{Exp} = 0.479$$

A rain zone droplet size is obtained by following an iterative procedure of minimizing the difference between the calculated rain zone Merkel number and experimentally obtained Merkel number. The rain zone droplet was found to be 2.203 mm

APPENDIX.E SAMPLE CALCULATION MODELLING OF A NDWCT USING A ONE DIMENSIONAL MODEL

This section covers the sample calculation for the NDWCT one dimensional model as given by Kröger (2004) example 7.3.2. The sample calculation is used for verification of the model which is used to do a parametric study and determine its effect on the heat rejection rate and cooling tower approach. Figure E-1 shows a labelled tower used for the sample calculation.
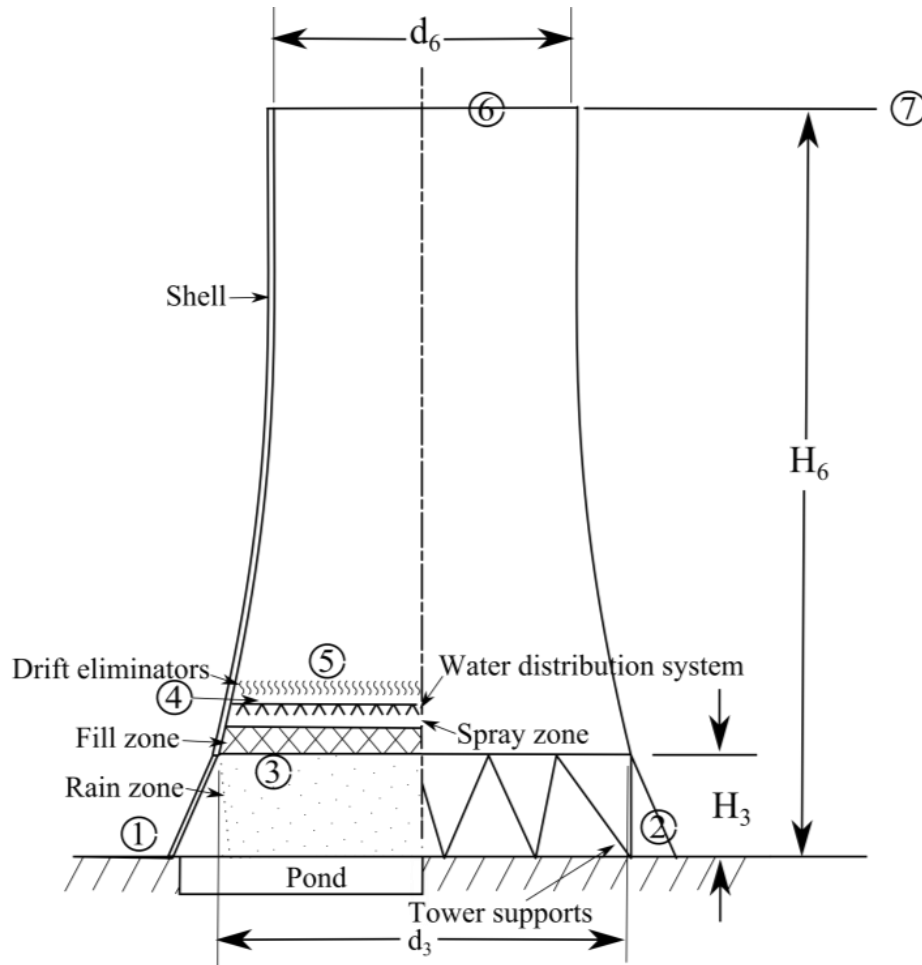
Figure E-1: Notated counter flow NDWCT

The input parameters are shown below.

Water conditions:

Water mass flow rate	m_w	=	12 500 kg/s
Water inlet temperature	T_{w5}	=	40 °C

Ambient conditions:

Air temperature at ground level	T_{a1}	=	15.45 $^{\circ}$C
Wetbulb temperature at ground level	T_{a1wb}	=	11.05 $^{\circ}$C
Atmospheric pressure	p_{a1}	=	84100 N/m^2
Ambient temperature gradient	dT_a/dz	=	-0.00975 K/m

Cooling tower specifications:

Tower height	H_6	=	147 m
Tower inlet height	H_3	=	10 m
Tower inlet diameter	d_3	=	104.5 m
Tower outlet diameter	d_6	=	60.85 m
Number of tower supports	n_{ts}	=	72
Length of tower supports	L_{ts}	=	11.6 m
Diameter of support	d_{ts}	=	0.8 m
Drag coefficient of tower support (round)	C_{Dts}	=	1.0
Shell thickness (inlet)	t_s	=	1.0 m

Fill specifications:

Fill height	L_{fi}	=	2.504 m

Fill performance characteristics:

Transfer coefficient:

$Me_{fi}(G_w, G_a) = 0.25575\ G_w^{-0.094}\ G_a^{0.6023}$

Loss coefficient:

$K_{fdm1}(G_w, G_a) = 1.851 G_w^{1.2752} G_a^{-1.0356}$

Other specifications:

Frontal area of fill	A_{fr}	=	8300 m^2
Depth of spray zone above fill	L_{sp}	=	0.5 m
Mean drop diameter in rain zone	d_d	=	0.0035 m

An iterative method is employed to solve this problem. Selecting the parameters as listed below solves both the energy and draught equation.

Iteration parameters:

Air-vapour mass flow rate through the fill	m_{av15}	=	16 808.98 kg/s
Pressure after drift eliminators	p_{a5}	=	83 937.72 N/m^2
Air temperature after drift eliminators	T_{a5}	=	26.44 ^{o}C
Mean temperature of water in basin	T_{wo}	=	21.39 ^{o}C
Pressure at tower outlet	p_{a6}	=	82 650.58 N/m^2

The thermophysical properties at the tower inlet conditions.

Thermophysical properties at tower inlet:

Air-vapour density	ρ_{av1}	=	1.0101 kg/m^3
Humidity ratio of air	w_1	=	0.008127 kg/kg dry air
Heat capacity of dry air	c_{pa1}	=	1006.44 J/kg.K
Heat capacity of water vapour	c_{pv1}	=	1869.2 J/kg.K
Latent heat at 273.15 K	i_{fgwo}	=	2.5016×10^6 J/kg.K
Enthalpy of the inlet air	i_{ma1}	=	36114.71 J/kg

Thermophysical properties immediately after the drift eliminators where it is assumed the air is saturated i.e. $T_{a5} = T_{awb5}$

Thermophysical properties immediately after the drift eliminators:

Saturated vapour pressure	p_{v5}	=	3445.27 N/m^2
Air-vapour density	ρ_{av5}	=	0.96079 kg/m^3
Humidity ratio of air	w_5	=	0.02676
Heat capacity of dry air	c_{pa5}	=	1006.5515 J/kgK
Heat capacity of water vapour	c_{pv5}	=	1873.812 J/kgK
Latent heat at 273.15 K	i_{fgwo}	=	2.5016×10^6 J/kgK
Dynamic viscosity of air	μ_{a5}	=	1.84×10^{-5} kg/ms
Dynamic viscosity of water vapour	μ_{v5}	=	1.0032×10^{-5} kg/ms
Dynamic viscosity of air-vapour	μ_{av5}	=	1.8173×10^{-5} kg/ms
Enthalpy of air immediately after drift eliminators	i_{ma5}	=	94865.621 J/kg

Thermophysical properties at water outlet:

Density of water	ρ_{wo}	=	997.8696 kg/m^3
Surface tension	σ_{wo}	=	0.07256 N/m

The harmonic mean density of air –vapour through the fill

$\rho_{av15} = 2/(1/\rho_{av1} + 1/\rho_{av5}) = 2/(1/1.0101+1/0.96079) = 0.9848$ kg/m^3

Mass flow rates:

The dry air mass flow rate is calculated as shown below

$m_a = (2m_{av15})/(2+w_1+w_5) = 2\times16\ 808.4/(2+0.008127 + 0.02676) = 16\ 520.57$ kg/s

Mass flow rate at position 1 and 5 from fig D-1 can be found to be:

$m_{av1} = m_a(1+w_1) = 16\ 520.57(1+0.008127) = 16\ 654.83$ kg/s

$m_{av5} = m_a(1+w_5) = 16\ 520.57(1+0.02676) = 16\ 963.13$ kg/s

Mass velocities:

The corresponding mass velocities are as follows:

$G_{av15} = m_{av15}/A_{fr} = 16\ 808.98/8\ 300 = 2.02518$ kg/s m^2

$G_a = m_a/A_{fr} = 16\ 520.57/8\ 300 = 1.99043\ kg/s\ m^2$

$G_{av1} = m_{av1}/A_{fr} = 16\ 654.83/8\ 300 = 2.007$ kg/sm^2

$G_{av5} = m_{av5}/A_{fr} = 16\ 963/8\ 300 = 2.04375$ kg/sm^2

$G_w = m_w/A_{fr} = 12\ 500/8\ 300 = 1.50602$ kg/sm^2

The heat and mass transfer in the cooling tower evaluation is dependent upon the frontal area of the cooling tower. However the frontal area is reduced due to flow distortion caused by the various flow resistances. An effective frontal area must thus be calculated. The loss coefficients of the various flow resistances are required to determine the effective frontal area.

Loss coefficients:

The specified loss coefficient due to the fill support structure and contraction loss of the fill is shown below.

$K_{fsfi} + K_{ctcfi} = (\rho_{av15}/\rho_{av1})(m_{av1}/m_{av15})^2 = 0.5(0.9848/1.0101)(16\ 654.83/16\ 808.4)^2$

$= 0.4786$

The specified fill loss coefficient

$K_{fdm} = 1.851L_{fi}G_w^{1.2752}G_a^{-1.0356} = 1.851\times2.504\times1.50602^{1.2752}\times1.99043^{-1.0356} = 3.83021$

The actual cooling tower fill loss coefficient relation is shown below

$$K_{fi} = K_{fdm} + (G_{av5}^2/\rho_{av5} - G_{av1}^2/\rho_{av1})/(G_{av15}^2/\rho_{av15})$$

$$= 3.83021 + (2.04375^2/0.96079 - 2.007^2/1.0101)/(2.02957^2/0.98484) = 3.90828$$

The expansion loss coefficient

$$K_{ctefi} = \left(1 - A_{fr}/A_3\right)^2 \left(\rho_{av15}/\rho_{av5}\right)(m_{av5}/m_{av15})^2$$

$$= \left[1 - 8\,300 \times \frac{4}{\pi \times 104.52^2}\right]^2 \times \left(\frac{0.98484}{0.96079}\right) \times \left(\frac{16\,963.13}{16\,808.4}\right)^2 = 0.00109$$

Loss coefficient through the spray zone above the fill

$$K_{spfi} = L_{sp}[0.4(G_w/G_a) + 1]\left(\rho_{av15}/\rho_{av5}\right) \times (m_{av5}/m_{av15})^2$$

$$= 0.5[0.4(1.506/1.995) + 1] \times (0.98/0.96) \times (16\,963.13/16\,808.4)^2 = 0.67995$$

The specified loss coefficient for the water distribution system

$$K_{wdfi} = 0.5\left(\rho_{av15}/\rho_{av5}\right)(m_{av5}/m_{av15})^2 = 0.5(0.98/0.96)(16\,963.13/16\,808.4)^2 = 0.5219$$

The loss coefficient for the specified type c drift eliminators based on fill conditions

$$K_{defi} = 27.4892\left[m_{av5}/(\mu_{av5}\ A_{fr})\right]^{-0.14247}\left(\rho_{av15}/\rho_{av5}\right) \times (m_{av5}/m_{av15})^2$$

$$= 27.4892\left[\frac{16\,963.13}{1.8 \times 10^{-5} \times 8\,300}\right]^{-0.14247} \times (0.98/0.96)(16\,963.13/16\,808.04)^2 = 5.47101$$

Sum of these loss coefficients

$$\left(K_{fs} + K_{ctc} + K_{fi} + K_{cte} + K_{sp} + K_{wd} + K_{de}\right)_{fi}$$

$$= 0.4786 + 3.9082 + 0.0011 + 0.6796 + 0.5219 + 5.4710 = 11.07164$$

The effective fill diameter

$$d_{e3} = [1.27 - 0.16722\ln(d_3/H_3) + \{0.043653\ln(d_3/H_3) - 0.062658\}$$

$$\times \ln\left(K_{fs} + K_{ctc} + K_{fi} + K_{cte} + K_{sp} + K_{wd} + K_{de}\right)_{fi}]$$

$$= 104.5[1.27 - 0.17\ln\left(\frac{104.5}{10}\right) + \left\{0.044\ln\left(\frac{104.5}{10}\right) - 0.063\right\}\ln(11.07164)] = 101.7 \text{ m}$$

The corresponding effective frontal area is as follows

$$A_{fre} = \pi d_{e3}^2/4 = \pi \times 101.7^2/4 = 8123.3 \text{ m}^2$$

The effective frontal area is approximately equal to the frontal area. This means that the frontal area will still be used in subsequent calculations.

The loss coefficient due to the tower supports

$$K_{tsfi} = \left[\frac{C_{dts}\ L_{ts}\ d_{ts}\ n_{ts}\ A_{fr}^2}{(\pi d_3\ H_3)^3}\right]\left(\rho_{av15}/\rho_{av1}\right)(m_{av1}/m_{av15})^2$$

$$= \left[1\times 11.6\times 0.8\times 72\times \frac{8\,300^2}{(\pi\times 104.5\times 10)^3} \right](0.98/1.01)(16\,654.8/16\,808.04)^2 = 1.2452$$

Tower inlet loss coefficient

$$K_{ctfi} = 1.5\exp(0.2d_3/H_3)\left(\rho_{av15}/\rho_{av1}\right)(m_{av1}/m_{av15})^2\left[4A_{fr}/(\pi d_3^2)\right]^2$$

$$\times [K_{fs}+K_{ctc}+K_{fi}+K_{cte}+K_{sp}+K_{wd}+K_{de}]_{fi}^{\left[-0.4645+\frac{0.2303d_3}{H_3}-0.00095\left(\frac{d_3}{H_3}\right)^2\right]}$$

$$= 1.5\exp\left(0.2\times\frac{104.5}{10}\right)\left(\frac{0.98484}{1.0101}\right)\left(\frac{16\,654.8}{16\,808.04}\right)^2\left[4\times\frac{8\,300}{\pi\times 104.5^2}\right]^2$$

$$\times 11.0605^{\left[-0.4645+0.02303\times\frac{104.5}{10}-0.00095\left(\frac{104.5}{10}\right)^2\right]} = 4.9453$$

Rain zone loss coefficient

$$K_{rz} = 3a_v v_{w3}\left(\frac{H_3}{d_d}\right)[0.22460-0.31467a_\rho\rho_{av1}+5263.04a_\mu\mu_{av1}+0.775526$$

$$\times\{1.4824163\exp(71.52a_L d_d)-0.91\}\{0.39064\exp(0.010912a_L d_3)$$

$$-0.17\}\{2.0892(a_v v_{av3})^{-1.3944}$$

$$+0.14\}\exp[\{0.8449\ln\left(\frac{a_L d_3}{2}\right)-2.312\}\times\{0.3724\ln(a_v v_{av3})+0.7263\}\ln\{206.757(a_L H_3)^{-2.83}$$

$$+0.43\}]]$$

$$=3\times1.0008\times0.001509\left(\frac{10}{0.0035}\right)[0.22460-0.31467\times1.0001\times1.0101+5263.04\times1.7857$$

$$\times10^{-5}+0.775526\{1.4824163\exp(71.52\times1.0003\times0.0035)-0.91\}\{0.39064\exp(0.010912$$

$$\times1.0003\times104.5)$$

$$-0.17\}\times[2.0892(1.0009\times1.9972)^{-1.3944}+0.14]\exp\{(0.8449\ln(1.0003\times104.5/2)-2.312\}$$

$$\times\{0.3724\ln(1.008\times1.99)+0.7263\}\times\ln(206.757(1.000\times10)^{-2.8344}+0.43\}]]$$

$$=7.22370$$

Transfer coefficients:

The parameters for the rain zone transfer coefficient. The "a" coefficients as shown below.

$$a_\mu = 3.061\times10^{-6}\left(\rho_{wo}^4\,g^9/\sigma_{wo}\right)^{0.25} = 3.061\times10^{-6}\left(997.84^4\times9.8^9/0.07257\right)^{0.25} = 1.0000$$

$$a_\rho = 998/\rho_{wo} = 998/997.87 = 1.0001$$

$$a_v = 73.298\left(g^5\sigma_{wo}^3/\rho_{wo}^3\right)^{0.25} = 73.298\left(9.8^5\times0.07257^3/997.87^3\right)^{0.25} = 1.0008$$

$$a_L = 6.122\left(g\sigma_{wo}/\rho_{wo}\right)^{0.25} = 6.122(9.8\times0.07257/997.87)^{0.25} = 1.0003$$

Schmidt number

$$Sc = \mu_{av1}/(\rho_{av1}D_1) = 1.7857\times10^{-5}/(1.0101\times2.2997\times10^{-5}) = 0.7687$$

The humidity ratio of saturated air at T_{w1} and diffusion coefficient at inlet conditions are given below

Humidity ratio of saturated air	w_{s1}	=	0.01950
Diffusion coefficient	D_1	=	2.2997×10^{-5} m^2/s

The air vapour velocity before the fill

$$v_{av3} = m_{av1}/(\rho_{av1}A_{fr})=1.99083 \text{ m/s}$$

Rain zone transfer coefficient

$$Me_{rz} = 12\left(\frac{D_1}{v_{av3}}\right)\left(\frac{H_3}{d_d}\right)\left(\frac{p_{a1}}{R_{wv}T_{a1}\rho_{wo}}\right)Sc^{0.33}\left[\frac{\ln\left(\frac{w_{s1}+0.622}{w_1+0.622}\right)}{w_{s1}-w_1}\right] \times [0.90757a_\rho\rho_{av1}$$

$$-30341.04a_\mu\mu_{av1}-0.37564 + 4.04016[\{0.55+41.7215\times(a_Ld_d)^{0.80043}\}$$
$$\times\{0.713+3.741(a_LH_3)^{-1.23456}\}\{3.11\exp(0.15a_vv_{av3})-3.13\}$$
$$\times\exp[\{5.3759\exp(-0.2092a_LH_3)\}\ln\{0.3719\times\exp(0.0019055a_Ld_3)$$
$$+0.55\}]]]$$

$$=12\left(\frac{2.2997\times10^{-5}}{1.9908\times0.0035}\right)\left(\frac{10}{0.0035}\right)\times\left(\frac{\frac{84100}{461.52\times288.6}}{997.87}\right)0.7687^{0.33}$$

$$\times[\ln\left(\frac{0.01950+0.622}{0.008127+0.622}\right)/(0.0195-0.008127)][0.90757\times1.00\times1.0101-30341.0$$
$$\times1.7857\times10^{-5}-0.37564+4.04016\times[\{0.55+41.7215(1.0003\times0.0035)^{0.80043}\}\times\{0.713$$
$$+3.741(1.0003\times10)^{-1.23456}\}\{3.11\exp(0.15\times1.0008\times1.9908)-3.13\}$$
$$\times\exp[\{5.3759(\exp(-0.2092\times1.0003\times10)\}\ln\{0.3719\exp(0.0019\times1.0003\times104.5)+0.55\}]]]$$
$$=0.414382$$

Fill transfer coefficient

$$Me_{fi} = 0.25575L_{fi}G_w^{-0.094}G_a^{0.6023}= 0.25575\times2.504\times1.50602^{-0.094}\times1.99043^{0.6023}$$

$$=0.932802$$

The spray zone transfer coefficient

$$Me_{sp} = 0.2L_{sp}(G_a/G_w)^{0.5}= 0.2\times0.5(1.99043/1.50602)^{0.5}$$

$$=0.114963$$

Overall transfer coefficient

$$Me_{rz} + Me_{fi} + Me_{sp} = 0.414382+0.932802+0.114963$$

$$=1.462147$$

The total Merkel ($Me_{rz} + Me_{fi} + Me_{sp} = Me_{CT}$) number can also be calculated using the Merkel method as shown below

$$\int_{T_{wo}}^{T_{wi}}\frac{c_{pw}dT_w}{i_{masw}-i_{ma}} \approx \frac{c_{pwm}(T_{wi}-T_{wo})}{4}\left(\frac{1}{\Delta i_1}+\frac{1}{\Delta i_2}+\frac{1}{\Delta i_3}+\frac{1}{\Delta i_4}\right)$$

The enthalpy differentials shown in the equation above are calculated at the following intermediate temperatures

$$T_{wi} = T_{wo}+0.1(T_{wi}-T_{wo}) = 294.526+0.1(313.15-294.526)=296.3884 \text{ K}$$

$$T_{w2} = T_{wo}+0.4(T_{wi}-T_{wo}) = 294.526+0.4(313.15-294.526)=301.9756 \text{ K}$$

$$T_{w3} = T_{wo}+0.6(T_{wi}-T_{wo}) = 294.526+0.6(313.15-294.526)=305.7004 \text{ K}$$

$$T_{w4} = T_{wo}+0.9(T_{wi}-T_{wo}) = 294.526+0.9(313.15-294.526)=311.2876 \text{ K}$$

E-7

In order to calculate the enthalpy differentials the thermophysical properties is calculated at their respective temperatures. This is done for T_{w1}.

Thermophysical properties at T_{w1}

Specific heat of air	c_{pa1}	=	1006.516 J/kg K
Specific heat of water vapour	c_{pv1}	=	1872.466 J/kg K
Pressure of the water vapour	p_{vs1}	=	2849.024 J/kg K
Humidity ratio	w_{s1}	=	0.021944 J/kg K

The corresponding enthalpy at T_{w1}

$$i_{masw1} = c_{pa1}(T_{w1}\text{-}273.15)+w_{s1}\left[i_{fgwo}+c_{pv1}(T_{w1}\text{-}273.15)\right]$$

$$=1006.52(296.39\text{-}273.15)+0.0219[2.5106\times10^6+1872.466(296.3884\text{-}273.15)]$$

$$=79\,294.418 \text{ J/kg dry air}$$

The enthalpy of air at T_{w1} away from the film of water

$$i_{ma1} = \frac{m_w c_{pwm}(T_{w1}\text{-}T_{wo})}{m_a}+i_{ma1}$$

$$=12\,500\times\frac{4\,178.833(296.3884\text{-}294.526)}{16\,551.58}+36\,114.729$$

$$=41\,998.4376 \text{ J/kg dry air}$$

The difference between the above calculated are shown for each of the enthalpy differentials at their respective temperatures.

$$\Delta i_x = i_{masw(x)}\text{-}i_{ma(x)}$$

$$\Delta i_1 = 37\,295.843 \text{ J/kg dry air}$$

$$\Delta i_2 = 48\,551.6031 \text{J/kg dry air}$$

$$\Delta i_3 = 60\,726.024 \text{ J/kg dry air}$$

$$\Delta i_4 = 88\,224.358 \text{ J/kg dry air}$$

Substitute these values into the approximate integral and find the combined Merkel number for all three zones

$$\int_{T_{wo}}^{T_{wi}}\frac{c_{pw}dT_w}{i_{masw}-i_{ma}} \approx \frac{c_{pwm}(T_{wi}\text{-}T_{wo})}{4}\left(\frac{1}{\Delta i_1}+\frac{1}{\Delta i_2}+\frac{1}{\Delta i_3}+\frac{1}{\Delta i_4}\right)$$

$$=1.4636735$$

The Merkel number obtained using the Merkel method agrees with the Merkel number previously obtained. This means that the chosen outlet water temperature (T_{wo}) is correct.

The heat rejected by the cooling tower

$$Q=m_w c_{pwm}(T_{wi}\text{-}T_{wo})=12\,500\times4\,178.33(313.15\text{-}294.526)$$

$$=972\,024\,218.951 \text{ W}$$

The heat absorbed by the air is shown below

$Q=m_a(i_{ma5}-i_{ma1}) = 16\ 520.57(94\ 951.920-36\ 114.72)$

972 024 081.2 W

The heat released by the water and absorbed by the air corresponds well thus confirming that T_{a5} is correct.

With all the loss coefficients known it is possible to confirm p_{a5}

$$p_{a5} = p_{a1}[1-0.00975(H_3+L_{fi}/2)/T_{a1}]^{3.5(1+w_1)\left\{1-\frac{w_1}{w_1+0.62198}\right\}}-(K_{fs}+K_{ctc}+K_{fi}+K_{cte}$$
$$+K_{sp}+K_{wd}+K_{de}+K_{rz}+K_{ts}+K_{ct})_{fi}(m_{av15}/A_{fr})^2/(2\rho_{av15})$$
$$=84100[1-0.00975(10+2.504/2)/288.6]^{3.5(1+0.008127)\left\{1-\frac{0.008127}{0.008127+0.62198}\right\}}$$
$$-24.486\times(16\ 808.04/8300)^2/(2\times0.98484)$$
$$=83\ 937.718\ \text{N/m}^2$$

This value is similar to the one used for previous calculations.

The temperature lapse rate above the drift eliminators as shown below

$$\xi_{Ta5} = -g(1+w_5)/\{c_{pma}+1.966\times10^{14}/p_{a5}T_{a5}^2[i_{fgwo}-(c_{pw}-c_{pv})(T_{a5}-273.15)]$$
$$\times\exp(-5406.1915/T_{a5})\}$$
$$=-9.8(1+0.02676)/\{1056.697+\frac{7.966\times10^{14}}{83937.56\times299.5719^2}\times[2.5016\times10^6-(4192.603-1873.8)$$
$$\times(299.5719-273.15)]\exp(-\frac{5406.1915}{299.5719})\}$$
$$= -0.002091057\ \text{K/m}$$

In order to find the pressure difference between the tower outlet and the ambient at the same elevation ($p_{a6} - p_{a7}$) the Froude number and air properties must be known. A value for pressure at 6 must be chosen to calculate the air properties. This value was chosen as 82 650.58912 N/m^2 .

The temperature at 6 can be found by using the temperature lapse rate from 5.

$$T_{a6} = T_{a5}+\xi_{Ta5}(H_6-H_3-L_{fi}-L_{sp}) = 299.5719-0.002092433(147-10-2.504-0.5)$$
$$=299.2916\ \text{K}$$

The density of the air-vapour mixture at the specified temperature and pressure.

$$\rho_{av6} = (1+w_5)\left[1-\frac{w_5}{w_5+0.62198}\right]p_{a6}/(RT_{a6})$$
$$= (1+0.02676)\left[1-\frac{0.02676}{0.02676+0.62198}\right]\times82\ 650.58/(287.08\times299.0291)$$
$$=0.946941\ \text{N/m}^2$$

With the temperature lapse rate of the ambient air known the temperature at 7 can be calculated.

$$T_{a7} = T_{a1}-0.00975H_6=288.6-0.00975\times147$$
$$=287.16675\ \text{K}$$

The corresponding pressure at 7 is found to be

$$p_{a7} = p_{a1}\left[1-\frac{0.00975H_6}{T_{a1}}\right]^{3.5(1+w_I)\left\{1-\frac{w_I}{w_I+0.62198}\right\}}$$

$$=84\ 100[1\text{-}0.00975\times\frac{147}{288.6}]^{3.5(1+0.008127)\left\{1-\frac{0.008127}{0.008127+0.62198}\right\}}$$

$$=82\ 654.268\ \text{N/m}^2$$

With the temperature and pressure known at 7 and assuming a uniform humidity ratio of w_1 the density of air-vapour mixture can be determined.

$$\rho_{av7} = (1+w_I)\left[1-\frac{w_I}{w_I+0.62198}\right]p_{a7}/(R\,T_{a7})$$

$$= \left(1+8.127\times10^{-3}\right)\left[1\text{-}8.127\times\frac{10^{-3}}{8.127\times10^{-3}+0.62198}\right]\times82\ 654.268/(287.08\times287.16675)$$

$$= 0.99771\ \text{N/m}^2$$

The Froud number is determined assuming there is no cold inflow

$$Fr_D = \left(\frac{m_{av5}}{A_6}\right)^2/[\rho_{av6}\left(\rho_{av7}\text{-}\rho_{av6}\right)gd_6\ ]$$

$$= \left[\frac{16\ 963.13}{0.25\times\pi\times60.85^2}\right]^2/[0.946941(0.9977\text{-}0.9469)\times9.8\times60.85]$$

$$=1.19$$

The relation shown below is used to confirm the value chosen for p_{a6} is correct

$$p_{a6} = p_{a7}+\left[0.02Fr_D^{-1.5}\text{-}\frac{0.14}{Fr_D}\right]\left(\frac{m_{av5}}{A_6}\right)^2/\rho_{av6}$$

$$=82\ 654.268+\left[0.02\times1.17033^{-1.5}\text{-}\frac{0.14}{1.17033}\right]\left(\frac{16\ 963.13}{0.25\times\pi\times60.85^2}\right)^2/0.946941$$

$$=82\ 650.581\ \text{N/m}^2$$

The draught equation can now be solved. The LHS of the draught equation is found to be

$$LHS = p_{a1}[\left\{1\text{-}\frac{0.00975\left(H_3+\frac{L_{fi}}{2}\right)}{T_{a1}}\right\}^{3.5(1+w_I)\{1-\frac{w_I}{w_I+0.62198}\}}$$

$$\times\left\{1+\frac{\xi_{Ta5}\left(H_6\text{-}H_3\text{-}\frac{L_{fi}}{2}\right)}{T_{a5}}\right\}^{-\frac{(1+w_5)\left\{1-\frac{w_5}{w_5+0.62198}\right\}g}{R\xi_{Ta5}}}$$

$$-\left\{1\text{-}\frac{0.00975H_6}{T_{a1}}\right\}^{3.5(1+w_I)\left\{1-\frac{w_I}{w_I+0.62198}\right\}}]-(0.02Fr_D^{-1.5}\text{-}0.14/Fr_D)\left(\frac{m_{av5}}{A_6}\right)^2/\rho_{av6}$$

$$= 84\ 100[\left\{1\text{-}\frac{0.00975\left(10+\frac{2.504}{2}\right)}{288.6}\right\}^{3.5(1+0.008127)\left\{1-\frac{0.008127}{0.008127+0.62198}\right\}}$$

$$\times\{1\text{-}0.0020924(147\text{-}10\text{-}\frac{2.504}{2})/299.5719\}^{-(1+0.02676)\left\{1-\frac{0.02676}{0.02676+0.62198}\right\}}$$

$$\times \frac{9.8}{\text{-}287.08\times0.00209}\text{-}\{1\text{-}0.0098\times147/288.6\}^{\,3.5(1+0.0081)\left\{1\text{-}\frac{0.0081}{0.0081+0.62198}\right\}}]$$

$$=68.4$$

The value on the right hand side

$$RHS=(K_{fs}+K_{ctc}+K_{fi}+K_{cte}+K_{sp}+K_{wd}+K_{de}+K_{rz}+K_{ts}+K_{ct})_{fi}\left(\frac{m_{av15}}{A_{fr}}\right)^{2}$$

$$\div (2\rho_{av15})[1+\zeta_{Ta5}(H_{6}\text{-}H_{3}\text{-}L_{fi}/2)/T_{a5}]^{\,\text{-}\frac{(1+w_5)\left[1\text{-}\frac{w_5}{w_5+0.62198}\right]g}{R\zeta_{Ta5}}}+\alpha_{e6}\left(\frac{m_{av5}}{A_{6}}\right)^{2}/(2\rho_{av6})$$

$$=24.456\times\left(\frac{16\,808.04}{8300}\right)^{2}/(2\times0.98484)[1\text{-}0.0020924\left(147\text{-}10\text{-}\frac{2.504}{2}\right)$$

$$\div 299.5719]^{\,\text{-}(1+0.02676)\left[1\text{-}\frac{0.02676}{0.02676+0.62198}\right]}\times\frac{9.8}{\text{-}287.08\times0.0020924}+\frac{1.01\left(\frac{16999.66}{2908.111}\right)^{2}}{2\times0.946941}$$

$$=68.4$$

The LHS of the draught equation is approximately equal to the RHS thus the air-vapour flowrate chosen is correct.

APPENDIX.F EXPERIMENTAL DATA

This section contains the experimental data for the entire tests done for all configurations.

Table F-1: Experimental data and results for H_{sp} = 300 mm, H_{fi} = 608 mm, H_{fg} = N/A, H_{gg} = N/A, H_{rz} = 280 mm (configuration 1)

p_a N/m²	L_{fi} mm	G_w kg/sm²	G_a kg/sm²	Me	K_{fdm}	T_{nzdb} °C	T_{nzwb} °C	T_{fidb} °C	T_{fiwb} °C	dp_{nz} N/m²	dp_{fi} N/m²	T_{wi} °C	T_{wo} °C
101720	608	4.65	3.45	0.92	13.89	7.90	6.21	8.74	6.70	552.11	74.50	46.83	29.01
101720	608	4.65	2.94	0.83	14.04	7.74	6.23	8.41	6.67	398.83	54.67	46.05	30.16
101720	608	4.61	1.91	0.62	15.91	7.38	5.94	7.84	6.32	166.71	26.01	45.07	33.25
101720	608	4.59	1.03	0.40	22.65	7.67	6.05	7.90	6.44	48.75	10.55	44.34	36.96
101720	608	3.01	1.03	0.60	20.00	8.00	6.28	8.05	6.47	49.38	9.30	42.76	33.05
101720	608	2.99	2.00	0.93	14.36	8.08	6.45	8.20	6.54	183.90	25.34	42.37	27.81
101720	608	3.00	2.93	1.20	13.13	7.76	6.25	8.34	6.58	396.61	49.52	41.75	24.42
101720	608	3.00	3.43	1.35	12.98	7.76	6.18	8.58	6.62	542.92	66.52	41.00	22.77
101720	608	1.50	1.04	1.12	17.29	7.86	6.27	7.92	6.44	49.44	7.88	40.14	25.76
101720	608	1.49	1.97	1.69	13.20	7.89	6.28	8.08	6.35	178.89	22.13	39.61	20.16
101720	608	1.49	2.93	2.20	12.20	7.16	5.86	7.90	6.19	394.84	44.79	39.32	16.68
101720	608	1.50	3.43	2.43	12.04	7.24	5.83	8.11	6.24	543.05	60.40	39.16	15.51
101720	608	4.61	1.04	0.42	22.28	7.79	6.17	8.01	6.47	49.86	10.42	38.96	33.26
101720	608	4.60	1.93	0.63	15.88	8.14	6.40	8.28	6.57	171.54	26.06	38.75	29.88
101720	608	4.59	2.92	0.84	14.19	8.29	6.53	8.77	6.85	394.15	53.14	38.32	26.99
101720	608	4.57	3.42	0.94	14.05	8.21	6.52	8.95	6.95	540.64	71.76	38.15	25.76
101720	608	3.02	1.03	0.62	19.93	8.24	6.62	8.40	6.87	49.00	9.06	37.62	30.10
101720	608	3.03	1.95	0.94	14.53	7.73	6.31	8.16	6.66	175.48	24.17	37.40	25.95
101720	608	3.03	2.82	1.19	13.28	7.51	6.10	8.17	6.52	367.51	46.00	37.30	23.20
101720	608	3.02	3.36	1.34	13.06	7.51	6.07	8.36	6.56	520.20	63.68	37.27	21.82
101720	608	1.55	1.04	1.11	17.37	7.77	6.15	7.90	6.38	49.46	7.88	37.01	24.75
101720	608	1.56	1.96	1.65	13.32	7.71	6.13	7.97	6.32	176.48	21.93	36.69	19.77
101720	608	1.56	2.97	2.17	12.25	7.71	6.13	8.30	6.44	408.08	46.26	36.71	16.53
101720	608	1.56	3.42	2.40	12.10	7.19	5.96	8.25	6.50	541.59	60.43	36.67	15.43
101720	608	4.56	1.02	0.43	22.29	7.39	6.00	7.84	6.39	47.89	9.95	36.90	31.78
101720	608	4.56	1.98	0.67	15.72	7.12	5.77	7.64	6.13	179.04	26.77	36.28	28.15
101720	608	4.55	2.89	0.85	14.25	7.24	5.84	7.93	6.26	383.94	51.64	35.52	25.51
101720	608	4.59	3.37	0.96	14.15	7.23	5.85	8.15	6.42	525.19	69.48	33.47	23.54
101720	608	3.03	0.93	0.56	21.15	7.52	5.95	7.72	6.25	40.22	7.73	32.32	27.14
101720	608	3.03	1.93	0.94	14.62	7.66	6.10	7.80	6.29	170.48	23.20	31.20	22.88
101720	608	3.03	2.95	1.26	13.29	7.78	6.13	8.12	6.33	401.36	49.33	30.64	20.12
101720	608	3.04	3.41	1.39	13.18	7.73	6.09	8.34	6.42	538.35	65.32	30.27	19.10
101720	608	1.57	0.96	1.06	17.80	8.06	6.33	7.87	6.35	42.84	6.85	29.44	21.69

p_a N/m^2	L_{fi} mm	G_w kg/sm^2	G_a kg/sm^2	Me	K_{fdm}	T_{nzdb} ^{o}C	T_{nzwb} ^{o}C	T_{fidb} ^{o}C	T_{fiwb} ^{o}C	dp_{nz} N/m^2	dp_{fi} N/m^2	T_{wi} ^{o}C	T_{wo} ^{o}C
101720	608	1.57	1.97	1.69	13.35	8.11	6.23	8.08	6.17	177.66	21.76	28.87	17.21
101720	608	1.59	2.88	2.15	12.43	7.97	6.25	8.38	6.40	381.54	43.26	28.59	14.91
101720	608	1.58	3.41	2.39	12.25	7.85	6.21	8.61	6.54	538.33	59.84	28.33	13.91

Table F-2: Experimental data and results for H$_{sp}$ = 300 mm, H$_{fi}$ = 608 mm, H$_{fg}$ = N/A, H$_{gg}$ = N/A, H$_{rz}$ = 2105 mm (configuration 2)

p_a N/m^2	L_{fi} mm	G_w kg/sm^2	G_a kg/sm^2	Me	K_{fdm}	T_{nzdb} ^{o}C	T_{nzwb} ^{o}C	T_{fidb} ^{o}C	T_{fiwb} ^{o}C	dp_{nz} N/m^2	dp_{fi} N/m^2	T_{wi} ^{o}C	T_{wo} ^{o}C
100700	608	4.51	3.36	0.97	16.29	12.15	11.48	13.19	11.95	532.14	84.49	49.10	30.25
100700	608	4.52	2.91	0.90	16.85	12.16	11.51	13.02	11.91	396.12	65.13	47.04	30.77
100700	608	4.52	1.97	0.71	20.41	12.24	11.56	12.80	11.86	180.41	36.10	45.67	33.37
100700	608	4.52	0.99	0.44	36.34	12.36	11.61	12.97	12.02	45.76	16.08	44.69	37.47
100700	608	3.02	1.00	0.61	30.02	12.40	11.61	12.78	11.90	46.54	13.32	43.70	34.28
100700	608	3.01	2.04	0.99	17.51	12.34	11.58	12.73	11.84	194.05	32.67	43.37	28.84
100700	608	3.00	2.92	1.26	15.09	12.22	11.50	12.90	11.84	399.28	57.38	43.13	25.83
100700	608	3.00	3.41	1.41	14.62	12.29	11.51	13.18	11.94	547.23	75.64	42.77	24.48
100700	608	1.68	1.03	1.06	22.79	12.60	11.58	12.64	11.67	49.88	10.61	41.42	28.12
100700	608	1.68	1.99	1.59	15.18	12.65	11.61	12.80	11.69	186.18	26.59	41.12	23.05
100700	608	1.68	2.96	2.05	13.38	12.70	11.64	13.14	11.84	410.81	51.14	40.72	20.12
100700	608	1.68	3.44	2.30	13.05	12.67	11.64	13.45	11.98	557.16	67.25	40.34	18.98
100700	608	4.39	1.03	0.45	34.94	12.73	11.72	13.18	12.03	49.64	16.43	39.68	34.01
100700	608	4.38	1.97	0.72	20.36	12.61	11.67	13.03	11.90	181.17	35.20	38.88	30.04
100700	608	4.38	2.90	0.93	16.90	12.71	11.79	13.36	12.10	396.08	63.31	38.15	27.32
100700	608	4.35	3.45	1.06	16.24	12.69	11.67	13.58	12.09	560.83	85.54	37.77	25.97
100700	608	3.14	1.03	0.62	29.42	12.67	11.71	13.00	11.95	49.96	13.71	36.57	30.24
100700	608	3.15	1.95	0.96	18.18	12.67	11.73	12.96	11.86	177.46	30.40	36.30	26.57
100700	608	3.13	2.91	1.26	15.34	12.72	11.76	13.28	12.01	399.20	57.21	35.90	23.89
100700	608	3.12	3.38	1.40	14.83	12.70	11.74	13.54	12.13	539.87	74.45	35.57	22.82
100700	608	1.57	0.98	1.12	23.03	12.78	11.86	12.85	11.89	45.67	9.65	34.78	25.26
100700	608	1.57	1.98	1.73	15.03	12.70	11.81	12.92	11.87	183.92	25.63	34.55	20.88
100700	608	1.57	2.94	2.23	13.28	12.74	11.76	13.27	11.98	406.20	49.61	34.39	18.47
100700	608	1.56	3.43	2.50	12.96	12.82	11.77	13.59	12.07	554.66	65.70	34.00	17.49
100700	608	4.39	1.02	0.43	34.86	12.80	11.81	13.20	12.10	49.21	15.89	33.13	29.45
100700	608	4.38	1.94	0.71	20.52	12.81	11.76	13.15	11.95	175.51	33.69	32.82	26.76
100700	608	4.37	2.90	0.94	16.95	12.81	11.71	13.38	11.97	394.76	62.21	32.44	24.64
100700	608	4.37	3.42	1.07	16.31	12.91	11.74	13.67	12.09	550.56	83.03	32.08	23.60
100700	608	3.09	1.03	0.63	28.90	13.04	11.78	13.14	11.91	49.55	13.15	31.37	26.83
100700	608	3.08	1.99	1.00	17.78	13.11	11.84	13.22	11.90	185.78	30.62	31.02	23.79
100700	608	3.08	2.96	1.32	15.20	13.10	11.84	13.58	12.06	413.75	57.97	30.93	21.76
100700	608	3.09	3.35	1.43	14.83	13.13	11.85	13.81	12.14	529.81	72.15	30.70	21.08

100700	608	1.59	1.03	1.18	21.99	13.12	11.88	13.10	11.88	50.10	10.03	30.33	22.95
100700	608	1.58	1.92	1.72	15.21	13.13	11.96	13.23	11.98	173.64	24.26	30.11	19.76
100700	608	1.58	2.97	2.25	13.30	13.15	12.03	13.56	12.15	415.82	50.41	29.96	17.62
100700	608	1.58	3.41	2.50	13.01	13.21	12.10	13.97	12.38	548.60	64.80	29.76	16.99

Table F-3: Experimental data and results for H_{sp} = 300 mm, H_{fi} = 608 mm, H_{fg} = 200 mm, H_{gg} = N/A, H_{rz} = 1905 mm (configuration 3)

p_a N/m^2	L_{fi} mm	G_w kg/sm^2	G_a kg/sm^2	Me	K_{fdm}	T_{nzdb} ^{o}C	T_{nzwb} ^{o}C	T_{fidb} ^{o}C	T_{fiwb} ^{o}C	dp_{nz} N/m^2	dp_{fi} N/m^2	T_{wi} ^{o}C	T_{wo} ^{o}C
101920	608	1.60	1.95	1.75	16.36	7.32	6.30	7.61	6.48	172.88	28.15	53.47	22.49
101920	608	3.06	1.98	1.04	19.76	7.62	6.53	7.89	6.70	178.17	35.39	54.10	30.52
101920	608	4.40	1.97	0.76	22.64	7.58	6.56	7.98	6.82	175.45	40.61	54.28	35.04
101920	608	1.58	2.00	1.81	19.84	7.63	6.50	7.91	6.62	180.93	28.88	52.80	22.00
101920	608	1.57	1.08	1.31	32.52	8.01	6.67	7.95	6.68	52.98	12.58	52.33	27.96
101920	608	1.56	1.94	1.73	19.58	7.54	6.42	7.90	6.59	170.47	27.57	51.30	22.30
101920	608	1.58	2.91	2.22	16.73	7.01	6.06	7.77	6.41	385.35	52.55	50.53	18.33
101920	608	1.58	3.44	2.60	16.20	6.87	5.97	7.86	6.45	539.16	70.03	49.83	16.29
101920	608	1.58	1.98	1.81	19.59	7.33	6.23	7.82	6.57	177.96	28.39	48.72	21.51

Table F-4: Experimental data and results for H_{sp} = 300 mm, H_{fi} = 608 mm, H_{fg} = 300 mm, H_{gg} = N/A, H_{rz} = 1905 mm (configuration 4)

p_a N/m^2	L_{fi} mm	G_w kg/sm^2	G_a kg/sm^2	Me	K_{fdm}	T_{nzdb} ^{o}C	T_{nzwb} ^{o}C	T_{fidb} ^{o}C	T_{fiwb} ^{o}C	dp_{nz} N/m^2	dp_{fi} N/m^2	T_{wi} ^{o}C	T_{wo} ^{o}C
101800	608	1.56	2.03	1.71	16.76	8.27	7.37	8.52	7.46	187.63	29.22	48.60	22.12
101800	608	3.00	2.01	1.08	20.41	8.20	7.40	8.51	7.52	184.42	35.47	49.29	29.12
101800	608	4.41	2.00	0.79	23.41	8.35	7.44	8.65	7.60	181.65	41.12	49.55	33.42
101800	608	3.08	2.02	1.07	19.58	7.84	6.99	8.26	7.24	184.81	36.05	49.31	29.24
101800	608	3.09	1.06	0.72	31.34	7.91	7.01	8.11	7.21	51.30	16.81	49.24	35.33
101800	608	3.09	1.96	1.02	19.44	7.91	7.07	8.27	7.38	175.17	35.05	49.22	29.78
101800	608	3.08	2.98	1.37	16.55	8.21	7.35	8.87	7.73	406.37	64.99	48.78	25.39
101800	608	3.08	3.42	1.51	16.08	8.05	7.24	9.01	7.76	537.39	82.05	48.35	23.93
101800	608	3.09	2.01	1.10	19.44	8.47	7.45	8.98	7.78	184.42	35.68	44.26	27.78

Table F-5: Experimental data and results for H_{sp} = 300 mm, H_{fi} = 608 mm, H_{fg} = 400 mm, H_{gg} = N/A, H_{rz} = 2105 mm (configuration 5)

p_a N/m^2	L_{fi} mm	G_w kg/sm^2	G_a kg/sm^2	Me	K_{fdm}	T_{nzdb} ^{o}C	T_{nzwb} ^{o}C	T_{fidb} ^{o}C	T_{fiwb} ^{o}C	dp_{nz} N/m^2	dp_{fi} N/m^2	T_{wi} ^{o}C	T_{wo} ^{o}C
101130	608	4.46	0.97	0.52	26.54	5.29	4.18	5.99	4.71	43.52	10.72	38.03	23.34
101130	608	4.48	1.99	0.82	17.25	6.20	4.79	6.59	5.05	166.28	27.32	44.23	20.30
101130	608	4.50	2.85	1.03	14.60	6.38	4.90	7.05	5.38	385.50	52.91	43.64	16.41

p_a N/m²	L_{fi} mm	G_w kg/sm²	G_a kg/sm²	Me	K_{fdm}	T_{nzdb} °C	T_{nzwb} °C	T_{fidb} °C	T_{fiwb} °C	dp_{nz} N/m²	dp_{fi} N/m²	T_{wi} °C	T_{wo} °C
101130	608	4.53	3.42	1.17	14.04	6.23	4.82	7.16	5.41	532.79	69.82	43.37	15.04
101130	608	3.21	0.99	0.69	37.07	6.24	4.91	6.22	4.98	44.49	16.13	47.57	35.16
101130	608	3.22	1.94	1.04	21.23	6.04	4.84	6.32	5.01	171.40	35.82	47.14	28.86
101130	608	3.22	2.88	1.35	17.34	5.91	4.72	6.41	5.05	379.03	63.90	46.77	24.76
101130	608	3.21	3.43	1.52	16.45	6.14	4.89	6.76	5.24	537.79	85.22	46.42	22.90
101130	608	1.56	1.04	1.34	43.98	5.70	4.54	5.85	4.63	43.37	19.09	49.91	39.27
101130	608	1.57	1.91	1.83	23.46	5.47	4.42	5.87	4.60	180.24	42.75	50.66	33.14
101130	608	1.57	2.90	2.40	19.24	5.30	4.27	5.86	4.72	368.45	71.33	52.49	29.95
101130	608	1.56	3.41	2.64	18.08	5.09	4.23	5.90	5.40	533.65	96.67	53.52	28.25
101130	608	4.37	1.06	0.53	25.79	6.26	4.85	6.29	4.99	49.28	12.04	45.12	26.05
101130	608	4.37	1.97	0.83	16.83	4.89	4.00	5.90	4.59	169.19	26.73	37.57	17.54
101130	608	4.37	2.90	1.08	14.45	5.42	4.24	6.33	4.88	380.91	51.07	37.03	14.19
101130	608	4.35	3.38	1.20	13.90	5.56	4.37	6.75	5.13	531.05	68.03	36.77	13.08
101130	608	3.18	0.97	0.71	37.72	6.22	4.80	6.58	5.08	42.64	15.30	40.26	31.44
101130	608	3.17	2.03	1.14	20.66	5.50	4.39	6.13	4.94	186.07	36.97	39.49	25.44
101130	608	3.17	2.85	1.41	17.48	5.25	4.24	6.06	4.71	369.01	61.48	39.07	22.36
101130	608	3.17	3.42	1.58	16.55	4.89	4.01	6.15	4.71	533.37	83.60	38.63	20.64
101130	608	1.41	0.98	1.41	41.53	6.45	4.94	6.78	5.20	48.32	19.44	42.87	34.87
101130	608	1.40	1.93	2.04	23.71	6.39	4.96	6.85	5.27	176.08	40.68	42.02	29.82
101130	608	1.40	2.89	2.64	19.19	6.27	4.90	7.02	5.51	383.42	71.07	41.61	26.44
101130	608	1.39	3.41	2.91	18.21	6.24	4.84	7.13	5.40	523.24	91.41	41.22	24.86
101130	608	4.36	1.07	0.59	26.97	5.37	4.23	6.02	4.66	44.59	11.06	33.09	22.10
101130	608	4.34	2.03	0.87	17.26	5.32	4.24	6.17	4.74	167.78	26.95	32.64	17.12
101130	608	4.34	2.95	1.12	14.62	5.30	4.21	6.30	4.76	402.33	54.23	32.57	13.99
101130	608	4.31	3.39	1.24	14.14	5.55	4.33	6.63	5.01	532.27	69.06	32.31	12.92
101130	608	3.17	1.00	0.78	36.59	5.51	4.31	6.33	4.81	45.29	15.52	34.31	27.54
101130	608	3.17	1.97	1.12	21.02	5.52	4.35	6.48	4.83	176.51	35.10	34.00	23.34
101130	608	3.17	2.95	1.46	17.31	5.42	4.26	6.49	4.91	395.05	64.23	33.77	20.33
101130	608	3.15	3.39	1.62	16.59	5.28	4.22	6.53	4.92	524.79	81.40	33.49	19.06
101130	608	1.53	0.99	1.31	40.12	5.80	4.50	6.62	5.02	51.70	19.66	36.19	30.27
101130	608	1.53	1.92	1.94	23.23	5.89	4.59	6.75	5.10	186.42	41.34	35.76	26.43
101130	608	1.54	2.97	2.50	19.08	5.98	4.66	7.02	5.31	395.82	71.61	35.47	23.72
101130	608	1.53	3.41	2.79	18.23	5.78	4.54	7.02	5.26	526.12	90.48	35.07	22.43

Table F-6: Experimental data and results for H_{sp} = 300 mm, H_{fi} = 608 mm, H_{fg} = 400 mm, H_{gg} = 400 mm, H_{rz} = 1905 mm (configuration 6)

p_a N/m²	L_{fi} mm	G_w kg/sm²	G_a kg/sm²	Me	K_{fdm}	T_{nzdb} ºC	T_{nzwb} ºC	T_{fidb} ºC	T_{fiwb} ºC	dp_{nz} N/m²	dp_{fi} N/m²	T_{wi} ºC	T_{wo} ºC
100540	608	1.64	2.02	1.78	17.83	11.08	10.30	11.16	10.49	190.25	32.05	42.53	22.09
100540	608	3.14	2.00	1.14	21.86	11.46	10.54	11.16	10.70	186.82	39.26	42.02	27.65
100540	608	4.33	1.98	0.89	24.89	11.57	10.56	11.39	10.70	183.74	44.10	40.73	29.86
100540	608	3.09	1.99	1.18	21.84	11.68	10.67	11.52	10.83	184.41	38.49	40.09	26.83
100540	608	3.09	1.00	0.82	38.47	11.57	10.54	11.45	10.77	46.65	17.03	39.64	31.26
100540	608	3.07	1.95	1.18	22.11	11.52	10.49	11.51	10.73	176.70	37.28	39.38	26.61
100540	608	3.08	2.90	1.50	18.21	11.11	10.22	11.38	10.58	395.03	68.00	39.09	23.51
100540	608	3.09	3.39	1.66	17.44	11.09	10.16	11.37	10.61	540.68	88.56	38.81	22.22
100540	608	3.06	1.99	1.25	21.75	11.44	10.40	11.43	10.78	185.27	38.32	37.95	25.71

Table F-7: Experimental data and results for H_{sp} = 300 mm, H_{fi} = 608 mm, H_{fg} = 400 mm, H_{gg} = 800 mm, H_{rz} = 1905 mm (configuration 7)

p_a N/m²	L_{fi} mm	G_w kg/sm²	G_a kg/sm²	Me	K_{fdm}	T_{nzdb} ºC	T_{nzwb} ºC	T_{fidb} ºC	T_{fiwb} ºC	dp_{nz} N/m²	dp_{fi} N/m²	T_{wi} ºC	T_{wo} ºC
100540	608	1.53	1.96	2.04	17.91	11.40	10.44	11.40	10.74	178.84	29.88	36.41	19.86
100540	608	3.07	1.94	1.23	22.21	11.45	10.48	11.32	10.75	176.30	37.12	36.80	25.40
100540	608	4.32	1.93	0.90	25.58	11.69	10.67	11.53	10.80	173.98	42.30	36.41	27.87
100540	608	3.08	1.94	1.19	22.27	11.80	10.65	11.65	10.84	176.42	37.15	36.29	25.37
100540	608	3.07	1.01	0.84	38.34	11.78	10.58	11.63	10.83	47.64	17.12	35.98	29.06
100540	608	3.06	2.00	1.11	22.09	11.83	10.72	11.69	10.85	187.15	38.93	35.82	25.36
100540	608	3.06	2.96	1.50	18.23	11.82	10.69	11.90	10.94	410.51	69.96	35.80	22.47
100540	608	3.06	3.42	1.64	17.53	12.01	10.81	12.00	11.26	552.35	90.00	35.47	21.44
100540	608	3.07	1.96	1.23	22.08	12.16	10.92	12.10	11.22	180.24	37.46	34.76	24.65

Table F-8: Experimental data and results for H_{sp} = 300 mm, H_{fi} = 608 mm, H_{fg} = N/A, H_{gg} = N/A, H_{rz} = 4168 mm (configuration 8)

p_a N/m²	L_{fi} mm	G_w kg/sm²	G_a kg/sm²	Me	K_{fdm}	T_{nzdb} ºC	T_{nzwb} ºC	T_{fidb} ºC	T_{fiwb} ºC	dp_{nz} N/m²	dp_{fi} N/m²	T_{wi} ºC	T_{wo} ºC
101480	608	1.62	2.02	1.54	17.59	6.02	4.36	6.16	4.84	185.31	31.00	45.85	21.90
101480	608	3.04	2.00	1.03	22.28	6.34	4.60	5.94	4.80	180.63	39.27	46.73	28.35
101480	608	4.55	2.02	0.77	26.80	6.62	4.89	7.45	5.97	184.76	49.17	47.19	32.56
101480	608	2.99	2.04	1.08	21.68	6.50	4.92	6.59	5.19	188.63	39.93	46.78	27.85
101480	608	3.00	1.06	0.73	40.57	6.59	4.87	6.62	5.23	50.86	20.11	46.40	33.66
101480	608	2.98	2.02	1.06	22.20	6.41	4.79	6.62	5.20	184.32	39.89	46.27	27.90
101480	608	2.98	3.02	1.37	17.29	6.11	4.62	6.61	5.11	413.92	68.91	46.02	23.92
101480	608	2.98	3.44	1.57	16.27	6.48	4.84	6.95	5.34	540.58	84.24	45.97	22.25
101480	608	3.00	2.02	1.09	21.93	6.16	4.57	6.50	5.23	185.42	39.48	44.40	27.14

Table F-9: Experimental data and results for H$_{sp}$ = 300 mm, H$_{fi}$ = 608 mm, H$_{fg}$ = 400, H$_{gg}$ = N/A, H$_{rz}$ = 4168 mm (configuration 9)

p_a N/m^2	L_{fi} mm	G_w kg/sm^2	G_a kg/sm^2	Me	K_{fdm}	T_{nzdb} ^{o}C	T_{nzwb} ^{o}C	T_{fidb} ^{o}C	T_{fiwb} ^{o}C	dp_{nz} N/m^2	dp_{fi} N/m^2	T_{wi} ^{o}C	T_{wo} ^{o}C
101480	608	1.40	2.05	2.33	18.07	6.75	5.18	5.96	5.18	190.24	32.15	38.27	16.77
101480	608	2.97	2.02	1.31	23.99	6.31	4.94	6.08	5.13	185.30	42.78	40.65	24.84
101480	608	4.59	2.00	0.85	30.11	6.49	5.00	6.90	6.01	181.18	52.56	38.43	28.36
101480	608	2.97	1.97	1.26	24.71	7.08	5.35	6.81	5.56	176.96	41.45	36.29	23.69
101480	608	2.96	1.05	0.92	46.64	7.11	5.41	6.84	5.60	50.57	22.24	35.90	27.70
101480	608	2.96	2.01	1.24	24.43	7.35	5.55	7.14	5.71	184.25	42.57	35.95	23.57
101480	608	2.96	2.96	1.57	18.86	7.60	5.68	7.44	5.80	400.79	70.82	35.70	20.56
101480	608	2.95	3.42	1.81	17.52	8.03	5.82	7.81	6.09	536.62	87.58	35.38	19.10
101480	608	2.95	1.95	1.31	24.65	8.29	6.10	8.40	6.60	174.42	40.56	34.66	23.13

Table F-10: Experimental data and results for H$_{sp}$ = 300 mm, H$_{fi}$ = 608 mm, H$_{fg}$ = 400, H$_{gg}$ = 800, H$_{rz}$ = 4168 mm (configuration 10)

p_a N/m^2	L_{fi} mm	G_w kg/sm^2	G_a kg/sm^2	Me	K_{fdm}	T_{nzdb} ^{o}C	T_{nzwb} ^{o}C	T_{fidb} ^{o}C	T_{fiwb} ^{o}C	dp_{nz} N/m^2	dp_{fi} N/m^2	T_{wi} ^{o}C	T_{wo} ^{o}C
100520	608	1.49	1.97	2.19	21.06	13.81	9.37	13.31	9.41	182.32	35.98	42.18	19.79
100520	608	2.95	1.95	1.36	27.70	13.27	9.35	13.41	9.44	178.60	47.58	42.88	26.33
100520	608	4.41	1.98	0.92	32.42	13.73	9.24	13.27	9.34	173.27	57.77	43.22	30.51
100520	608	3.01	2.00	1.33	27.46	14.22	9.49	13.45	9.43	189.13	49.78	43.11	26.51
100520	608	2.99	1.05	0.89	54.08	14.40	9.61	13.49	9.60	52.10	27.05	43.10	31.99
100520	608	3.00	2.01	1.29	27.46	14.51	9.89	13.78	9.59	190.86	50.16	43.07	26.65
100520	608	2.98	2.98	1.75	20.72	14.55	9.75	13.97	9.77	419.97	82.32	43.03	22.80
100520	608	2.97	3.39	1.94	19.39	14.44	9.57	14.62	9.74	546.87	99.80	42.96	21.50
100520	608	2.97	1.99	1.38	27.35	14.55	9.74	14.14	9.71	186.56	48.93	42.97	26.29

Table F-11: Experimental data and results for H$_{sp}$ = 300 mm, H$_{fi}$ = 608 mm, H$_{fg}$ = 400-450, H$_{gg}$ = N/A, H$_{rz}$ = 4168 mm (configuration 11)

p_a N/m^2	L_{fi} mm	G_w kg/sm^2	G_a kg/sm^2	Me	K_{fdm}	T_{nzdb} ^{o}C	T_{nzwb} ^{o}C	T_{fidb} ^{o}C	T_{fiwb} ^{o}C	dp_{nz} N/m^2	dp_{fi} N/m^2	T_{wi} ^{o}C	T_{wo} ^{o}C
100520	608	1.38	2.02	2.16	17.64	14.35	9.81	13.79	9.73	192.99	31.65	40.59	19.37
100520	608	3.11	2.00	1.19	24.16	14.33	9.89	13.74	9.82	188.22	43.49	42.32	27.15
100520	608	4.40	1.98	0.89	28.82	14.38	9.89	14.01	9.69	184.94	51.28	41.88	30.12
100520	608	3.07	2.01	1.16	24.16	14.36	9.82	13.89	9.61	189.49	43.28	39.26	26.14
100520	608	3.05	0.96	0.78	50.64	14.39	9.88	13.59	9.65	44.02	20.92	37.99	30.32
100520	608	3.06	1.96	1.16	24.70	14.29	9.75	13.80	9.50	180.25	41.83	36.99	25.34
100520	608	3.05	2.91	1.54	18.85	14.31	9.68	14.13	9.52	401.44	70.28	35.91	21.94

p_a N/m^2	L_{fi} mm	G_w kg/sm^2	G_a kg/sm^2	Me	K_{fdm}	T_{nzdb} ^oC	T_{nzwb} ^oC	T_{fidb} ^oC	T_{fiwb} ^oC	dp_{nz} N/m^2	dp_{fi} N/m^2	T_{wi} ^oC	T_{wo} ^oC
100520	608	3.05	3.45	1.73	17.41	14.45	9.79	14.51	9.69	565.07	90.76	35.44	20.62
100520	608	3.08	1.93	1.25	24.79	14.41	9.71	14.01	9.48	175.64	40.71	34.73	24.23